CASE REPORTS IN NEUROSURGERY: 2021

EDITED BY: Philipp Taussky
PUBLISHED IN: Frontiers in Surgery

frontiers Research Topics

ISSN 1664-8714
ISBN 978-2-88976-453-2
DOI 10.3389/978-2-88976-453-2

About Frontiers

Frontiers is more than just an open-access publisher of scholarly articles: it is a pioneering approach to the world of academia, radically improving the way scholarly research is managed. The grand vision of Frontiers is a world where all people have an equal opportunity to seek, share and generate knowledge. Frontiers provides immediate and permanent online open access to all its publications, but this alone is not enough to realize our grand goals.

Frontiers Journal Series

The Frontiers Journal Series is a multi-tier and interdisciplinary set of open-access, online journals, promising a paradigm shift from the current review, selection and dissemination processes in academic publishing. All Frontiers journals are driven by researchers for researchers; therefore, they constitute a service to the scholarly community. At the same time, the Frontiers Journal Series operates on a revolutionary invention, the tiered publishing system, initially addressing specific communities of scholars, and gradually climbing up to broader public understanding, thus serving the interests of the lay society, too.

Dedication to Quality

Each Frontiers article is a landmark of the highest quality, thanks to genuinely collaborative interactions between authors and review editors, who include some of the world's best academicians. Research must be certified by peers before entering a stream of knowledge that may eventually reach the public - and shape society; therefore, Frontiers only applies the most rigorous and unbiased reviews.
Frontiers revolutionizes research publishing by freely delivering the most outstanding research, evaluated with no bias from both the academic and social point of view. By applying the most advanced information technologies, Frontiers is catapulting scholarly publishing into a new generation.

What are Frontiers Research Topics?

Frontiers Research Topics are very popular trademarks of the Frontiers Journals Series: they are collections of at least ten articles, all centered on a particular subject. With their unique mix of varied contributions from Original Research to Review Articles, Frontiers Research Topics unify the most influential researchers, the latest key findings and historical advances in a hot research area! Find out more on how to host your own Frontiers Research Topic or contribute to one as an author by contacting the Frontiers Editorial Office: frontiersin.org/about/contact

CASE REPORTS IN NEUROSURGERY: 2021

Topic Editor:
Philipp Taussky, The University of Utah, United States

Citation: Taussky, P., ed. (2022). Case Reports in Neurosurgery: 2021. Lausanne: Frontiers Media SA. doi: 10.3389/978-2-88976-453-2

Table of Contents

frontiers | Frontiers in Surgery

EDITORIAL
published: 06 June 2022
doi: 10.3389/fsurg.2022.906371

Editorial: Sharing One's Experience and Advancing Medicine through Case Reports

*Philipp Taussky**

Department of Neurosurgery, Clinical Neurosciences Center, The University of Utah, Salt Lake City, UT, United States

Keywords: case reports, surgery, complications, knowledge acquisition, technique, radiology

Editorial on the Research Topic

Sharing One's Experience and Advancing Medicine through Case Reports

One of our residents recently pointed out that there are three distinct ways to learn as a surgeon: From one's own mistakes, which is the least attractive way, from mistakes reported in the literature, and from directly witnessing other people's mistakes. The last two instances may be the most advantageous way of learning in a surgical setting. The publication of case reports exactly addresses these last two scenarios. It allows surgeons to share their experience, insights, or mistakes with a wider audience and to create the opportunity for others to learn without making the same mistake or unknowingly facing the same challenge. In its most fundamental sense, case reports speak to a higher academic calling. They transform one's own experience into something much larger, by publishing and sharing it, it becomes part of our common literature of collectively gained knowledge in an academic framework.

In many ways, this aspect of case reports speaks directly to the core mission of Frontiers in Surgery: To create a discussion and knowledge platform of advances and research findings in surgical practice today to continuously improve clinical management of patients and foster innovation in this field. But case reports also have limitations. In the publishing world, they are not popular, since they are rarely cited and therefore tend not to improve a journal's impact factor. For researchers and physicians, case reports are considered minor intellectual achievements relegated to a different category in an academic CV, separate from your more impactful publications.

Yet, despite their relatively small academic stature, case reports play an important part in medicine and its long history. Case reports have been identified in an Egyptian antiquity papyrus from the 16th to 17th dynasty, circa 1,600 BC (1). Interestingly, the case reports (a few dozen have been found) follow a modern presentation: Diagnosis in the title, examination and prognosis, and treatment. Case reports are also found in Greek medical literature, in the Hippocratic Corpus, probably written around 400 BC (2). In the middle ages, case reports were disseminated in the Islamic medical literature (3). Rhazes (865–929 AD), a famous Persian physician, scholar, and philosopher, whose full name was Abu Bakr Muhamed Ibn Zakariya al-Razi, left a large collection of case reports (3). While medicine lacked major progress in Europe during the Middle Ages, during the Renaissance and Enlightenment, the study of human anatomy and physiology gradually advanced and a recent linguistic analysis of publications in

Edited by:
Francesco Certo,
Neurological Surgery Unit,
University of Catania, Italy

****Correspondence:***
Philipp Taussky
philipp.taussky@gmail.com

Specialty section:
This article was submitted to Neurosurgery, a section of the journal Frontiers in Surgery

Received: *28 March 2022*
Accepted: *25 April 2022*
Published: *06 June 2022*

Citation:
Taussky P (2022) Editorial: Sharing One's Experience and Advancing Medicine through Case Reports. Front. Surg. 9:906371. doi: 10.3389/fsurg.2022.906371

the Edinburgh Medical Journal (the oldest continuing medical journal in English) from 1735 to 1985 found that by the end of the 18th century case narratives had become standardized in their structure and form (4).

The significant medical value of case reports is beautifully illustrated in this current collection of case reports published in Frontiers in Surgery, the Neurosurgery section, in 2021. Case reports, such as these presented here, transform an individual clinical experience or insight into something larger: A contribution to the literature shared with other practitioners thus advancing our knowledge and the field in a fundamental academic way by being transparent and sharing knowledge.

Some of the case reports in our collection share surgical and technical nuances, such as novel bypass surgical approaches, a novel technique for cranioplasties, the novel use of an exoscope for an orbital cavernous hemangioma resection, a rare anterior inferior cerebellar artery aneurysm treated by re-anastomosis, and the use of a novel shunt for hydrocephalus (5–9). Unusual pathologies are reported on colliding pituitary adenoma and primary pituitary lymphoma, a de-novo mutation in an infant with Pallister-Hall syndrome and radiological and clinical findings of multiple cerebellar liponeurocytomas, and an unusual case of creeping growth in a lymphoplasmacyte-rich meningioma (10–13). And finally, lessons learned from unusual complications are shared in a rare case of fourth ventricle to spinal subarachnoid space shunt migration and contrast-induced encephalopathy after endovascular treatment of an intracranial aneurysm (14, 15).

These case reports represent the best of academic medicine but also the best of what an open-access journal like Frontiers has to offer: An online platform of international researchers sharing their rare insights, surgical techniques but also surgical complications, and lessons learned. The 2021 pandemic year was difficult for all of us, but the current collection of neurosurgical case reports also illustrates that despite difficulties stretching the capabilities of our healthcare systems, surgeons worldwide continued to treat patients with neurological disease, sharing their respective experiences by contributing to the field in a fundamental academic way.

AUTHOR CONTRIBUTIONS

Philipp Taussky conceived, drafted and wrote the manuscript. All authors contributed to the article and approved the submitted version.

REFERENCES

1. Allen JP. *The Art of Medicine in Ancient Egypt. The Metropolitan Museum of Art, New York*. New Haven and London: Yale University Press (2005).
2. The Internet Classics Archive. Available from: http://classics.mit.edu/Hippocrates/epidemics.2.ii.html (Accessed April 26, 2012).
3. Alvarez Millan C. Graeco-Roman case histories and their influence on Medieval Islamic clinical accounts. *Soc Hist Med.* (1999) 12:19–43. doi: 10.1093/shm/12.1.19
4. Atkinson D. The evolution of medical research writing from 1735 to 1985: the case of the Edinburgh Medical Journal. *Appl Linguist*. (1992) 13:337–74. doi: 10.1093/applin/13.4.337
5. Huang C, Qin S, Cao G, Huang W, Yu Y. Internal maxillary artery-radial artery-middle cerebral artery bypass and STA-MCA bypass for the treatment of complex middle cerebral artery bifurcation aneurysm: a case report. *Front Surg*. (2022) 8:773371. doi: 10.3389/fsurg.2021.773371
6. Perng PS, Lee PH, Hsu HH, Huang CC, Huang CY, Lee JS. Technical case report of a cranioplasty with *ex vivo* frozen ostoblastic bone graft from large skull metastasis. *Front Surg*. (2021) 8:746034. doi: 10.3389/fsurg.2021.746034
7. Peron S, Paulli S, Stefini R. Case report: high-definition 4K-3D exoscope for removal of an orbital cavernous hemangioma using a transpalpebral approach. *Front Surg*. (2021) 8:671423. doi: 10.3389/fsurg.2021.671423
8. Huang C, Qin S, Huang W, Yu Y. Anterior inferior cerebellar aneurysm treated by aneurysm resection and intracranial artery anastomosis *in situ*: a case report and literature review. *Front Surg*. (2021) 8:669433. doi: 10.3389/fsurg.2021.669433
9. Guo X, Popal AM, Zhu Z, Cai C, Lin J, Jiang H, et al. Ventriculosternal shunt for the treatment of idiopathic normal pressure hydrocephalus: a case report. *Front Surg*. (2021) 8:607417. doi: 10.3389/fsurg.2021.607417
10. Shangjun R, Qingyang L, Yilei X, Yiming Z, Lianqun Z, Bin L, et al. Coexistence of pituitary adenoma and primary pituitary lymphoma: a case report and review of the literature. *Front Surg*. (2022) 9:842830. doi: 10.3389/fsurg.2022.842830
11. Yang Y, Shen F, Jing XP, Zhang N, Xu SY, Li DD, et al. Case report: whole-exome sequencing of hypothalamic hamartoma from an infant with pallister-hall syndrome revealed novel *de novo* mutation in the *GLI3*. *Front Surg*. (2021) 8:734757. doi: 10.3389/fsurg.2021.734757
12. Wang S, Xu X, Wang C. Radiological and clinical findings of multiple cerebellar liponeurocytoma: a case report. *Front Surg*. (2021) 8:686892. doi: 10.3389/fsurg.2021.686892
13. Li J, Zan X, Feng M, Deng X, Zhang S, Liu W. Case report: creeping growth in lymphoplasmacyte-rich meningioma-a radiologic variant. *Front Surg*. (2021) 8:775560. doi: 10.3389/fsurg.2021.775560
14. Serratrice N, Faddoul J, Tarabay B, Taifour S, Lahoud GN A. Case report: a rare case of fourth ventricle to spinal subarachnoid space shunt migration: surgical pearl and literature review. *Front Surg*. (2021) 8:696457. doi: 10.3389/fsurg.2021.696457
15. Zhang Y, Zhou M, Wang D, Liu T, Chang P, Zhang J, et al. Case report: a 62-year-old woman with contrast-induced encephalopathy caused by embolization of intracranial aneurysm. *Front Surg*. (2021) 8:689713. doi: 10.3389/fsurg.2021.689713

Conflict of Interest: The authors declare that the research was conducted in the absence of any commercial or financial relationships that could be construed as a potential conflict of interest.

frontiers in Surgery

CASE REPORT
published: 25 May 2021
doi: 10.3389/fsurg.2021.669433

Anterior Inferior Cerebellar Aneurysm Treated by Aneurysm Resection and Intracranial Artery Anastomosis *in situ*: A Case Report and Literature Review

Chaojue Huang†, Shixing Qin*†, Wei Huang** and Yongjia Yu

Department of Neurosurgery, First Affiliated Hospital of Guangxi Medical University, Nanning, China

Background: Anterior inferior cerebellar artery (AICA) aneurysms are relatively rare in clinical practice, accounting for <1% of all intracranial arteries. After the diagnosis and location are confirmed by angiography, magnetic resonance, and other imaging examinations, interventional, or surgical treatment is often used, but some complex aneurysms require reconstructive surgery.

Case Description: An 8-year-old male child was admitted to the hospital due to sudden disturbance of consciousness for 2 weeks. The head CT showed hematocele in the ventricular system with subarachnoid hemorrhage in the basilar cistern and annular cistern. On admission, he was conscious, answered correctly, had a soft neck, limb muscle strength was normal, and had no cranial nerves or nervous system abnormalities. A preoperative examination showed the right side of the anterior distal arteries class under the circular wide neck aneurysm, the distal anterior inferior cerebellar artery supplying a wide range of blood to the cerebellum, the ipsilateral posterior inferior cerebellar artery absent, and the aneurysm close to the VII, VIII nerves. The aneurysm was successfully treated by aneurysm resection and intracranial artery anastomosis *in situ* of a2 AICA-a2 AICA.

Conclusions: AICA aneurysms are relatively rare; in this case, a complex wide-necked aneurysm was successfully treated by aneurysm resection and anastomosis *in situ* of a2 AICA-a2 AICA. This case can provide a reference for the surgical treatment of complex anterior cerebellar aneurysms.

Keywords: aneurysms, complex aneurysms, anterior inferior cerebellar aneurysm, aneurysm resection, arterial anastomosis *in situ*

OPEN ACCESS

Edited by:
Michael Sughrue, University of New South Wales, Australia

Reviewed by:
Hiroki Toda, Kitano Hospital, Japan
Jorge Marcelo Mura, Instituto de Neurocirugía, Chile

***Correspondence:**
Wei Huang
13977166636@126.com
Chaojue Huang
310046542@qq.com

†These authors have contributed equally to this work

Specialty section:
This article was submitted to Neurosurgery, a section of the journal Frontiers in Surgery

Received: *18 February 2021*
Accepted: *13 April 2021*
Published: *25 May 2021*

Citation:
Huang C, Qin S, Huang W and Yu Y (2021) Anterior Inferior Cerebellar Aneurysm Treated by Aneurysm Resection and Intracranial Artery Anastomosis in situ: A Case Report and Literature Review. Front. Surg. 8:669433. doi: 10.3389/fsurg.2021.669433

HIGHLIGHTS

- In the treatment of complex aneurysms, bypass reconstruction can effectively ensure the patency of the distal posterior circulation artery and avoid cerebral infarction.
- *In situ* anastomosis technology has good matching of vascular diameter and wall and high expected patency rate, and its patency can be effectively verified by intraoperative fluorescence contrast and ultrasound Doppler.

- It can provide reference for the surgical treatment of complex anterior cerebellar small aneurysms.

INTRODUCTION

Anterior inferior cerebellar artery (AICA) aneurysms are rare clinically, accounting for <1% of all intracranial artery aneurysm. After the diagnosis and location are confirmed by angiography, magnetic resonance, and other imaging examinations, aneurysms are usually treated with intervention embolization or surgery (1–3). However, under the different anatomical locations and morphology of an AICA aneurysm, what kind of treatment is the most effective? There is still no unified conclusion. We report a case of a complex AICA aneurysm. The patient was admitted due to sudden disturbance of consciousness 2 weeks earlier. Physical examination on admission: clear, accurate answers; soft neck; normal muscle strength of limbs; no abnormality in cranial nerve and nervous system examination. CT showed that the ventricular system had hematocele, accompanied by subarachnoid hemorrhage in the basal cistern and annular cistern. Digital subtraction angiography revealed a circular wide-necked aneurysm of the distal AICA with an aneurysm size of about 5.2*4.8 mm. The aneurysm was isolated and resected; intracranial anastomosis *in situ* of a2 AICA-a2 AICA was performed. As far as we know, reports of similar cases are rare. Combined with the patient's clinical characteristics, surgical techniques, results, and literature review, the report is as follows:

CASE DESCRIPTION

The patient, an 8-year-old male, was admitted December 4, 2020, due to sudden disturbance of consciousness 2 weeks earlier. The patient had a sudden headache and consciousness disturbance 2 weeks earlier, and the head CT showed that the ventricular system had hematocele, accompanied by subarachnoid hemorrhage in the basal cistern and annular cistern. The patient was conscious after symptomatic treatment and then transferred to our hospital for further diagnosis and treatment. Physical examination on admission: clear, accurate answers, soft neck, normal muscle strength of limbs, no abnormality in cranial nerve, and nervous system examination. Digital subtraction angiography revealed a circular wide-necked aneurysm of the distal AICA with an aneurysm size of about 5.2*4.8 mm. The distal AICA supplied a wide range of blood, and the ipsilateral posterior inferior cerebellar artery was absent as shown in **Figures 1A–C**. Magnetic resonance imaging (MRI) shows that the aneurysm was located lateral to the internal auditory canal (IAC), near the VII, VIII nerves. The right AICA was diagnosed, Hunt–Hess class I.

Craniotomy of the aneurysm by retrosigmoid approach and anastomosis of the AICA was performed under general anesthesia. Intraoperatively, the aneurysm was found to be located in the middle segment of the right AICA, between the facial auditory nerve and the posterior cranial nerve. The aneurysm was closely adhered to the surrounding arachnoid with a wide neck and unclear boundary between the neck and the parent artery (**Figure 3A**). It is estimated that simple clamping is difficult to ensure patency of the parent artery, so we decided to separate the aneurysm from the surrounding adhesion carefully and remove it and part of the parent artery. After dissociating the proximal and distal vessels of the AICA, end-to-end intracranial vascular anastomosis of a2 AICA-a2 AICA was performed *in situ* (the schematic diagram of the operation is shown in **Figure 2**), and intraoperative fluorescence angiography was performed to confirm the patency of the anastomotic vessels (**Figures 3B,C**). The patient recovered well after the operation with no facial paralysis, hoarseness, or dysphagia, and limb muscle strength is normal with no ataxia. Cerebrovascular angiography before discharge indicated that the aneurysm disappeared, the distal and proximal ends of the AICA had patency, and the blood supply range was the same as before operation (**Figures 1D–F**).

DISCUSSION

AICA aneurysms are relatively rare, and the treatment reports of each center are mainly individual cases and small case series. The total number of aneurysms of the AICA reported by major neurosurgery centers in China accounts for about 0.15–0.3% (1, 2, 4). Symptomatic rupture of the AICA aneurysm is mainly associated with subarachnoid hemorrhage. Some patients show symptoms of mass effect in the cerebellar pontine angle, such as hearing loss, facial paralysis, hoarseness, dysphagia, dizziness, etc., which is related to the location of the aneurysm. Preoperative imaging, the thin layer of magnetic resonance, the bone of the skull base combination CTA reconstruction can effectively locate the aneurysm. AICA aneurysms can be cured by interventional embolization, craniotomy clipping, isolation, and other methods, and the overall effect is satisfied (3, 5–8). A few complex aneurysms require vascular reconstruction (9) and artery anastomosis of the occipital artery. Anterior inferior cerebellar is more common.

According to the relationship between different segments of AICA and the IAC, aneurysm of the AICA can be divided into anterior, internal, and posterior segments of IAC (2). According to the AICA and cerebellar pontine angle region nerve anatomical position relationship, it can be divided into the a1: anterior pontine segments, a2: lateral pontine segments, a3: flocculopeduncular segments, and a4: cortical segments (5, 10). a2 gives rise to the labyrinthine, recurrent perforating, and subarcuate arteries (9). As the a1 segment is deep, and the a4 segment has tiny vessels, a2 and a3 segments can make full use of the space in the CPA region, and the vessels are usually curled and of moderate diameter. They are often used as ideal bypass vessels (9, 11).

When the aneurysm is located in the anterior or internal segment of the IAC, namely segment a1 or a2, interventional embolization is the primary choice of treatment due to the difficulty of anatomical exposure. However, in the case of the tiny AICA, it is difficult to completely ensure the patency of the parent artery during interventional embolization of a complex wide-necked aneurysm, and some patients need to occlude the parent artery (5, 12). Due to the existence of potential

Abbreviations: CT, computed tomography; DSA, digital subtraction angiography; MRI, Magnetic resonance imaging; AICA: Anterior Inferior Cerebellar Artery; IAC: internal auditory canal; PICA: posterior inferior cerebellar artery; SCA: superior cerebellar artery; IAA: internal auditory artery; OA: occipital artery.

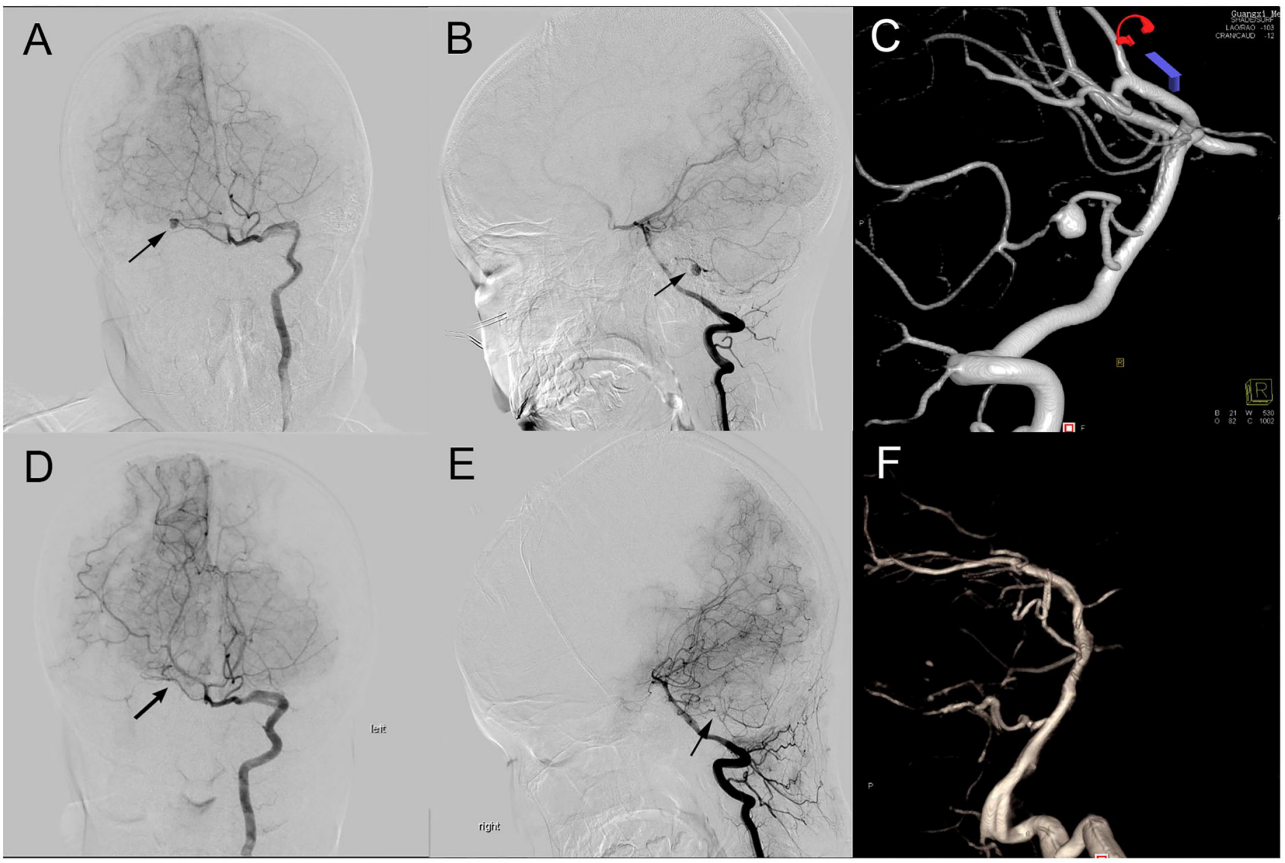

FIGURE 1 | Preoperative and postoperative DSA comparison. **(A–C)**: Preoperative DSA (A, A-P view; B, lateral view) showing an aneurysm (black arrow) located at main trunk of the right AICA; **(D–F)**: Preoperative DSA (D, A-P view; E, lateral view) showing the aneurysm disappeared and the distal AICA patency.

perforating arteries, occluding the AICA may lead to facial paralysis, dysphagia, water choking, occipital lobe infarction, binocular hemianopia, etc. (2).

When the aneurysm is located in the posterior segments of IAC, namely segment a3 or a4, application of a retrosigmoid sinus approach can obtain effective surgical anatomy of the exposure; previous literature has reported that the clipping effect is good (1, 4, 13). However, there are also some cases due to the aneurysm shape being broad neck or fusiform, which are difficult to clip. Once the parent artery is narrowed or the aneurysm has a residual neck after clipping, it leads to an increased risk of rebleeding, and these cases can only choose the aneurysm isolation technique. However, when the ipsilateral PICA and SCA is hypoplasia or tiny, when AICA is the mutation of PICA, or when you cannot be sure that variations in the course of the internal auditory artery (IAA) arise from the distal AICA, pure isolated aneurysm or occlusion of the anterior artery can produce a wide range of cerebral infarction and severe neurological dysfunction.

Therefore, for these complex AICAs, the application of the bypass vessel reconstruction technique is an effective strategy to preserve the distal vessel patency and avoid cerebral infarction. This paper reviews and summarizes previous literature reports on vascular reconstruction for complex AICA aneurysms, and most of them achieve good efficacy as shown in **Table 1**. Pasler et al. (16) and Baranoski et al. (9), respectively, report one case of complex AICA resection by the retrosigmoid sinus approach, followed by end-to-end anastomosis of AICA *in situ*, which effectively avoided postoperative cerebral infarction. Baranoski et al. (9) and Lee et al. (11) also, respectively, report that the p3 segment of PICA was anastomotic with the a3 segment of AICA to isolate proximal aneurysms of AICA and effectively avoid cerebral infarction. No matter which type of vascular reconstruction, this requires the surgeon to be proficient in deep vascular anastomosis. Comparatively, on the one hand, the distal anastomosis between the OA and AICA is superficial but usually requires the application of an incision flap similar to the distal lateral approach. Besides this, there is a risk that the diameter and wall of bypass vessels will not match very well, which affects the anastomosis effect. On the other hand, the anastomosis of PICA-AICA must first be anatomically similar to the branch vessels, and the additional intraoperative risk of blocking PICA may lead to more extensive cerebral infarction after surgery. Compared with the above two vascular reconstruction techniques, end-to-end anastomosis of AICA *in situ* for craniotomy using a retrosigmoid sinus approach can achieve good matching of vascular diameter and wall of bypass vessels, recovery of original hemodynamics, closer to natural anatomy, and high expected patency rate.

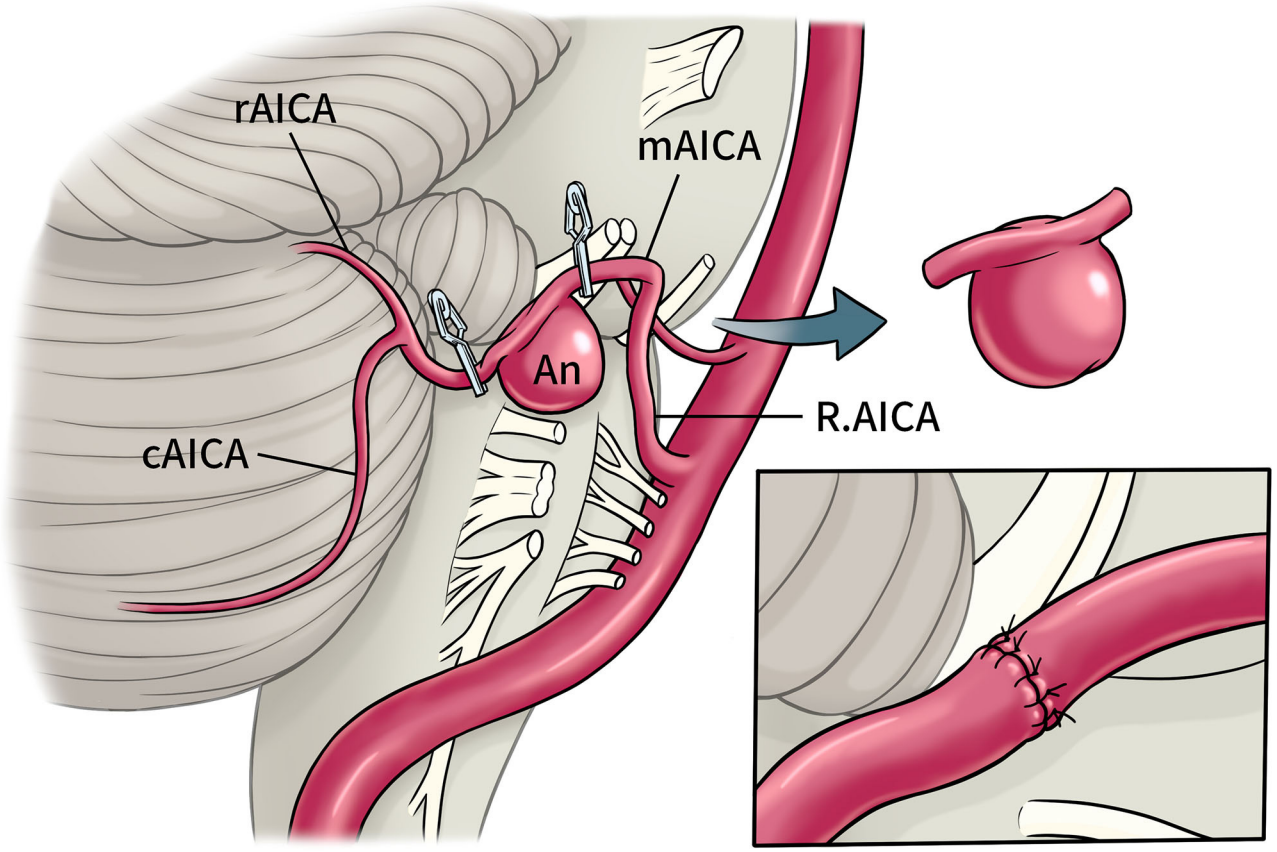

FIGURE 2 | Schematic diagram of operation. Right AICA aneurysm located in a2 segments, intracranial artery anastomosis *in situ* was perform after trapping and resection. (cAICA, caudal trunk of AICA; mAICA, main trunk of AICA; rAICA, rostral trunk of AICA; a2, lateral pontine segments of AICA).

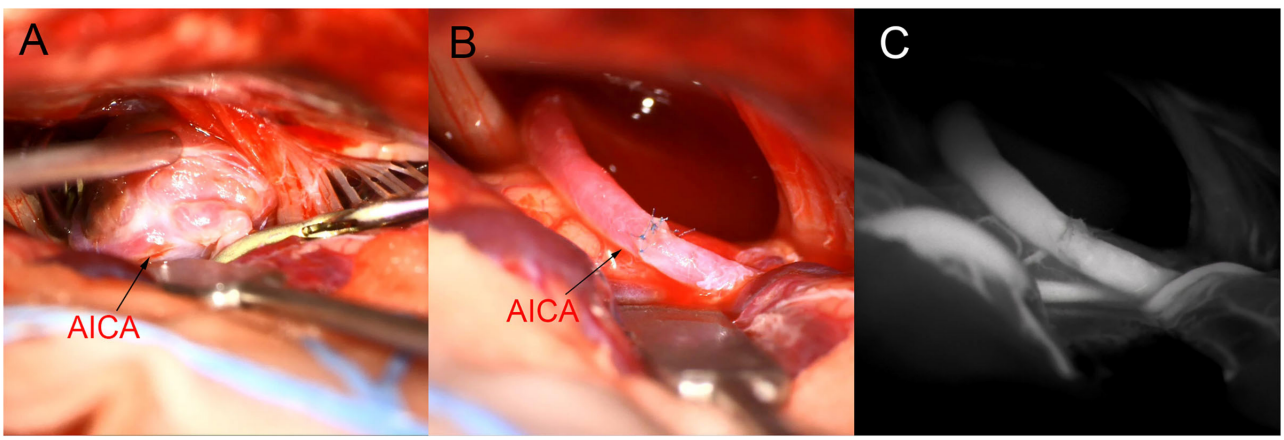

FIGURE 3 | Intraoperative image. **(A)**: Aneurysm neck and parent artery were not clearly defined. **(B,C)**: a2AICA-a2AICA anastomosis *in situ* after aneurysm resection, intraoperative fluorescence imaging confirmed patency.

CONCLUSIONS

In this case, preoperative angiography suggested that the right PICA was absent, and the blood supply range of the right AICA was extensive. If aneurysm isolation was performed alone, the risk of postoperative cerebellar and brainstem infarction was high. Therefore, the aneurysm was treated by excision of the aneurysm and anastomosis *in situ* of AICA. Intraoperative fluorescence angiography and Doppler imaging confirmed that the vessel patency. Postoperative angiography also indicated that

TABLE 1 | Literature review of AICA aneurysms treated by vascular reconstruction.

No.	Year	Author	Age/sex	Onset	Primary	Location	Size (mm)	Types	Operation	Outcome
1	2009	Fukushima et al. (14)	15/F	N/A	Yes	a2	14*10.8	Dissecting	OA-AICA bypass	DSA not prompt vascular patency, then interventional embolism aneurysms
2	2010	Oyama et al. (15)	65/F	ICH	Yes	a2	N/A	Fusiform	OA-AICA bypass+trapping+thrombectomy	Legacy swallowing dysfunction, left limbs hemiplegia and gait disorder
3	2011	Päsler et al. (16)	22/M	N/A	Yes	a2	N/A	Globular	Excising the aneurysmal segment, reanastomosis: a2 AICA-a2 AICA	Hearing impairment and headache recurrence 1 year later, MR indicate vascular patency
4	2012	Fujimura et al. (17)	77/F	SAH	Yes	a2, cAICA	N/A	Fusiform	OA-AICA bypass+trapping	Hearing impairment, no infarction, DSA prompt patency.
5	2016	Kanamori et al. (18)	62/M	SAH	Yes	a3, AICA-PICA variant	13	Saccular	OA-AICA bypass+trapping	Right hemiplegia improved, but right abducens nerve palsy did not improve, DSA prompt patency
6	2018	Lee et al. (11)	59/M	N/A	Yes	a2, cAICA	7	Irregular	*In situ* bypass: p3PICA-a3AICA, trapping+thrombectomy	Without neurologic deficits after 6 weeks follow-up, DSA prompt patency
7	2018	Umekawa et al. (19)	78/M	N/A	No	a2, mAICA	5.6	pseudo	OA-AICA bypass+trapping	DSA prompt patency, mRS = 1
8	2020	Hou et al. (20)	53/F	SAH	Yes	a2, cAICA	N/A	dissecting	Excising the aneurysmal, *In situ* suturing: a2AICA-a2AICA	The mild facial paralysis on the right side improved, DSA prompt patency 9 months later
9	2020	Baranoski et al. (9)	75/F	N/A	Yes	a1, mAICA	N/A	fusiform	*In situ* bypass: p3PICA-a3AICA, trapping+thrombectomy	Symptoms improved, after 6 months later, mRS = 0
10	2020	Baranoski et al. (9)	51/F	SAH	No	a2, mAICA	N/A	fusiform	Excising the aneurysmal segment, reanastomosis: a2 AICA-a2 AICA	Recover well, after 1 year follow-up, mRS = 1

AICA, anterior inferior cerebellar artery; PICA, posterior inferior cerebellar artery; F, female; M, male; mRS, modified Rankin Scale; N/A, not available; OA, occipital artery; SAH, subarachnoid hemorrhage; cAICA, caudal trunk of AICA; mAICA, main trunk of AICA; rAICA, rostral trunk of AICA; a2, lateral pontine segments of AICA; a3, flocculopeduncular segments of AICA; p3, tonsillomedullary segments of PICA.

anastomosis patency, and the blood supply range of the anterior cerebellar artery was the same as before. There are few reports on the application of vascular reconstruction in the treatment of AICA aneurysms. This case can provide a reference for the surgical treatment of complex AICA aneurysms.

DATA AVAILABILITY STATEMENT

The original contributions presented in the study are included in the article/supplementary material, further inquiries can be directed to the corresponding author/s.

AUTHOR CONTRIBUTIONS

CH and WH: conceptualization and study design. CH and SQ: data collection, literature research, and manuscript drafting. WH and YY: revision. CH: funding. All authors contributed to the article and approved the submitted version.

FUNDING

This work was supported by Guangxi Medical and Health Key Scientific Research Project (No. Z20190610).

REFERENCES

1. Li X, Zhang D, Zhao J. Anterior inferior cerebellar artery aneurysms: six cases and a review of the literature. *Neurosurg Rev.* (2012) 35:111–9. doi: 10.1007/s10143-011-0338-1
2. Kai-ming G, Xiao-guang T. Surgical treatment for ruptured anterior inferior cerebellar artery aneurysms. *Chin J Contemp Neurol Neurosurg.* (2013) 13:201–10. doi: 10.3969/j.issn.1672-6731.2013.03.009
3. Anil G, Sein L, Nga V, Teo K, Chou N, Yeo TT. Dissecting distal cerebellar artery aneurysms: options beyond a parent vessel sacrifice. *Neurosurg Rev.* (2019) 43:771–80. doi: 10.1007/s10143-019-01119-y
4. Xin C, Hao W, Peng-Jun J, Yu-Ming J, Yong C, You-Xiang L, et al. Clinical analysis of 11 cases of anterior inferior cerebellar artery aneurysms. *Chin J Stroke.* (2020) 15:631–6. doi: 10.3969/j.issn.1673-5765.2020.06.011
5. Rodríguez-Hernández A, Zador Z, Rodríguez-Mena R, Lawton MT. Distal aneurysms of intracranial arteries: application of numerical nomenclature, predilection for cerebellar arteries, and results of surgical management. *World Neurosurgery.* (2013) 80:103–12. doi: 10.1016/j.wneu.2012.09.010
6. Tokimura H, Ishigami T, Yamahata H, Yonezawa H, Yokoyama S, Haruzono A, et al. Clinical presentation and treatment of distal anterior inferior cerebellar artery aneurysms. *Neurosurg Rev.* (2012) 35:497–503. doi: 10.1007/s10143-012-0390-5

7. Lv X, Ge H, He H, Jiang C, Li Y. Anterior inferior cerebellar artery aneurysms: segments and results of surgical and endovascular managements. *Interv Neuroradiol.* (2016) 22:643–8. doi: 10.1177/1591019916656474
8. Khayat HA, Alshareef F, Alshamy A, Algain A, Alhejaili E, Alnabihi O, et al. Pure endovascular management of an arteriovenous malformation and an aneurysm both supplied by anterio-inferior cerebellar artery: a case report and a review of literature. *Front Neurol.* (2017) 8:382. doi: 10.3389/fneur.2017.00382
9. Baranoski JF, Przybylowski CJ, Mascitelli JR, Lang MJ, Lawton MT. anterior inferior cerebellar artery bypasses: the 7-bypass framework applied to ischemia and aneurysms in the cerebellopontine angle. *Operat Neurosurg.* (2020) 19:165–74. doi: 10.1093/ons/opz347
10. Rodríguez-Hernández A, Rhoton AL Jr, Lawton MT. Segmental anatomy of cerebellar arteries: a proposed nomenclature. laboratory investigation. *J Neurosurg.* (2011) 115:387–97. doi: 10.3171/2011.3.JNS101413
11. Lee BS, Witek AM, Moore NZ, Bain MD. Treatment of an anterior inferior cerebellar artery aneurysm with microsurgical trapping and *in situ* posterior inferior cerebellar artery to anterior inferior cerebellar artery bypass: case report. *Operat Neurosurg.* (2018) 15:418–24. doi: 10.1093/ons/opx275
12. Hou K, Li G, Xu B, Xu K, Yu J. Which patients with aneurysms involving the a1-a2 segment of the anterior inferior cerebellar artery would benefit from parent artery occlusion? *World Neurosurgery.* (2019) 126:301–9. doi: 10.1016/j.wneu.2019.03.070
13. Bambakidis NC, Manjila S, Dashti S, Tarr R, Megerian CA. Management of anterior inferior cerebellar artery aneurysms: an illustrative case and review of literature. *Neurosurg Focus.* (2009) 26:E6. doi: 10.3171/2009.1.FOCUS0915
14. Fukushima S, Hirohata M, Okamoto Y, Yamashita S, Ishida S, Shigemori M. Anterior inferior cerebellar artery dissecting aneurysm in a juvenile: case report. *Neurol Med Chir.* (2009) 49:81–4. doi: 10.2176/nmc.49.81
15. Oyama H, Kito A, Maki H, Hattori K, Tanahashi K. Compression of the medulla oblongata and acute respiratory failure caused by rupture of a thrombosed large aneurysm of the anterior inferior cerebellar artery. *Neurol Med Chir.* (2010) 50:571–3. doi: 10.2176/nmc.50.571
16. Päsler D, Baldauf J, Runge U, Schroeder HW. Intrameatal thrombosed anterior inferior cerebellar artery aneurysm mimicking a vestibular schwannoma. *J Neurosurg.* (2011) 114:1057–60. doi: 10.3171/2010.9.JNS10491
17. Fujimura M, Inoue T, Shimizu H, Tominaga T. Occipital artery-anterior inferior cerebellar artery bypass with microsurgical trapping for exclusively intra-meatal anterior inferior cerebellar artery aneurysm manifesting as subarachnoid hemorrhage. case report. *Neurol Med Chir.* (2012) 52:435–8. doi: 10.2176/nmc.52.435
18. Kanamori F, Kawabata T, Muraoka S, Kojima T, Watanabe T, Hatano N, et al. Ruptured partially thrombosed anterior inferior cerebellar artery aneurysms: two case reports and review of literature. *Nagoya J Med Sci.* (2016) 78:517–22. doi: 10.18999/nagjms.78.4.517
19. Umekawa M, Hasegawa H, Shin M, Kawashima M, Nomura S, Nakatomi H, et al. Radiosurgery-induced anterior inferior cerebellar artery pseudoaneurysm treated with trapping and bypass. *World Neurosurg.* (2018) 116:209–13. doi: 10.1016/j.wneu.2018.04.161
20. Hou K, Xu K, Guo Y, Yu J. *In situ* suturing of a post-meatal segment of the anterior inferior cerebellar artery dissected by an aneurysm: a technical note. *Neuroradiol J.* (2020) 34:49–52. doi: 10.1177/1971400920964717

Conflict of Interest: The authors declare that the research was conducted in the absence of any commercial or financial relationships that could be construed as a potential conflict of interest.

frontiers in Surgery

CASE REPORT
published: 07 July 2021
doi: 10.3389/fsurg.2021.686892

Radiological and Clinical Findings of Multiple Cerebellar Liponeurocytoma: A Case Report

*Shan Wang, Xiaopei Xu and Chao Wang**

Department of Radiology, The Second Affiliated Hospital, Zhejiang University School of Medicine, Hangzhou, China

Background: Cerebellar liponeurocytoma is an extremely rare benign tumor which generally occurs in cerebellum and is almost always solitary. Multifocal cerebellar liponeurocytoma is exceedingly rare, only 8 cases has been reported so far. Herein we present the 9th case of multifocal cerebellar liponeurocytoma in a 70-year-old woman with the complete clinical course and comprehensive imaging findings.

Case Presentation: A 70-year-old woman presented with a history of intermittent headache for 5 years. Computed tomography (CT) and magnetic resonance imaging (MRI) of the brain have been performed and suggested a diagnosis of teratoma based on the imaging findings. After the surgical resection of the lesion, histopathological and immunohistochemical analyses revealed neuronal, glial, and lipomatous components and confirmed the diagnosis of multifocal cerebellar liponeurocytoma after surgical resection. During the 2-year follow-up period, the patient showed no signs of recurrence or metastasis.

Conclusion: We described the radiological characteristics and clinical course of an exceedingly rare case of multifocal cerebellar liponeurocytoma in the cerebellar vermis and temporal lobe. The clear multifocality makes this case unusual.

Keywords: brain tumor, computed tomography, magnetic resonance imaging, liponeurocytoma, cerebellum

OPEN ACCESS

Edited by:
Chenlong Yang, Center for Precision Neurosurgery and Oncology of Peking University Health Science Center, China

Reviewed by:
Aldo Spallone, Peoples' Friendship University of Russia, Russia
Hiroaki Matsumoto, Yoshida Hospital, Japan

****Correspondence:***
Chao Wang
2514110@zju.edu.cn

Specialty section:
This article was submitted to Neurosurgery, a section of the journal Frontiers in Surgery

Received: *28 March 2021*
Accepted: *09 June 2021*
Published: *07 July 2021*

Citation:
Wang S, Xu X and Wang C (2021) Radiological and Clinical Findings of Multiple Cerebellar Liponeurocytoma: A Case Report. Front. Surg. 8:686892. doi: 10.3389/fsurg.2021.686892

INTRODUCTION

Cerebellar liponeurocytoma (CLN), which was first described in 1978 by Bechtel et al. (1), is classified as a WHO grade II tumor and is now considered as a clinicopathologic entity distinct from medulloblastoma. The major symptoms of the disease include headache, vomiting, gait disturbance, dysphonia, or cerebellar signs depending on the tumor location, and progressive visual symptoms are common in the later stages of the disease (2) due to raised intra-cranial pressure. Complete tumor resection is usually the cornerstone of management of CLN. In previous reports, CLN is almost always solitary and located in the cerebellum. This makes the presence of multifocal CLN an unusual condition, thus adds to the challenges in the diagnosis and management of the disease due to limited knowledge of the biological behaviors and clinical features. So far, only eight cases of multifocal have been reported and herein we report the 9th case of multifocal CLN in both cerebellar vermis and left temporal lobe. Details of the radiological characteristics and complete clinical course are provided and a review of the pertinent literatures is also given.

CASE PRESENTATION

Clinical History

A 70-year-old woman presented with unsteady walk without any obvious inducement in June 2018. She also described a history of occasionally falls, memory loss, hearing and vision loss, nausea, and vomiting for 3 months. In her previous medical history, she had intermittent headache and dizziness for 5 years. Neurological examinations at admission were unremarkable. An elevated level of neuron-specific enolase (NSE, 37.6 ng/ml) was found. Blood pressure, pulse, temperature, routine laboratory tests (complete blood count, liver function, renal function, and C-reactive protein) and other serum tumor markers were within normal ranges, including carbohydrate antigen 242 (CA242, 3.3 ng/ml), carbohydrate antigen 125 (CA125, <1 U/ml), carbohydrate antigen 153 (CA242, <0.5 U/ml), carbohydrate antigen 199 (CA199, 2.0 U/ml), alpha-fetoprotein serum (0.0 ng/ml), carcinoembryonic antigen (0.5 ng/ml), and β-human choriogonadotropin (2.6 U/L).

Radiological Findings

Computed tomography (CT) and contrast-enhanced magnetic resonance imaging (MRI) were performed in June 2018. CT revealed a large heterogeneous mass (5 cm * 3.4 cm) in the temporal lobe with curvilinear calcification (**Figure 1A**), and a small hypodense lesion (3.6 * 2.8 * 3 cm) in the cerebellar vermis with predominantly fatty density and ill-defined margin caused compression of ambient cisterns. The bone window showed the mild compression of perilesional cranial bones (**Figure 1B**). MRI revealed two lesions in the cerebellar vermis and left temporal lobe. The lesions were hyperintense on T1-weighted images (WI) (**Figure 1C**) and iso-to hyperintense on T2WI (**Figure 1D**), indicating the lipomatous component of the lesion. Gadolinium-enhanced T1WI revealed obvious heterogeneous enhancement, particularly in the cerebellar vermis (**Figure 1E**). The cerebellar lesion extended through the tentorium cerebelli and caused obstructive hydrocephalus (**Figure 1F**). After reviewing patient's previous medical records, a brain MRI was performed in October 2013 revealed two lesions in the cerebellar vermis and left temporal lobe. Back then, the cerebellar lesion was relatively small (6.4 * 4.3 * 4.6 cm) (**Figure 1G**) without any sign of obstructive hydrocephalus (**Figure 1H**). Judging from the radiological appearance and the benign nature of the disease, a diagnosis of teratoma was made, and vigilantly monitoring without interventions was recommended then.

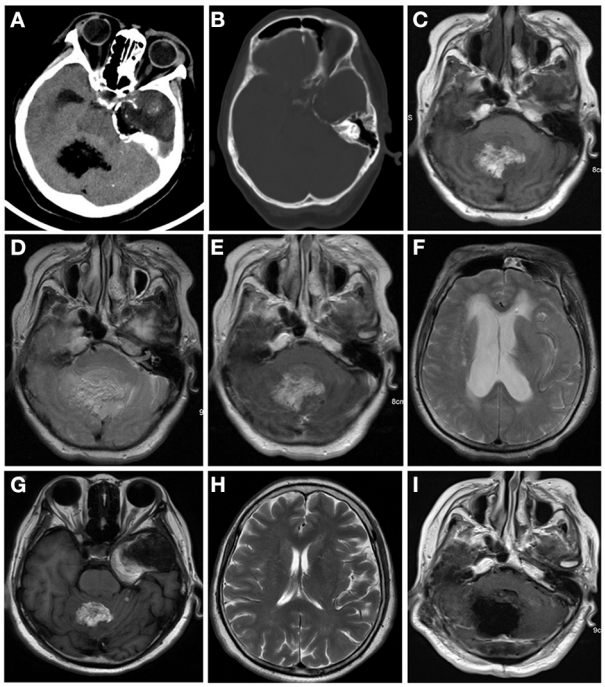

FIGURE 1 | Computed tomography (CT) and contrast-enhanced magnetic resonance imaging (MRI) were performed in June 2018 **(A–E)**. CT images of brain window images demonstrated a well-demarcated mass with fat density in the left temporal lobe and cerebellar vermis with calcification **(A,B)**. MRI revealed a hyper- and isointense mixed mass on T1-weighted image **(C)** and iso- and hyperintense mixed mass on T2-weighted image **(D)**. Gadolinium-enhanced T1-weighted image showed heterogeneous enhancement **(E)**. The lesion in the cerebellum compressed the fourth ventricle **(E)** and caused supratentorial obstructive hydrocephalus **(F)**. In 2013, the cerebellum lesion was relatively small **(G)** and did not cause obstructive hydrocephalus **(H)**. Postoperative MRI indicated the cerebellar mass was near-totally removed **(I)**.

Intra-Operative Findings and Pathological Examination Results

Due to the unbearable headache caused by obstructive hydrocephalus, midline suboccipital craniotomy, and near-total excision of the cerebellar mass was performed, and the left temporal lobe lesions was left untreated since it is asymptomatic at time. On intraoperative examination, we observed a grayish cerebellar tumor with firm consistency, and abundant blood supply, that was not well-demarcated from the surrounding tissue. Microscopic examination showed a glioneuronal tumor with dense and diverse tumor cells, accompanied by extensive vascular hyperplasia, and papillary structures along with scattered adipose tissue and lymphatic structures in excised tumor mass (**Figures 2A,B**). Generally, the tumor cells had a low cell proliferation index and expressed glial and neuronal markers. Immunohistochemical staining showed the tumor cells had a positive expression for NeuN (**Figure 2C**), GFAP (**Figure 2D**), CD56, ATRX, Olig-2, and negative expression for CD45 (LCA), CD20, EMA. The Ki-67 proliferation index was low (5–10%) in tumor cells (**Figure 2E**). Although, the confirmed diagnosis of temporal lobe tumor was not obtained, it was considered to be liponeurocytoma because of its similar imaging features to the cerebellar mass.

Postoperative Course

The patient was discharged 12 days after the surgery. Postoperative MRI indicated the cerebellar mass was removed near-total (**Figure 1I**). The temporal lobe mass was as usual. During the 2-years follow-up period, the patient had no signs of recurrence or metastasis.

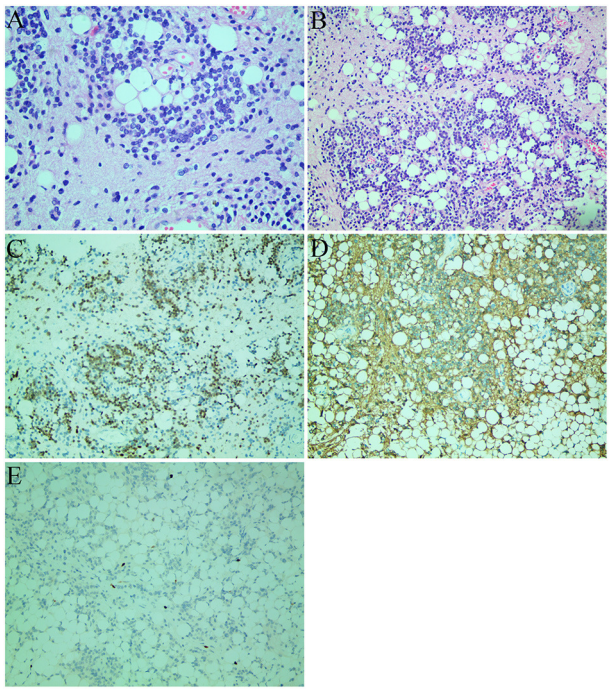

FIGURE 2 | Histological images **(A,B)** and immunohistochemical staining images **(C–E)**. **(A)** The tumor consisted of uniform round cells with small, round, or oval nuclei with finely speckled chromatin and large lipid vacuoles (hematoxylin and eosin staining; original magnification: ×400). **(B)** The tumor cells were accompanied by a large number of vascular hyperplasia and papillary structure. There were scattered adipose tissue and lymphatic structures in the tumor (hematoxylin and eosin staining; original magnification: ×200). **(C)** Strong NeuN immunopositivity of neoplastic cells. **(D)** GFAP-positive component and immunonegative neurocytic fields. **(E)** The Ki-67 proliferation index was 5–10%.

DISCUSSION

The first case of CLN was reported by Bechtel et al. in 1978 (1). CLN is a rare neoplasm of the central nervous system with low proliferative potential. The WHO listed CLN as an independent entity in 2000 and later 2007, WHO categorized CLN as a grade II tumor (3). Although, it is named as CLN, it also occurs in supratentorial regions such as intracranial ventricles and temporal lobe (4). When it appears in the cerebellum, the clinical symptoms are usually related to intracranial hypertension and cerebellar neurological deficit (3). Patients with CLN commonly present between the third and fifth decades of life (5) and there is no gender predominance (6). Familial cases have also been reported with possible autosomal dominant inheritance (7).

CLN is composed of cells with neuronal differentiation and focal lipomatosis (8). The histopathological hallmarks are cellular tumor arranged in lobular aggregates with hyperchromatic nuclei and clear cytoplasm. In addition, CLN has other features such as brisk mitotic activity, microvascular proliferation, and foci of calcification. On immunohistochemistry analyses, CLN was positive for early and mature neuronal markers such as glial fibrillary acidic protein (GFAP), NSE, and synaptophysin. The MIB-1 labeling index tumor may elevated in some cases (9).

Our patient presented with multifocal lesions involving both temporal lobe and cerebellar vermis. Only eight cases with multifocal lesions have been previously reported. In 1997, the first case of multifocal CLNs in a 44-year-old man was reported by Horoupian et al. (10) Subsequently, seven similar cases were reported. Details of these cases are summarized in **Table 1**. Of the nine cases in **Table 1**, seven CLNs (77.8%) occurred in the cerebellum, and four CLNs (44.4%) occurred in the intracranial ventricles/cisterns. Almost all patients had headaches. Four patients (44.4%) had vomiting caused by intracranial hypertension. Among seven patients with follow-up records in **Table 1**, only one case (1/7, 14.2%) had recurrence. Seven out of nine cases had gone through complete surgical removal. Based on Khatri et al.'s report (17), surgical resection of the larger lesion was performed amid multiple lesions when the larger lesion was responsible for the clinical symptoms. The smaller lesions were usually left untreated and monitored regularly by CT/MRI. In 4 out of 9 cases, radiotherapy was performed yet the role of the treatment has not been well-defined.

In our case, the relative small lesion in the cerebellum increased slowly in size and showed an aggressive feature during the 5-years follow-up period. Jenkinson et al. (18) reported a similar invasive case, emphasizing that the behavior of these tumors might be less predictable than previously thought. Long-term follow-up and further investigation of future cases is certainly necessary for a better understanding of the nature of these neoplasms.

Cerebellar hemisphere is the most common site, while fourth ventricle is the second common site for CLN. The fat composition was observed within the tumor in all cases. Calcification and hemorrhage were observed in one case, while cystic changes were found in five cases. CLN was typically isointense or hyperintense on T1WI. On T2WI and fluid-attenuated inversion recovery (FLAIR) images, the tumor was hyperintense. Heterogeneous contrast enhancement was found in nearly all cases. Edema in surrounding tissue was rare. On CT, the tumor was variably iso-to hypodense (compared to brain parenchyma) with focal areas of marked hypoattenuation corresponding to fat component (19). The key imaging feature was the fat density or signal inside the mass (20). The lesion was typically isointense/hypointense on T1WI and hyperintense on T2WI; high signal (fat signal) can be found on T1WI and T2WI/FLAIR in some areas of the mass. Sometimes edema was found around the mass on T2WI. Calcification was occasionally seen. On the contrast-enhanced scan, the mass commonly showed heterogeneous enhancement. CLN might show space-occupying effect and compress the adjacent structure. In our case, the smaller lesion compressed the fourth ventricle and caused obstructive hydrocephalus. Few tumors showed invasive nature.

Differential diagnosis of CLN includes medulloblastoma and intracranial teratoma. Medulloblastoma usually presents at younger age (<20 years old) with CT showing a slightly hyperintense lesion in the fourth ventricle. Cystic changes and calcification are commonly seen in tumors. The lesion is usually isointense or hypointense on T1WI, while hyperintense on T2WI

TABLE 1 | Summary of previously reported cases of multiple cerebellar liponeurocytoma.

Authors, year (ref)	Age(years)/sex	Location	Symptoms	Surgery	Adjuvant therapy	Follow-up (months)	Tumor recurrence	Recurrence/growth after (months)
Horoupian et al. 1997 (10)	44/M	The right lateral ventricle, the fourth ventricle	Dizziness, nausea and vomiting, episodic headaches	A transcallosal resection of the tumor arising from the septum pellucidum	3,900 cGy RT	36	No	No
Aker et al. 2005 (11)	49/F	The vermis, the fourth ventricle	Hypertension, vertigo and vomiting and progressive vision and gait disturbances	Microscopic subtotal tumor resection	36 Gy/20 WBRT	19	nm	nm
Pelz et al. 2013 (12)	54/F	The fourth ventricle, in the lateral right cerebellar hemisphere	Headaches and upper neck pain	Yes	No	24	Yes	Residual tumor 24 months after surgery after first surgery, 24 months after second surgery
Scoppetta et al. 2015 (13)	42/M	Peripheral cerebellar	Headache	No	No	nm	nm	nm
Dhar et al. 2015 (14)	49/F	Left cerebellopontine angle, cerebellar hemisphere	Headache accompanied by recurrent episodes of vomiting	Left retro-mastoid sub occipital craniotomy	No	nm	nm	nm
Konovalov et al. 2015 (15)	42/M	The head of the brain and all the vertebrae	Neck pain and bad arm feeling	Yes	RT	36	No	No
Sivaraju et al. 2017 (16)	37/M	The left side of the cerebellar vermis, the cerebellar hemispheres	Headache, vomiting, and gait disturbance	No	60 Gy WBRT	24	No	No
Khatri et al. 2018 (17)	36/F	The left cerebellar hemisphere, the right cerebellar hemisphere	Headache and difficulty in walking	Left paramedian suboccipital craniectomy	No	8	No	No
Present case	70/F	The temporal lobe, the cerebellar vermis	Headache and walking unstable	A midline suboccipital craniotomy and near total removal of the cerebellar mass	No	24	No	No

F, female; M, male; nm, not mentioned; WBRT, whole brain radiation therapy; RT, radiation therapy.

on MRI. Intracranial teratoma are benign tumors occurring mainly in the pineal and sellar region, mostly in young men.

In conclusion, CLN is a rare intracranial tumor with unknown etiology, which can occur in the cerebellum or supratentorial parenchyma. The distinctive imaging feature of CLN is the fatty component within the lesion. An accurate diagnosis based solely on its imaging findings preoperatively is usually is difficult due to its rarity. Surgery is the primary treatment of choice for large masses causing symptoms. Long-term follow-up is needed for unresected small lesions.

DATA AVAILABILITY STATEMENT

The original contributions presented in the study are included in the article/**Supplementary Material**, further inquiries can be directed to the corresponding author/s.

ETHICS STATEMENT

The studies involving human participants were reviewed and approved by the ethics committee of the Second Affiliated Hospital, Zhejiang University School of Medicine. The patients/participants provided their written informed consent to participate in this study.

AUTHOR CONTRIBUTIONS

CW performed the data acquisition. CW and SW performed the radiological images analysis. CW, SW, and XX performed the manuscript preparation. All authors contributed to the article and approved the submitted version.

FUNDING

This research was supported by Zhejiang Provincial Natural Science Foundation of China under Grant No. LY21H180003.

SUPPLEMENTARY MATERIAL

The Supplementary Material for this article can be found online at: https://www.frontiersin.org/articles/10.3389/fsurg.2021.686892/full#supplementary-material

REFERENCES

1. Bechtel JT, Patton JM, Takei Y. Mixed mesenchymal and neuroectodermal tumor of the cerebellum. *Acta Neuropathol.* (1978) 41:261–3. doi: 10.1007/BF00690447
2. Chakraborti S, Mahadevan A, Govindan A, Yasha TC, Santosh V, Kovoor JME, et al. Supratentorial and cerebellar liponeurocytomas: report of four cases with review of literature. *J Neurooncol.* (2011) 103:121–7. doi: 10.1007/s11060-010-0361-z
3. Limaiem F, Bellil S, Chelly I, Bellil K, Mekni A, Jemel H, et al. Recurrent cerebellar liponeurocytoma with supratentorial extension. *Can J Neurol Sci.* (2009) 36:662–5. doi: 10.1017/S0317167100008222
4. Pinar K, Aydin S, Necmettin P. Does "cerebellar liponeurocytoma" always reflect an expected site? An unusual case with a review of the literature. *Folia Neuropathol.* (2014) 1:101–5. doi: 10.5114/fn.2014.41749
5. Oliver G, Andreas J, Yahya A, Ulrich S, Elias L. Cerebellar liponeurocytoma – a rare entity: a case report. *J Med Case Rep.* (2018) 12:170. doi: 10.1186/s13256-018-1706-z
6. Patel N, Fallah A, Provias J, Jha NK. Cerebellar liponeurocytoma. *Can J Surg.* (2009) 52:E117.
7. Wolf A, Alghefari H, Krivosheya D, Staudt MD, Bowden G, Macdonald DR, et al. Cerebellar liponeurocytoma: a rare intracranial tumor with possible familial predisposition. Case report. *J Neurosurg.* (2016) 125:57–61. doi: 10.3171/2015.6.JNS142965
8. George DH, Scheithauer BW. Central liponeurocytoma. *Am J Surg Pathol.* (2001) 25:1551–5. doi: 10.1097/00000478-200112000-00013
9. Kakkar A, Sable M, Suri V, Sarkar C, Garg A, Satyarthee GD, et al. Cerebellar liponeurocytoma, an unusual tumor of the central nervous system–ultrastructural examination. *Ultrastruct Pathol.* (2015) 39:419–23. doi: 10.3109/01913123.2015.1027435
10. Horoupian DS, Shuster DL, Kaarsoo-Herrick M, Shuer LM. Central neurocytoma: one associated with a fourth ventricular PNET/medulloblastoma and the second mixed with adipose tissue. *Hum Pathol.* (1997) 28:1111–4. doi: 10.1016/s0046-8177(97)90066-6
11. Aker FV, Zkara S, Eren P, Peker N, Armaan S, Hakan T. Cerebellar liponeurocytoma/lipidized medulloblastoma. *J Neurooncol.* (2005) 71:53–9. doi: 10.1007/s11060-004-9172-4
12. Pelz D, Khezri N, Mainprize T, Phan N, Keith J, Bilbao J, et al. Multifocal Cerebellar Liponeurocytoma. *Canad J Neurol Sci.* (2013) 40:870–2. doi: 10.1017/s0317167100016048
13. Scoppetta TLPD, de Brito MCB, de Almeida Prado JLM, Scoppetta LCD. Multifocal cerebellar liponeurocytoma. *Neurology.* (2015) 85:1912. doi: 10.1212/WNL.0000000000002156
14. Dhar A, Vaish M, Gupta R, Jain K, Abrahim M, Marda M. Multiple cerebellar liponeurocytoma mimicking left cerebellopontine angle and right cerebellar dermoid: a case report. *EC Neurol.* (2015) 2:55–60.
15. Konovalov AN, Konovalov NA, Pronin IN, Shishkina LV, Timonin SI. Multiple primary liponeurocytoma of the central nervous system. *Zh Vopr Neirokhir Im N N Burdenko.* (2015) 79:87–96. doi: 10.17116/neiro201579287-96
16. Sivaraju L, Aryan S, Ghosal N, Hegde AS. Cerebellar liponeurocytoma presenting as multifocal bilateral cerebellar hemispheric mass lesions. *Neurol India.* (2017) 65:422–4. doi: 10.4103/neuroindia.NI_1379_15
17. Khatri D, Bhaisora KS, Das KK, Behari S, Pal L. Cerebellar liponeurocytoma: the dilemma of multifocality. *World Neurosurg.* (2018) 120:131–7. doi: 10.1016/j.wneu.2018.08.156
18. Jenkinson MD, Bosma JJD, Du Plessis D, Ohgaki H, Kleihues P, Warnke P, et al. Cerebellar liponeurocytoma with an unusually aggressive clinical course: case report. *Neurosurgery.* (2003) 53:1425–8. doi: 10.1227/01.NEU.0000093430.61239.7E
19. Nishimoto T, Kaya, B. Cerebellar liponeurocytoma. *Arch Pathol Lab Med.* (2012) 136:965–9. doi: 10.5858/arpa.2011-0337-RS
20. Cai J, Li W, Du J, Xu N, Gao P, Zhou J, et al. Supratentorial intracerebral cerebellar liponeurocytoma: a case report and literature review. *Medicine.* (2018) 97:e9556. doi: 10.1097/MD.0000000000009556

Conflict of Interest: The authors declare that the research was conducted in the absence of any commercial or financial relationships that could be construed as a potential conflict of interest.

frontiers in Surgery

CASE REPORT
published: 08 July 2021
doi: 10.3389/fsurg.2021.696457

Case Report: A Rare Case of Fourth Ventricle to Spinal Subarachnoid Space Shunt Migration: Surgical Pearl and Literature Review

Nicolas Serratrice[1]*, *Joe Faddoul*[1], *Bilal Tarabay*[1], *Sarkis Taifour*[2] and *Georges Naïm Abi Lahoud*[1]

[1] ICVNS - CMC Bizet, Paris, France, [2] CIMOP - CMC Bizet, Paris, France

Background: In the event of syringomyelia communicating with the fourth ventricle, a fourth ventricle to cervical subarachnoid space shunting could be proposed.

Case Report: In this review article, we describe the case of a 40-year-old woman who had a previously implanted fourth ventricle to spinal subarachnoid space shunt for the treatment of syringomyelia in the context of Chiari syndrome. The catheter migrated intradurally to the lumbosacral space, but in the absence of neurological repercussions, we decided to leave it in place.

Conclusions: To the best of our knowledge, this is the first case described in the literature review of a catheter migration in the subarachnoid space from occipitocervical to lumbosacral level.

Keywords: cranio-cervical junction, syringomyelia, trapped fourth ventricle, trapped fourth ventricle with syrinx, fourth ventricle to spinal subarachnoid space shunt, catheter migration, Chiari syndrome

OPEN ACCESS

Edited by:
Michael Sughrue, University of New South Wales, Australia

Reviewed by:
Mario Ganau, University of Toronto, Canada
Fahd Derkaoui Hassani, Cheikh Zaid International University Hospital, Morocco

***Correspondence:**
Nicolas Serratrice
n.serratrice@clinique-bizet.com; nico.serratrice@orange.fr

Specialty section:
This article was submitted to Neurosurgery, a section of the journal Frontiers in Surgery

Received: *16 April 2021*
Accepted: *14 June 2021*
Published: *08 July 2021*

Citation:
Serratrice N, Faddoul J, Tarabay B, Taifour S and Abi Lahoud GN (2021) Case Report: A Rare Case of Fourth Ventricle to Spinal Subarachnoid Space Shunt Migration: Surgical Pearl and Literature Review. Front. Surg. 8:696457. doi: 10.3389/fsurg.2021.696457

INTRODUCTION

Syringomyelia is frequently associated with Chiari syndrome (1, 2). When syrinx cavities communicate with the fourth ventricle, a fourth ventricle to spinal subarachnoid space shunting could be proposed with good clinical results (3, 4). Neurological complications reported with this surgical technique are mainly related to the misplacement of the shunt (5, 6), but the migration of the catheter itself has never been described. In this review article, we report for the first time a case of migration of a subarachnoid catheter from the craniocervical level into the lumbosacral intradural space. We also propose a review of the literature concerning the complications and, in particular, the migration of the different types of shunts used at present.

CASE REPORT

This is the case of a 40-year-old woman who was referred to our institution for the assessment of a complex pathology. She was operated three times for Chiari syndrome between 2010 and 2012. During the second intervention in 2011, a ventriculoperitoneal shunt was placed for neurological deterioration secondary to hydrocephalus. During the last intervention, a fourth ventricle to spinal subarachnoid space shunt with a 15 cm catheter was placed for the progression of syringomyelia associated with a fourth ventricle entrapment. The patient presented significant sequelae including right-side

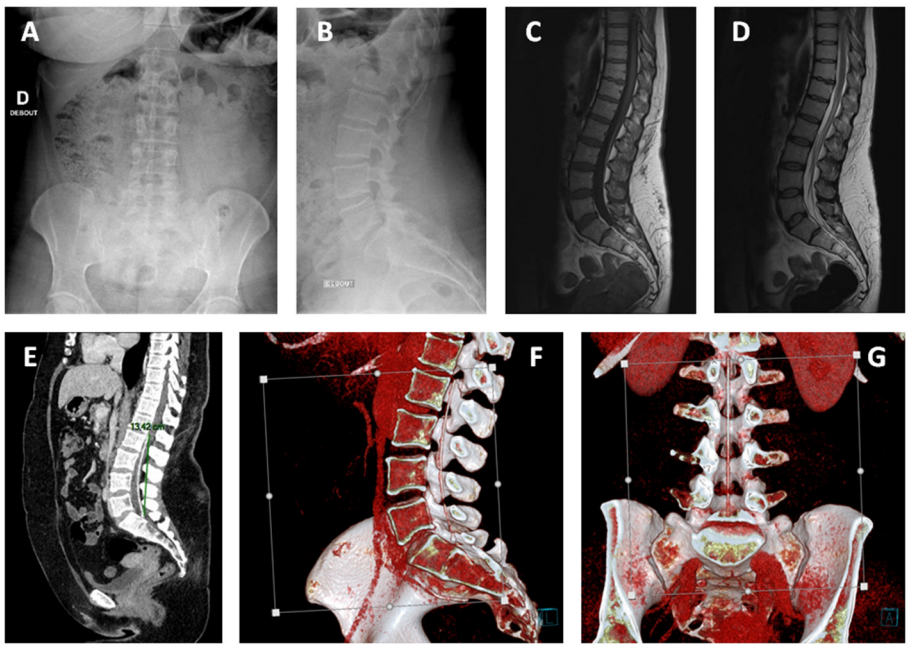

FIGURE 1 | Lumbar x-rays: anteroposterior **(A)** and lateral views **(B)**, MRI sagittal view, respectively, T1 **(C)**, and T2 **(D)** sequences. The presence of the catheter was hard to identify even for experienced radiologists, as its intensity on T1-weighted and T2-weighted images was similar to that of the cauda equina nerve roots. **(E)** Lumbar CT scanner sagittal view showing the initially placed fourth ventricle to cervical subarachnoid space shunt located at L2-S1 level measuring around 15 cm in length and 2.5 mm in diameter. **(F,G)** Three-dimensional (3D) reconstructions. There is no local compression of neurological elements.

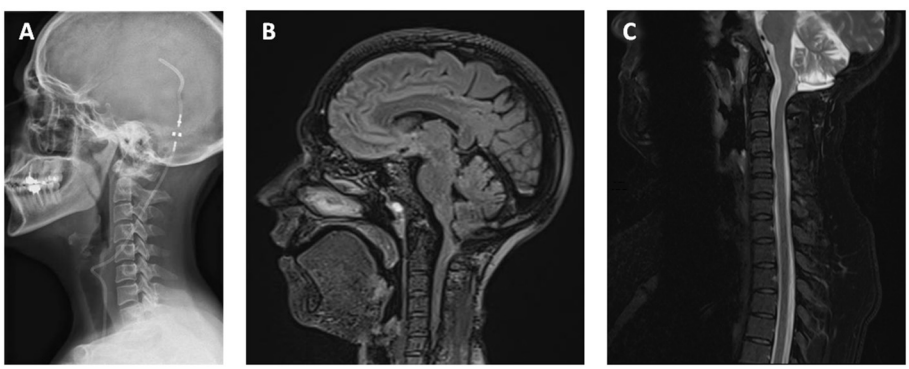

FIGURE 2 | (A) Lateral x-ray showing the ventriculoperitoneal shunt. **(B)** No hydrocephaly and dilatation of fourth ventricles on MRI sagittal view T1 sequence. The syrinx has completely regressed **(C)** on MRI sagittal view T2 sequence.

hemiparesis, permanent dizziness, and diffuse chronic pain. In the course of the assessment of recent abdominal pain, the patient benefited from an abdominal CT (**Figure 1**). The CT showed no intra-abdominal complications. However, the presence of an intradural catheter at the L2-S1 level measuring around 15 cm in length and 2.5 mm in diameter was noted. When looking back to a spine MRI taken in 2018 carried out to investigate mechanical low back pain, the presence of the catheter was hard to identify even for experienced radiologists, as its intensity on T1-weighted and T2-weighted images were similar to that of the cauda equina nerve roots. We concluded that this catheter must have migrated intradurally since it was put in place in 2012. To date, this is the first time such migration of the fourth ventricle to spinal subarachnoid space shunt is described in the literature review. Its presence is not responsible for pain or neurological symptoms as it is well-confirmed clinically and on the electromyogram. The ventriculoperitoneal shunt seemed to be functional, and no fourth ventricle entrapment was found (**Figure 2**). No residual syringomyelia was detected on the spine MRI. Hence, we found no indication to place a new shunt nor to remove the migrated one.

DISCUSSION

In this review article, we describe the case of a 40-year-old woman with a history of syringomyelia in a context of Chiari syndrome (1), who had a previously implanted fourth ventricle to cervical subarachnoid space shunt that migrated to the subdural lumbosacral level. Because of the absence of syringomyelia and ventricular dilation, as well as the absence of neurological repercussions, we decided to leave the catheter in place.

Several types of shunts can be used in the treatment of syringomyelia, namely, fourth ventricle to cervical subdural, syringo-subarachnoid, syringo-peritoneal, syringo-pleural, lumboperitoneal, and ventricular shunts. Each of these techniques has its well-known advantages and complications. Among the complications, catheter migration remains extremely rare. However, to be safe and effective, it is recommended to perform such techniques selectively by an experienced neurosurgeon.

In 1995, Lee et al. reported five complications on 12 patients treated by fourth-ventricular shunting for symptomatic posterior fossa cysts of the Dandy-Walker malformation and trapped the fourth ventricle: Three patients developed new cranial nerve dysfunction caused by direct injury to the floor of the fourth ventricle, one patient suffered an intracystic hemorrhage and acute shunt malfunction, and one patient had the catheter tip in the brainstem on postoperative studies without new neurological deficit (5). These complications were mainly related to the misplacement of the catheter, and even if the techniques have evolved, options include, nowadays, the following: open fenestration through a suboccipital craniotomy, fourth-ventricular shunting, and minimally invasive procedures including endoscopic stenting and fenestration. These techniques are associated with complications in 42% of cases (6–10).

Trapped fourth ventricle with or without syringomyelia is a rare condition, and there is still no consensus on its management strategy. However, in this context of migration of the fourth ventricle to subarachnoid space shunt, the ventriculoperitoneal shunt previously implanted might have in itself induced the long-term resolution of the syringomyelia. This would, therefore, suggest the limited impact of the fourth ventricle to subarachnoid space shunting. Such a view is also shared by a growing portion of the adult and pediatric neurosurgical community (11).

Syringomyelia associated with spinal arachnoiditis or arachnoid adhesions can be treated by adhesiolysis using a conventional microscopic approach or an endoscopic technique in order to place a spinal cysto-subarachnoid shunt (12).

A thorough neuroradiological workup is the best way to ensure the least number of perioperative and postoperative complications and maximal chances of satisfactory long-term clinical improvement in Chiari syndrome (13). When there is persistence, recurrence, or progression of the syrinx after a foramen magnum decompression (30% of the patients), syringomyelia can be treated with a syringo-subarachnoid shunt (14). However, rare neurological complications have been reported (15).

Complications of migration of lumboperitoneal shunt are frequent (16, 17). General complications are similar to ventriculoperitoneal shunt, i.e., abdominal pseudocyst, distal catheter migration, inguinal hernia, catheter disconnection, infection, and intestinal obstruction (18).

CONCLUSIONS

To our knowledge, this is the first described case of catheter migration from the fourth ventricle to the lumbar subarachnoid space in the context of Chiari syndrome associated with syringomyelia. Because of the absence of radiological and neurological repercussions, we decided to leave the catheter in place.

DATA AVAILABILITY STATEMENT

The original contributions presented in the study are included in the article/supplementary material, further inquiries can be directed to the corresponding author/s.

ETHICS STATEMENT

Ethical review and approval was not required for the study on human participants in accordance with the local legislation and institutional requirements. The patients/participants provided their written informed consent to participate in this study.

AUTHOR CONTRIBUTIONS

NS: investigation, writing—original draft, and visualization. JF: writing—review and editing and visualization. BT and ST: writing—review and editing. GNAL: supervision and writing—review and editing. All authors contributed to the article and approved the submitted version.

ACKNOWLEDGMENTS

We are grateful to coauthors for the rereading of the article.

REFERENCES

1. Di Rocco C. Should we stop using the term "malformation" for Chiari type I? *Childs Nerv Syst.* (2019) 35:1649–50. doi: 10.1007/s00381-019-04311-z
2. Hidalgo JA, Tork CA, Varacallo M. *Arnold Chiari Malformation*. Treasure Island, FL: StatPearls Publishing (2020).
3. Fukushima T, Yoshinaga S, Matsuda T, Tomonaga M, Takahashi S, Oita J, et al. [Syringomyelia, its pathogenesis and surgical treatment based on 4 cases' experience]. *No Shinkei Geka.* (1986) 14:909–16.
4. Davidoff CL, Liu S, Wong JHY, Koustais S, Rogers JM, Stoodley MA. Treatment of Syringomyelia in patients with arachnoiditis at the craniocervical junction. *World Neurosurg.* (2017) 107:565–73. doi: 10.1016/j.wneu.2017.08.064

5. Lee M, Leahu D, Weiner HL, Abbott R, Wisoff JH, Epstein FJ. Complications of fourth-ventricular shunts. *Pediatr Neurosurg.* (1995) 22:309–313; discussion 314. doi: 10.1159/000120921
6. Dollo C, Kanner A, Siomin V, Ben-Sira L, Sivan J, Constantini S. Outlet fenestration for isolated fourth ventricle with and without an internal shunt. *Childs Nerv Syst.* (2001) 17:483–6. doi: 10.1007/s003810100444
7. Udayakumaran S, Biyani N, Rosenbaum DP, Ben-Sira L, Constantini S, Beni-Adani L. Posterior fossa craniotomy for trapped fourth ventricle in shunt-treated hydrocephalic children: long-term outcome. *J Neurosurg Pediatr.* (2011) 7:52–63. doi: 10.3171/2010.10.PEDS10139
8. Yadav YR, Parihar V. The endoscopic trans-fourth ventricle aqueductoplasty and stent placement for the treatment of trapped fourth ventricle; stent blockage complications under estimated? *Neurol India.* (2012) 60:455. doi: 10.4103/0028-3886.100743
9. Say I, Dodson V, Tomycz L, Mazzola C. Endoscopic fourth ventriculostomy: suboccipital transaqueductal approach for fenestration of isolated fourth ventricle: case report and technical note. *World Neurosurg.* (2019) 129:440–4. doi: 10.1016/j.wneu.2019.06.010
10. Tyagi G, Singh P, Bhat DI, Shukla D, Pruthi N, Devi BI. Trapped fourth ventricle-treatment options and the role of open posterior fenestration in the surgical management. *Acta Neurochir.* (2020) 162:2441–9. doi: 10.1007/s00701-020-04352-3
11. Singhal A, Cheong A, Steinbok P. International survey on the management of Chiari 1 malformation and syringomyelia: evolving worldwide opinions. *Childs Nerv Syst.* (2018) 34:1177–82. doi: 10.1007/s00381-018-3741-x
12. Tan DCH, Vaughan KA, Koeck H. Endoscopic-assisted spinal arachnoiditis adhesiolysis and placement of a spinal cysto-subarachnoid shunt. *World Neurosurg.* (2019) 131:43–6. doi: 10.1016/j.wneu.2019.07.160
13. D'Arco F, Ganau M. Which neuroimaging techniques are really needed in Chiari I? A short guide for radiologists and clinicians. *Childs Nerv Syst.* (2019) 35:1801–8. doi: 10.1007/s00381-019-04210-3
14. Soleman J, Roth J, Bartoli A, Rosenthal D, Korn A, Constantini S. Syringo-subarachnoid shunt for the treatment of persistent syringomyelia following decompression for chiari type I malformation: surgical results. *World Neurosurg.* (2017) 108:836–43. doi: 10.1016/j.wneu.2017.08.002
15. Levi V, Franzini A, Di Cristofori A, Bertani G, Pluderi M. Subacute posttraumatic ascending myelopathy (SPAM): a potential complication of subarachnoid shunt for syringomyelia? *J Spinal Cord Med.* (2020) 43:714–8. doi: 10.1080/10790268.2018.1512735
16. Kanai M, Kawano K, Uehara S. Upward migration of the L-P shunt catheter into the cranial base. *Osaka City Med J.* (1999) 45:123–7.
17. Yoshida S, Masunaga S, Hayase M, Oda Y. Migration of the shunt tube after lumboperitoneal shunt–two case reports. *Neurol Med Chir.* (2000) 40:594–6. doi: 10.2176/nmc.40.594
18. Ferreira Furtado LM, Da Costa Val Filho JA, Moreira Faleiro R, Lima Vieira JA, Dantas Dos Santos AK. Abdominal complications related to ventriculoperitoneal shunt placement: a comprehensive review of literature. *Cureus.* (2021) 13:e13230. doi: 10.7759/cureus.13230

Conflict of Interest: The authors declare that the research was conducted in the absence of any commercial or financial relationships that could be construed as a potential conflict of interest.

frontiers in Surgery

CASE REPORT
published: 19 July 2021
doi: 10.3389/fsurg.2021.689713

Case Report: A 62-Year-Old Woman With Contrast-Induced Encephalopathy Caused by Embolization of Intracranial Aneurysm

Ying Zhang[1], *Ming Zhou*[1], *Dong Wang*[1], *Tao Liu*[1], *Pengfei Chang*[1], *Jie Zhang*[1], *Rui Zhang*[1], *Yumin Luo*[2] *and Ping Liu*[2]*

[1] *Department of Encephalopathy, Traditional Chinese Medicine Hospital of Weifang, Weifang, China,* [2] *Department of Neurology, Xuanwu Hospital of Capital Medical University, Beijing, China*

Contrast-induced encephalopathy (CIE) is a rare complication of endovascular treatment and is extensively reported as a transient and reversible phenomenon. This report describes a 62-year-old woman for embolization of an internal carotid artery (ICA) aneurysm. The operation was successful, but postoperation the patient suffered unconsciousness, blindness, hemiplegia, ophthalmoplegia, fever, and seizures. CT of the brain without the contrast showed widespread edema in the right cerebral hemisphere, which is involved in the frontal, parietal, temporal, and occipital lobes. She was diagnosed with CIE in time and treated with supportive management as soon as possible, and fortunately, the patient improved a benign course and was discharged without any neurological deficits. This study emphasizes the prevention of the CIE and the importance of early diagnosis and symptomatic treatment.

Keywords: contrast-induced encephalopathy, complication of endovascular treatment, aneurysm embolization, computer tomography, cerebral edema

OPEN ACCESS

Edited by:
Gilberto Ka Kit Leung, The University of Hong Kong, SAR China

Reviewed by:
Jorge Marcelo Mura, Instituto de Neurocirugía, Chile
Mario Ganau, University of Toronto, Canada

***Correspondence:**
Ping Liu
pingliu@xwhosp.org

Specialty section:
This article was submitted to Neurosurgery, a section of the journal Frontiers in Surgery

Received: *12 April 2021*
Accepted: *16 June 2021*
Published: *19 July 2021*

Citation:
Zhang Y, Zhou M, Wang D, Liu T, Chang P, Zhang J, Zhang R, Luo Y and Liu P (2021) Case Report: A 62-Year-Old Woman With Contrast-Induced Encephalopathy Caused by Embolization of Intracranial Aneurysm. Front. Surg. 8:689713. doi: 10.3389/fsurg.2021.689713

INTRODUCTION

Contrast-induced encephalopathy (CIE) is a rare complication of angiography. The first case of CIE was described in 1970 as transient cortical blindness after coronary angiography (1). Clinical manifestations include encephalopathy, seizures, cortical blindness, and focal neurological deficits, such as ophthalmoplegia (2). Herein, a case of CIE following embolization of intracranial aneurysm is described, in which the severe neurological deficits were reversed.

CASE REPORT

A 62-year-old woman with a history of hypertension was admitted to our hospital due to headache for 20 days. On physical examination, blepharoptosis was found in the right eye. MRI of the brain detected changes in signals that consist of multiple lacunar infarctions in the right basal ganglia and bilateral demyelination in the centrum semiovale (**Figure 1A**). Magnetic resonance angiography (MRA) of the brain indicated an aneurysm in the communicating segment of the right internal carotid artery (ICA) (**Figure 1B**). Then, the patient underwent digital silhouette angiography

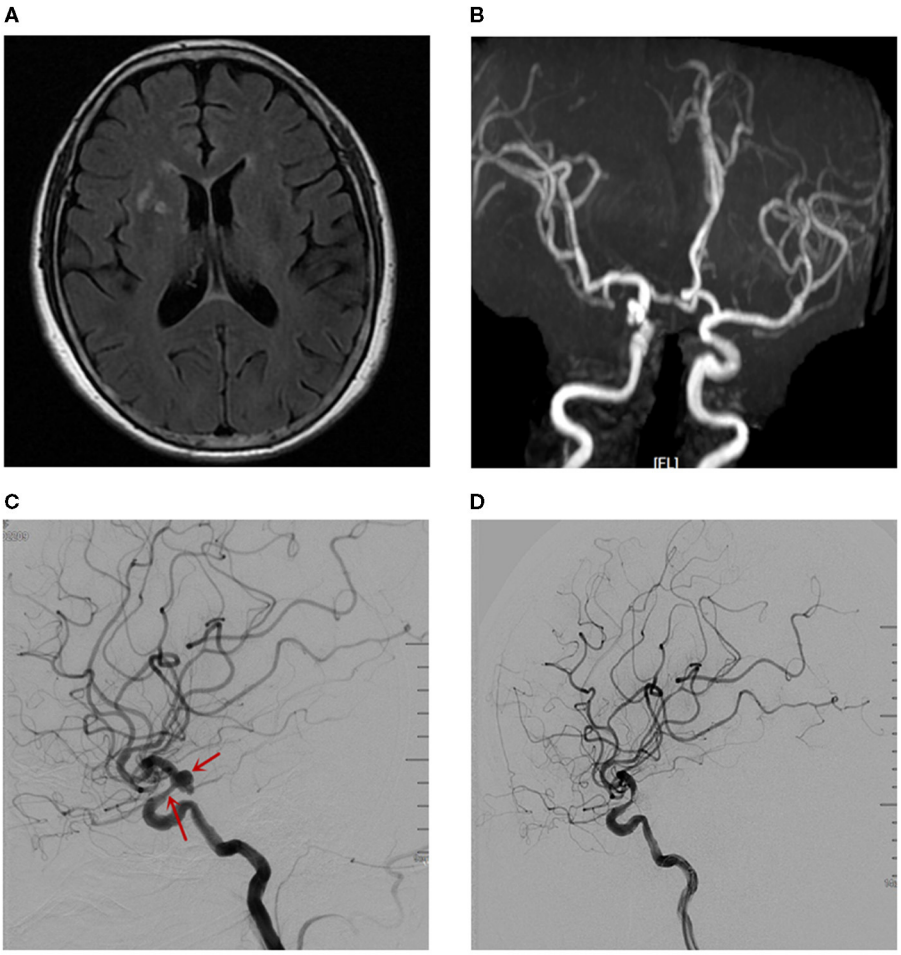

FIGURE 1 | The imaging examinations before CIE. **(A)** MRI of the brain. **(B)** MRA detected the aneurysm in the communicating segment of the right ICA. **(C)** The DSA revealed an aneurysm with size of 7.4mm*6.1mm in the right ICA-communicating segment, and mild stenosis in right ICA-ophtalmic segment. **(D)** The DSA revealed a coiling embolization of the aneurysm.

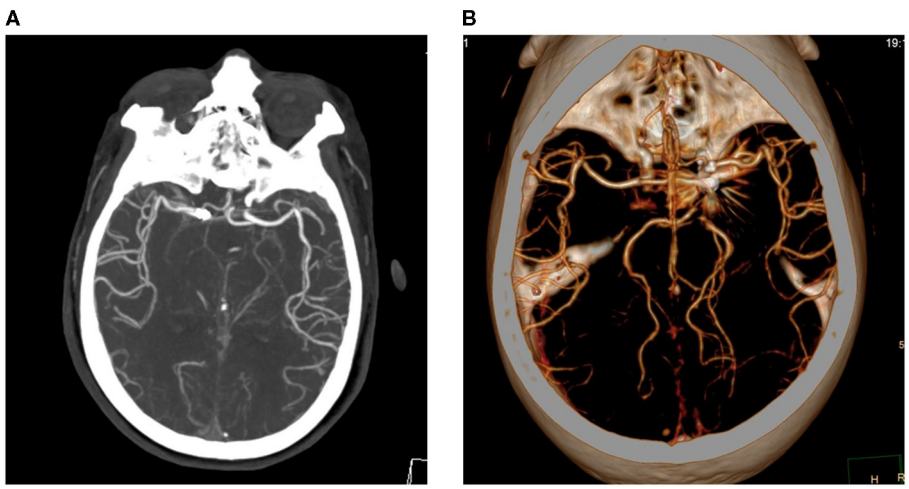

FIGURE 2 | CTA performed 2 hours later indicated no occlusion of the right ICA **(A,B)**.

(DSA) for a further assessment, with the total amount of 200 ml iodixanol (iodine concentration 270 mgi/ml; osmotic pressure 290 mOsm/kg H_2O, Yangtze River Pharm, China). The DSA revealed an aneurysm with a size of 7.4 mm * 6.1 mm in the right communicating segment of ICA, and mild stenosis in right ophthalmic segment of ICA (**Figure 1C**). There was no complication during and after the operation.

The patient received oral aspirin (100 mg/day) and clopidogrel (75 mg/day) for 5 days, after which a coiling embolization of the aneurysm was performed under general anesthesia. She received successful coiling of the aneurysm using two stent remodeling techniques (**Figure 1D**). Postcoiling angiography showed completed occlusion of the aneurysm, and all the arteries were shown to be patent in the final angiogram. The total amount of iodixanol (iodine concentration 270 mgi/ml; osmotic pressure 290 mOsm/kg H_2O, Yangtze River Pharm, China) administrated during this procedure was also 200 ml, and the systolic blood pressure (SBP) was maintained at about 110 mmHg during the intraoperative period. About 10 min after the operation, the patient woke up, but she became confused and suffered blindness, and the eyes stared to the right side. The diameters of the pupils were 3 mm bilaterally with light reflex sensitivity. One hour later, the weakness in the left limb decreased (regained 4/5 strength), and the SBP gradually increased to about 180 mmHg. A non-contrast CT of the brain performed immediately after the operation showed edema in the right cerebral hemisphere and involved the frontal, parietal, temporal, and occipital lobes, and there was no hemorrhage (**Figure 3A**). CT angiography (CTA) performed 2 h later indicated no occlusion of the right ICA (**Figures 2A,B**). She was diagnosed with CIE based on the acute onset of symptoms after cerebral angiography and distinctive CT findings. We initiated hydration therapy for the excretion of the contrast agent and used urapidil to control SBP at about 140 mmHg; meanwhile, mannitol was used to improve the cerebral edema. On the following day, the patient had a fever up to 38.5°C, weakness in the left limb decreased (regained 0/5 strength), and suffered generalized tonic-clonic seizures for twice. CT reviewed persistent edema in the right cerebral hemisphere (**Figure 3B**). We applied methylprednisolone pulse 80 mg/day for CIE and diazepam 10 mg/day for symptomatic epilepsy. Fortunately, her clinical manifestations disappeared gradually on the third day and the follow-up brain CT showed resolution of the cerebral edema (**Figure 3C**).

DISCUSSION

This case report demonstrated the following points: First, minimization of the amount of contrast medium and hydration may prevent the CIE. Second, early diagnosis, active blood pressure control, and symptomatic treatment are important to reduce the incidence of CIE and alleviate its disability. CIE is a very rare complication of endovascular interventions. The incidence of CIE seems to be lower in recent years due to the increased use of nonionic contrast agents. Though neurological status usually occurs self-limiting over a period of days (3), there are persistent neurological deficits and irreversible fatal cerebral edema cases reported (4, 5). Therefore, CIE should be kept in mind as a complication of angiography and supportive therapy should be initiated as soon as possible.

The mechanism and cause of CIE are associated with the disruption of the blood-brain barrier (BBB). Contrast agents can damage the BBB and facilitate its own entry into the brain, which is considered to be one of the mechanisms of CIE (4). Studies have been indicated that the risk factors of CIE included hypertension, renal disorder, acute cerebral infarction, the low temperature of contrast media, and endovascular surgery requiring a higher dose of contrast agents (6). In our case, though the total amount of contrast agents is not excessive, the contrast agent was injected repeatedly into a single vessel, and the cumulative injection may disrupt the BBB. Meanwhile, the case presented with lacunar infarction and white matter lesion indicated small vessel disease with a certain degree of vascular endothelial damage, and the damaged BBB was vulnerable to be disrupted by the repeated injection of contrast agents into the territory of ICA with endothelial damage induced by small vessel disease.

The diagnosis of CIE is not easy, as its presentation may resemble embolism and hemorrhagic complications following angiography and percutaneous interventions. The typical radiological findings, including abnormal cortical contrast enhancement and cerebral edema, subarachnoid contrast enhancement, and striatal contrast enhancement, could help us to differentiate CIE from hemorrhage or infarction. Measuring the Hounsfield units (HU) can help differentiate subarachnoid hemorrhage (SAH) from CIE, as blood usually measures at 30–45 HU, and contrast usually measures at 80–160 HU (7). On MRI, gyral swelling and hyperintensity on T2 fluid-attenuated inversion recovery (FLAIR) image and diffusion-weighted imaging (DWI), not accompanied by changes on apparent diffusion coefficient (ADC), have been described in the previous report (8). In this case, we diagnosed CIE by the acute onset of symptoms after cerebral angiography, typical CT and CTA findings, and rapid improvement in clinical and imaging findings.

There is no definitive treatment for CIE, and hydration and close observation of the patient in the postprocedural period are recommended (6). Steroids are also commonly used to improve cerebral edema by stabilizing the BBB (9). Mannitol is another type of drug used to relieve cerebral edema; however, it is because that mannitol opens the BBB and conversely induces contrast medium into the brain tissue (10). Hemodialysis is useful for the removal of the contrast medium from the blood, with approximately 80% of the contrast medium having been removed within 4 h, and there have been cases where symptoms were improved by hemodialysis (11). It is also reported the deterioration of neurological symptoms caused by cerebral edema is attributed to an osmotic gradient between the brain and the blood as a result of rapid removal of urea by hemodialysis (10, 11). For fatal cerebral edema cases, craniectomy should be considered (12), while further research studies are needed to develop the evidence-based treatment for CIE.

Though the rare incidence of CIE renders their prevention, which may help minimize the severe complication very

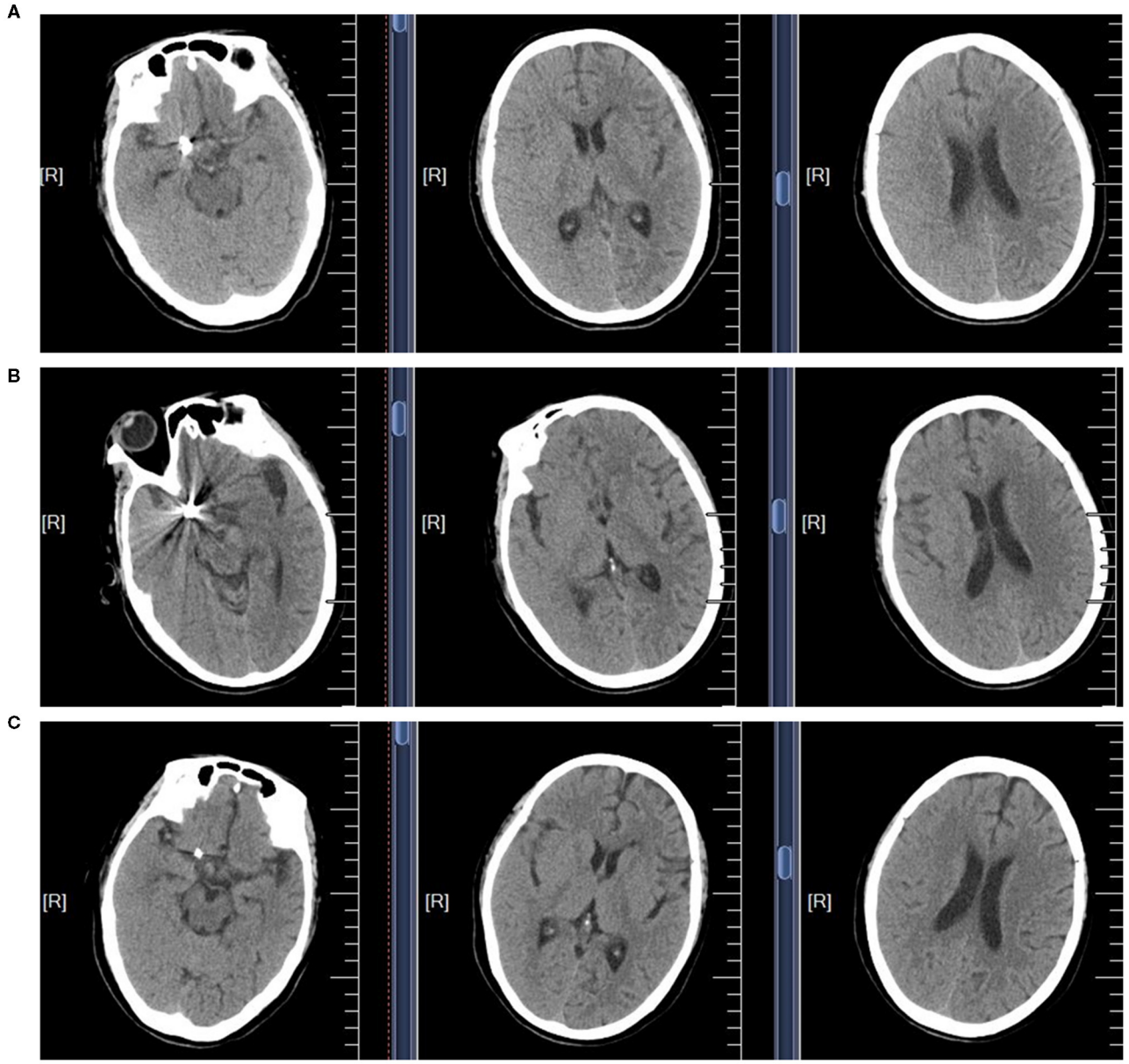

FIGURE 3 | The non-contrast CT scans of the brain in CIE patient. **(A)** The brain CT scan performed immediately after the operation. **(B)** The brain CT scan performed in the following day. **(C)** The brain CT scan performed in the third day.

difficult, following measures should be considered during the perioperative period. First, it is reported that CIE is an idiosyncratic response to a small dose of contrast agent, a variety of preoperative tests for contrast agents should be performed, and it is generally accepted that antiallergic drugs or corticosteroids should be used for patients who were allergic to contrast media (13). Second, hydration should be sufficient to accelerate the excretion of contrast medium during and after the operation, as long as the cardiac function is tolerated. Third, it is reported that BBB is affected by the injection of high concentrations, low temperatures, and repeated injections with short interval into the same blood vessel (14); therefore, during the procedure we should minimize the amount of contrast medium while keeping the image clear and pay attention to the details mentioned above. Fourth, with regard to hypertension, it is thought that the BBB is affected by a decline in the autoregulation blood vessels (15). We should control blood pressure in a reasonable range and avoid fluctuation of blood pressure during the whole perioperative period. Recent research studies display that improving contrast media using nanocarriers, such as nanoparticles, liposomes, micelles, nanobodies, and quantum dots, may enhance its tolerability and bioavailability because they leverage on the bioinert potential of their coating agents and also decrease the risk of CIE (16, 17).

In conclusion, we emphasize the prevention of the CIE, as well as the importance of early diagnosis and symptomatic treatment, in order to reduce the incidence of CIE and alleviate its disability. However, in the clinic, it needs experienced doctors to judge CIE quickly It may be more reasonable to extend the interval between two injections of contrast agents.

DATA AVAILABILITY STATEMENT

The original contributions presented in the study are included in the article/supplementary material, further inquiries can be directed to the corresponding author/s.

ETHICS STATEMENT

Written informed consent was obtained from the individual(s) for the publication of any potentially identifiable images or data included in this article.

AUTHOR CONTRIBUTIONS

YZ, MZ, DW, TL, PC, JZ, and RZ contributed to the search and assessment of the available literature. YZ and PL wrote the manuscript. YL and PL helped revise the text to the final form. All authors contributed to the article and approved the submitted version.

FUNDING

This work was funded by the Natural Science Foundation in China (81601157 and 81971222) and the General projects of Scientific and Technological Plan of Beijing Municipal Education Commission (KM201910025019).

REFERENCES

1. Fischer-Williams M, Gottschalk PG, Browell JN. Transient cortical blindness. An unusual complication of coronary angiography. *Neurology.* (1970) 20:353–5. doi: 10.1212/WNL.20.4.353
2. Yu J, Dangas G. Commentary: New insights into the risk factors of contrast-induced encephalopathy. *J Endovasc Ther.* (2011) 18:545–6. doi: 10.1583/11-3476C.1
3. Niimi Y, Kupersmith MJ, Ahmad S, Song J, Berenstein A. Cortical blindness, transient and otherwise, associated with detachable coil embolization of intracranial aneurysms. *AJNR Am J Neuroradiol.* (2008) 29:603–7. doi: 10.3174/ajnr.A0858
4. Kamimura T, Nakamori M, Imamura E, Hayashi Y, Matsushima H, Mizoue T, et al. Low-dose contrast-induced encephalopathy during diagnostic cerebral angiography. *Intern Med.* (2021) 60:629–33. doi: 10.2169/internalmedicine.5139-20
5. Leong S, Fanning NF. Persistent neurological deficit from iodinated contrast encephalopathy following intracranial aneurysm coiling. A case report and review of the literature. *Interv Neuroradiol.* (2012) 18:33–41. doi: 10.1177/159101991201800105
6. Iwata T, Mori T, Tajiri H, Miyazaki Y, Nakazaki M. Repeated injection of contrast medium inducing dysfunction of the blood-brain barrier: case report. *Neurol Med Chir (Tokyo).* (2013) 53:34–6. doi: 10.2176/nmc.53.34
7. Lantos G. Cortical blindness due to osmotic disruption of the blood-brain barrier by angiographic contrast material: CT and MRI studies. *Neurology.* (1989) 39:567–71. doi: 10.1212/WNL.39.4.567
8. Spina R, Simon N, Markus R, Muller DW, Kathir K. Contrast-induced encephalopathy following cardiac catheterization. *Catheter Cardiovasc Interv.* (2017) 90:257–68. doi: 10.1002/ccd.26871
9. Potsi S, Chourmouzi D, Moumtzouoglou A, Nikiforaki A, Gkouvas K, Drevelegas A. Transient contrast encephalopathy after carotid angiography mimicking diffuse subarachnoid haemorrhage. *Neurol Sci.* (2012) 33:445–8. doi: 10.1007/s10072-011-0765-3
10. Matsubara N, Izumi T, Miyachi S, Ota K, Wakabayashi T. Contrast-induced encephalopathy following embolization of intracranial aneurysms in hemodialysis patients. *Neurol Med Chir (Tokyo).* (2017) 57:641–8. doi: 10.2176/nmc.oa.2017-0132
11. Donepudi B, Trottier S. A seizure and hemiplegia following contrast exposure: understanding contrast-induced encephalopathy. *Case Rep Med.* (2018) 2018:9278526. doi: 10.1155/2018/9278526
12. Zhao W, Zhang J, Song Y, Sun L, Zheng M, Yin H, et al. Irreversible fatal contrast-induced encephalopathy: a case report. *BMC Neurol.* (2019) 19:46. doi: 10.1186/s12883-019-1279-5
13. Lasser EC, Berry CC, Talner LB, Santini LC, Lang EK, Gerber FH, et al. Pretreatment with corticosteroids to alleviate reactions to intravenous contrast material. *N Engl J Med.* (1987) 317:845–9. doi: 10.1056/NEJM198710013171401
14. Clark BA, Kim D, Epstein FH. Endothelin and atrial natriuretic peptide levels following radiocontrast exposure in humans. *Am J Kidney Dis.* (1997) 30:82–6. doi: 10.1016/S0272-6386(97)90568-0
15. Alakbarzade V, Pereira AC. Cerebral catheter angiography and its complications. *Pract Neurol.* (2018) 18:393–8. doi: 10.1136/practneurol-2018-001986
16. Teleanu DM, Chircov C, Grumezescu AM, Volceanov A, Teleanu RI. Contrast agents delivery: an Up-to-date review of nanodiagnostics in neuroimaging. *Nanomaterials (Basel).* (2019) 9:542. doi: 10.3390/nano9040542
17. Ganau M, Syrmos NC, D'Arco F, Ganau L, Chibbaro S, Prisco L, et al. Enhancing contrast agents and radiotracers performance through hyaluronic acid-coating in neuroradiology and nuclear medicine. *J Nucl. Med.* (2017) 20:166–8. doi: 10.1967/s002449910558

Conflict of Interest: The authors declare that the research was conducted in the absence of any commercial or financial relationships that could be construed as a potential conflict of interest.

frontiers in Surgery

CASE REPORT
published: 06 August 2021
doi: 10.3389/fsurg.2021.671423

Case Report: High-Definition 4K-3D Exoscope for Removal of an Orbital Cavernous Hemangioma Using a Transpalpebral Approach

Stefano Peron[1*†], *Stefano Paulli*[2†] *and Roberto Stefini*[1]

[1] Department of Neurosurgery, Azienda Socio Sanitaria Territoriale (ASST) Ovest Milanese - Legnano Hospital, Milan, Italy, [2] Department of Maxillofacial Surgery, Azienda Socio Sanitaria Territoriale (ASST) Ovest Milanese - Legnano Hospital, Milan, Italy

Background: Cavernous hemangioma, also known as cavernous vascular malformation (CVM), is the most common primary lesion of the orbit in adults. The management of these lesions is challenging and is strongly dependent on their location, as well as the patient's symptoms and expectations. The trans-palpebral approach is currently used in surgery for orbital tumors, anterior skull base tumors, and even more, orbital reconstruction, because of its well-demonstrated esthetic advantages. Similarly, the use of magnification can be provided by surgical loupes, microscope, or more recently, endoscope, which is well-documented for its advantages in terms of minimal invasiveness and safety. In the last years, the use of exoscopes in microsurgery has been proposed due to their greater and sharper intraoperative magnification, but never for the removal of orbital tumors.

Clinical Presentation: We describe a case of a 38-year-old woman with a right orbital intraconic CVM removed using an inferior transpalpebral approach performed under 4K-3-dimensional (4K-3D) exoscopic vision. Navigation and ultrasound were also used, with the former allowing better identification of the lesion within the orbit and the second overcoming the limitations of navigation, in terms of the retraction on the ocular globe before or just after periorbital incision.

Conclusion: The use of a 4K-3D exoscope allowed us to perform the surgery safely, thanks to the high magnification and definition of anatomical details, with the surgeon operating in an upright, comfortable position. The CVM was completely removed with excellent results from both functional and esthetic points of view.

Keywords: 4K-3D exoscope, navigation, orbital cavernous venous malformation, transpalpebral approach, ultrasound

OPEN ACCESS

Edited by:
Marco Cenzato, Niguarda Ca' Granda Hospital, Italy

Reviewed by:
Francesco Acerbi, Fondazione IRCCS Istituto Neurologio Carlo Besta, Italy
Davide Locatelli, Neurosurgey University Varese, Italy

***Correspondence:**
Stefano Peron
stefano.peron@asst-ovestmi.it

†These authors have contributed equally to this work and share first authorship

Specialty section:
This article was submitted to Neurosurgery, a section of the journal Frontiers in Surgery

Received: *23 February 2021*
Accepted: *07 July 2021*
Published: *06 August 2021*

Citation:
Peron S, Paulli S and Stefini R (2021) Case Report: High-Definition 4K-3D Exoscope for Removal of an Orbital Cavernous Hemangioma Using a Transpalpebral Approach. Front. Surg. 8:671423. doi: 10.3389/fsurg.2021.671423

INTRODUCTION

Cavernous venous malformation (CVM), also called cavernous hemangioma, is a benign, well-capsulated, vascular malformation, representing the most common primary orbital lesion of adults, with an incidence between 14.5 and 21.3% of all orbital tumors (1, 2). These lesions occur more often in women with clinical symptoms appearing typically in the fourth and fifth decades of life.

The most common sign of CVM is progressive axial proptosis due to the typical involvement of the intraconic orbital space. Optic nerve damage and other signs of orbital disturbance, such as visual impairment or diplopia, may be detected, but with a variable degree and frequency. The risk of orbital CVM rupture is very low, although, it is a described cause of non-traumatic retro-orbital hemorrhage.

Magnetic resonance imaging (MRI) of the orbits is the most important exam for correct diagnosis, with a combination of MRI, ultrasound, and computed tomography being accurate to precisely define the lesion in almost all cases (3).

Different surgical techniques have been proposed to remove these lesions, with lateral orbitotomy and anterior transconjunctival, or transpalpebral approaches as the most preferred for lateral CVMs, and an endoscopic endonasal approach is an effective and attractive alternative for medial CVMs (3–5).

Nonetheless, dealing with a small anatomical compartment with many delicate structures such as the orbit, all procedures for removal of intraconic lesions, either by trans-cranial or trans-palpebral approaches, require a magnified view of the anatomical details, which are traditionally provided by loupes or microscope.

In recent years, thanks to developments in surgical technology with procedures performed on head-up displays, exoscopes have also been introduced as an alternative or to assist microscopic vision.

To date, the use of the exoscope in surgery has been reported in the literature for cranial, spine, and otologic surgery (6–11). However, the use of a 4K-3D exoscopic system in a transpalpebral approach to the retro-orbital space has not yet been described.

CASE PRESENTATION

A 38-year-old woman presented to the maxillofacial surgery clinic of the Department of Neurosciences at ASST Ovest Milanese complaining of mild proptosis of the right eye and minimal binocular diplopia in the right gaze, which had appeared a few months earlier.

MRI of the orbits showed an enhanced, T2-hyperintense, T1-isointense, intraconic lesion in the inferior lateral part of the right orbit just behind the ocular globe (**Figures 1A,B**).

Preoperatively, the patient underwent contrast-enhanced MRI with volumetric acquisition (1–1.20-mm slice thickness) for 3D reconstruction. The woman underwent surgery to remove the lesion with a transpalpebral approach through the right inferior eyelid. The surgical procedure was performed by the second author (S.P.), who has substantial experience in transpalpebral approaches for orbital tumors and orbital reconstruction.

The patient was placed in a supine position, with the head slightly rotated to the left side.

The entire surgical procedure, starting from the skin incision, was performed under 4K-3D exoscopic vision. After the skin incision of the lower eyelid, a blunt dissection to expose the inferior orbital rim up to the lateral canthus was performed, and then gently dissecting the periorbit from the lateral wall.

Minimally-invasive removal of the lesion was aided by the use of intraoperative navigation (electromagnetic StealthStation S8, Medtronic) and ultrasound (BK 5000®, BK Medical) in order to limit retraction on the ocular globe, and to reduce the incision of the periorbita and manipulation of intraconic structures within the periorbital fat (**Figure 2**). The main steps of the surgical procedure are clearly visible in the attached Video as well as summarized in **Figure 3**.

There were no complications during the procedure.

The surgical time was comparable to that of the same procedures previously performed by the same surgeon with loupes.

Postoperative MRI showed complete removal of the lesion (**Figure 1C**). The esthetic result for the patient was optimal (**Figure 1D**). Histological examination returned a diagnosis of cavernous hemangioma.

EXOSCOPE CHARACTERISTICS

Our exoscope (ORBEYE, Sony Olympus Medical Solutions Inc., Tokyo, Japan) is equipped with an external 4K-3D orbital camera with a semi-robotic arm, which allows positioning above the operating field in multiple angles and a high optical zoom, with instant digital zoom for extra-detailed vision.

In addition to the camera, there are two medical 4K-3D monitors with 55-inch and 31-inch screens, respectively. The monitors can be positioned anywhere inside the operating room (OR) for the convenience of both surgeons and scrub nurses. Polarized 3D glasses are required to view the monitor images in 3D.

For better understanding, the OR setting in our clinical case is shown in **Figure 4**.

DISCUSSION

It is widely accepted that symptomatic benign neoplasms of the orbit require treatment, with surgical resection as the treatment of choice for most CVMs. While the management of extraconic lesions can be easier, intraconic pathologies require a certain degree of expertise in manipulating the delicate muscle and nerve structures within the intraconic space.

The success of the procedure depends on the localization of the CVM in particular with respect to the optic nerve and the extrinsic musculature. For this reason, the choice of the surgical approach to be adopted depends not only on the site of the lesion, but also on the personal experience of the surgeon, always with the aim of less invasiveness and, consequently, of a better functional and esthetic result (3, 4).

It is thus clear that the best approach should ensure adequate visualization of the intraorbital muscular and neurovascular structures and the lesion, minimizing manipulation of the former.

Currently, the lateral aspect of the orbital content is generally approached *via* transcranial routes, such as fronto-orbitozygomatic, fronto-temporal, or supraorbital craniotomies,

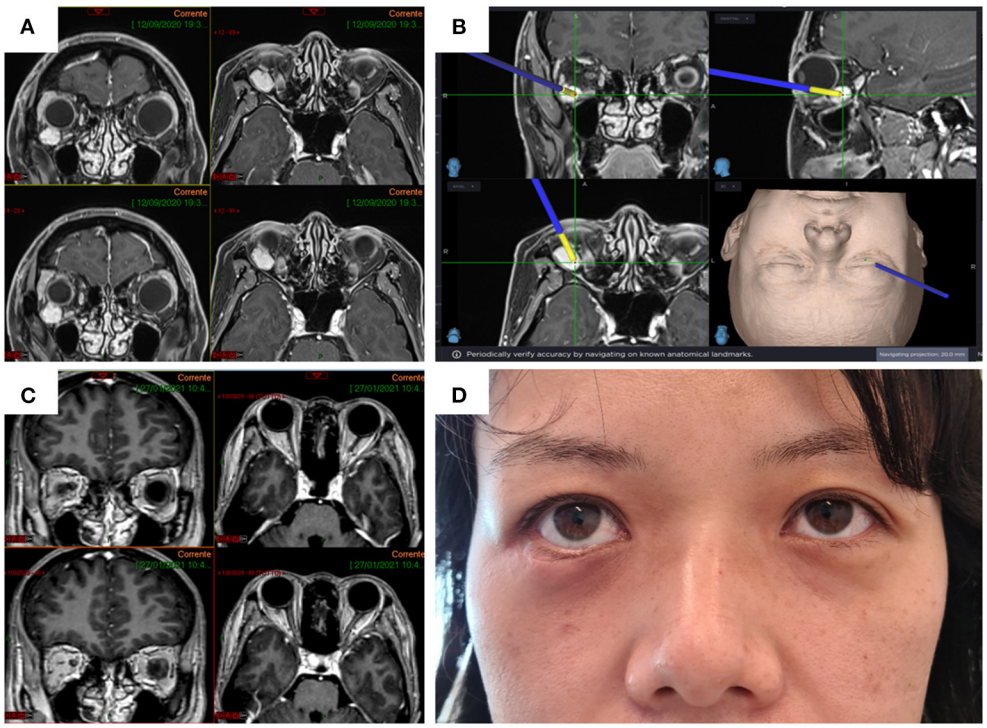

FIGURE 1 | Preoperative enhanced MRI of the orbits (left, axial; right, coronal) showing the cavernous hemangioma located in the inferior lateral part of the right orbital intraconic space **(A)** and detail of tumor localization using navigation **(B)**. Postoperative MRI showing complete removal of the hemangioma **(C)**. The transpalpebral approach allows a minimally invasive access to the retro-orbital space ensuring excellent esthetic and functional results **(D)**.

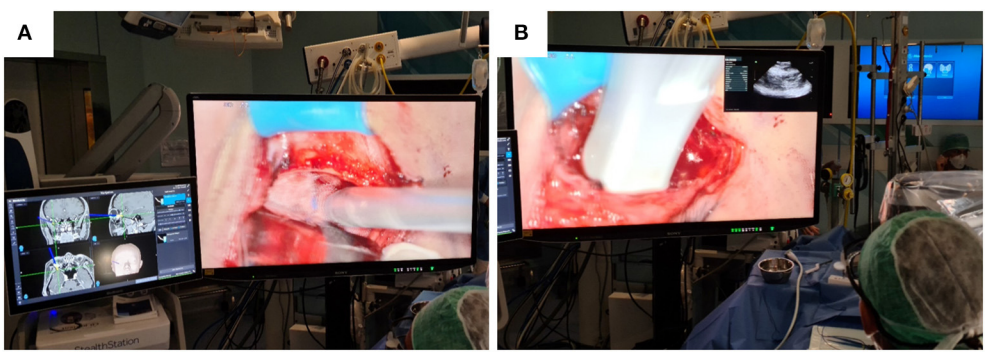

FIGURE 2 | On the 55-inch monitor, the navigation device **(A)** and ultrasound probe **(B)** used for precise localization of the hemangioma inside the periorbita are clearly visible. The PiP mode **(B)** allows the surgeon to control the position of the ultrasound probe without having to look away from the operating field.

especially for lesions located posteriorly, and *via* lateral orbitotomy for more anterior ones (3, 4).

In recent years, the endoscopic transnasal approach to the orbital cavity has gained interest as a feasible and safe surgical technique for the management of CVMs located in the inferior medial and superior medial part of the orbit. In a review, Lenzi reported on 17 cases of CVMs, all located in the inferior medial part of the orbit, which were removed through an endonasal endoscopic approach, with few and minor complications except for a case of enophthalmos requiring surgical revision (12).

The advent of endoscopic approaches in orbital surgery has introduced the concept of less invasiveness, better esthetic result, and gain in terms of visualization. In this regard, Dallan et al. (13) emphasized how endoscopic visualization allows high magnification with angled view, if required, and with the light close to the structures, for better identification of anatomical details and, consequently, more precise surgery.

These authors concluded that new technologies, such as 3D screens, will be able to ensure even better visualization, and manipulation of orbital structures,

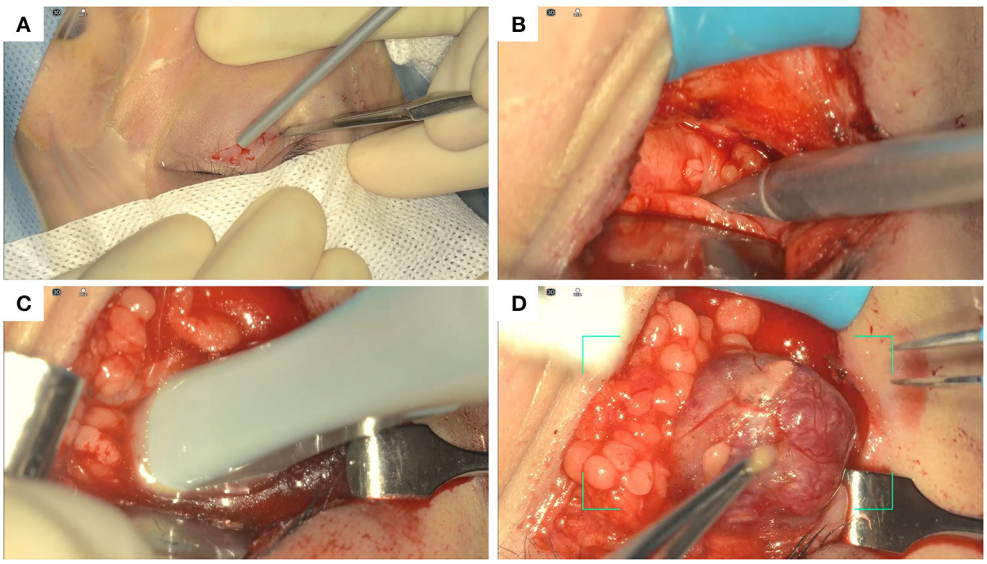

FIGURE 3 | Summary of the main surgical steps. Skin incision of the lower eyelid **(A)**; localization of the hemangioma before the opening of the periorbit using navigation **(B)**; localization of the hemangioma within the periorbit using ultrasound **(C)**; blunt dissection and removal of the hemangioma **(D)**.

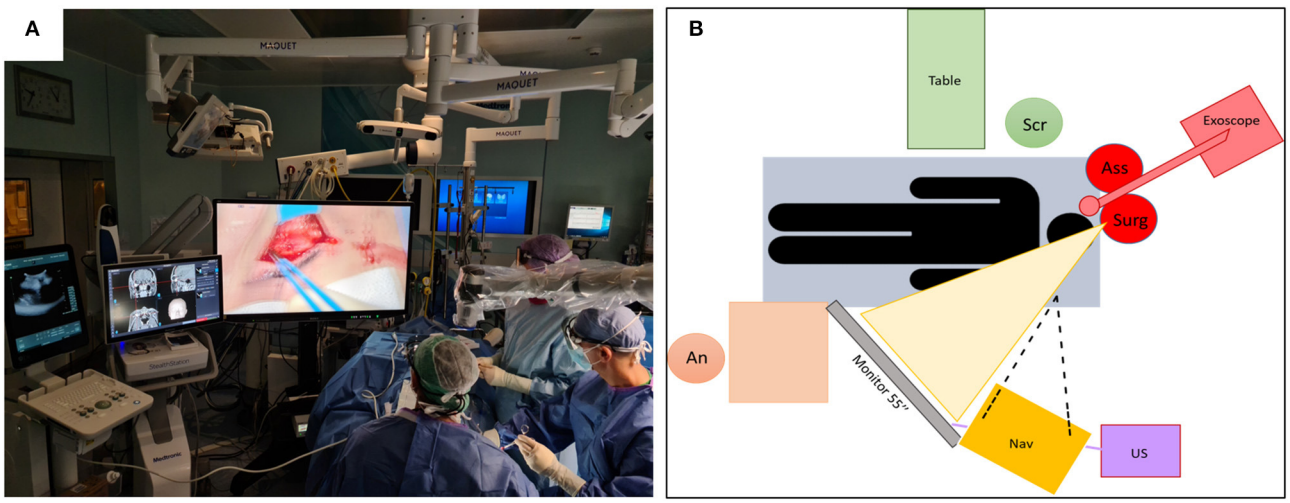

FIGURE 4 | Placement of the technologies in use (4K-3D camera, 55-inch monitor, navigator, and ultrasound) and staff within the OR during surgery for right transpalpebral approach **(A)** and scheme **(B)**. Note the comfortable position of the surgeon who can operate while looking at the monitor with the head in an upright position.

working with the principles, more familiar to most surgeons, of microsurgery.

Over the years, transpalpebral and transconjunctival approaches, with or without osteotomies, have gained increasingly more space in orbital tumor and anterior skull base surgery due to their minimal invasiveness and optimal esthetic and functional outcomes (5, 13–15).

In case of CVMs located in the inferior lateral or superior lateral aspect of the intraconic space, the trans-eyelid approach is usually preferred, avoiding lateral or superior orbitotomy according to its position.

Zoli et al. recently performed a review of endonasal and transpalpebral endoscopic approaches for removal of orbital lesions, most of which were cavernous hemangiomas. They selected 23 lesions, of which 16, located medially, were removed by an endonasal approach and 7, located laterally, by a transpalpebral approach. In transpalpebral access, the use of an exoscope is reported in the initial part (i.e., skin incision) of the procedure and then abandoned in favor of the endoscope. The advantages of ultrasound in localizing the lesion within the orbit is also reported (5). In that publication, it was highlighted that knowledge of both endoscopic, endonasal, and transpalpebral

techniques allows for 360° management of the anatomy of the orbit and thus the possibility to remove orbital lesions wherever they are located, whether lateral or medial, extraconic or intraconic.

Our expertise in transpalpebral approaches has grown over time thanks to the collaboration between neurosurgeons and maxillofacial surgeons, with the latter being more experienced in these approaches, mainly used by them in reconstructive surgery for orbital fractures. Experience to date suggests that trans-eyelid (superior or inferior) approaches provide adequate exposure of the entire orbital region, both medial and lateral, as well as inferior and superior.

In particular, as in the clinical case reported, an inferior transpalpebral approach offers complete extraconic exposure of the orbital floor up to the inferior third of the medial or lateral wall and posteriorly up to the inferior orbital fissure, enabling, by incision of periorbita, access to intraconic contents.

In daily surgical practice, where the endoscopic approach is not chosen, due to the surgeon's preference or lack of confidence with this technique, transpalpebral approaches are usually performed with visualization provided by loupes or operating microscope (OM). In recent years, exoscopes have been proposed as a possible alternative to the OM by offering very high magnification, high quality images, superior ergonomics, and ease of use. In the recent literature, different procedures have been performed with 4K-2D or 4K-3D exoscopic systems, in particular in plastic surgery as well as cranial, spine, and otologic surgery (6–11). A case of endoscopic dacryocystorhinostomy assisted by a 3D-2D exoscope has also been reported (16). These telescopes aim to combine the advantages of the OM with those of the endoscope, and at the same time, try to overcome the limits of both, such as the poor ease of movement and ability to adapt to the operating room setting, limits in the depth of field, and poor ergonomics for surgeons.

The high-resolution 4K-3D images of the orbital structures provided by the exoscope, starting with skin incision, make surgery more accurate, with optimal perception of depth, colors, and magnification. The high quality of the images, which allows precise manipulation of orbital structures, can be appreciated by watching the 4K-2D video of our case.

It should not be forgotten that the exoscope offers high quality, 4K-3D images not only for surgeons, but for everyone who watches the 55-inch or 31-inch monitor using polarized glasses. This advantage can also be used for educational purposes for students and residents, because the use of external monitors and glasses gives them the same high-resolution view as the surgeon.

An important disadvantage in using the exoscope is the difficulty in assisting the surgeon from a position of the assistant (5). This disadvantage is greatly reduced in our case, where the surgeon and the assistant worked side by side and therefore are able to look at the same 55-inch monitor placed in front of them, ensuring a precise manipulation for the assistant as well.

Moreover, the exoscope allows for neutral cervical spine posture by placing the monitor at eye level, directly in front of the surgeon, or at any angle desired. This ensures an upright and neutral posture, thus avoiding long hours spent in a fixed position looking through a microscope, or with the head bent over the patient wearing loupes.

We have no experience yet on the use of the exoscope in deep fields in orbital surgery. However, we do have extensive experience in this regard in intracranial surgery, e.g., for deep-seated lesions and with very angled surgical corridors, where the exoscope, compared to other visualization technologies and thanks to the possibility of easily tilting the camera, offers even in these cases the advantage of a clear view without forcing the surgeon to assume uncomfortable positions.

Furthermore, the exoscope allows more space around the operating table and patient. This is especially useful in procedures where multiple equipment is required, e.g., navigation devices or ultrasound, as in our surgical case.

The use of navigation allowed us to reduce the invasiveness of the procedure by addressing the tumor within the orbit. Even more, the choice of using ultrasound was driven by the desire to further reduce the margin of error before and just after periorbital incision due to the medial displacement of anatomical landmarks, and consequently poor navigation reliability, during ocular globe retraction. In fact, the use of a small size, high-frequency probe allowed us to limit even minimal errors of navigation, ensuring gentle manipulation of the delicate intraconic structures within periorbital fat.

In addition, throughout the time of hemangioma removal, the surgeon was able to look at the ultrasound images directly on the 55-inch monitor thanks to the Picture-in-Picture (PiP) mode offered by the exoscope (**Figure 2**). As reported by the surgeon, this was very useful because it allowed him to avoid frequently looking away from the operating field toward the ultrasound screen, reducing the risk of applying too much pressure on the ocular globe or minimal probe movement resulting in less accuracy in identifying the CVM within the intraconic space.

A slight difficulty in gaining a proprioceptive ability when manipulating the instruments by looking at the 3D monitor can be noticed by a surgeon who is unfamiliar with this technology. In our experience, the adaptation time is usually short and easily appreciable already during the same procedure. Indeed, as for all new technologies, a learning curve is required even for the exoscope.

In our opinion, the exoscope, by offering 4K-3D images with very high-definition and very high zoom, allows detailed anatomical visualization. This is very effective in procedures where high magnification is required, as in a minimal invasive approach to a small compartment such as the orbit. Moreover, the exoscope allows surgeons to operate in a comfortable position, even for extended periods, with all the images required in the same monitor. The use of navigation and ultrasound, which can be easily integrated with the exoscope thanks to the large space available above the operating field, makes the trans-eyelid approach even more minimally invasive, targeting surgical dissection, and consequently, minimizing manipulation of orbital intraconic structures, with optimal results for the patient from both functional and esthetic points of view.

DATA AVAILABILITY STATEMENT

The original contributions presented in the study are included in the article/**Supplementary Material**, further inquiries can be directed to the corresponding author/s.

ETHICS STATEMENT

Ethical review and approval was not required for the study on human participants in accordance with the local legislation and institutional requirements. The patients/participants provided their written informed consent to participate in this study. Written informed consent was obtained from the individual(s) for the publication of any potentially identifiable images or data included in this article.

AUTHOR CONTRIBUTIONS

SPe and SPa designed the study, wrote the manuscript, and collected the data and images. RS reviewed the manuscript. All authors gave their final approval before submission, contributed to the article and approved the submitted version.

SUPPLEMENTARY MATERIAL

The Supplementary Material for this article can be found online at: https://www.frontiersin.org/articles/10.3389/fsurg.2021.671423/full#supplementary-material

Supplementary Video 1 | Image definition and high magnification of anatomical details, as well as the use of navigation and ultrasound devices, can be clearly noticed and appreciated in this 4K-3D video.

REFERENCES

1. Zhang L, Li X, Tang F, Gan L, Wei X. Diagnostic imaging methods and comparative analysis of orbital cavernous hemangioma. *Front Oncol.* (2020) 10:577452. doi: 10.3389/fonc.2020.577452
2. Shields JA, Shields CL, Scartozzi R. Survey of 1264 patients with orbital tumors and simulating lesions: the 2002 montgomery lecture, part 1. *Ophthalmology.* (2004) 111:997–1008. doi: 10.1016/j.ophtha.2003.01.002
3. Calandriello L, Grimaldi G, Petrone G, Rigante M, Petroni S, Riso M, et al. Cavernous venous malformation (cavernous hemangioma) of the orbit: current concepts and a review of the literature. *Surv Ophthalmol.* (2017) 62:393–403. doi: 10.1016/j.survophthal.2017.01.004
4. Montano N, Lauretti L, D'Alessandris QG, Rigante M, Pignotti F, Olivi A, et al. Orbital tumors: report of 70 surgically treated cases. *World Neurosurg.* (2018) 119:e449–58. doi: 10.1016/j.wneu.2018.07.181
5. Zoli M, Sollini G, Milanese L, La Corte E, Rustici A, Guaraldi F, et al. Endoscopic approaches to orbital lesions: case 326 series and systematic literature review. *J Neurosurg.* (2020) 1–13. doi: 10.3171/2019.10.JNS192138
6. Murai Y, Sato S, Yui K, Morimoto D, Ozeki T, YamaguchiM, et al. Preliminary clinical microneurosurgical experience with the 4K3-Dimensional Microvideoscope (ORBEYE) system for microneurological surgery: observation study. *Oper Neurosurg (Hagerstown).* (2019) 16:707–16. doi: 10.1093/ons/opy277
7. Rubini A, Di Gioia S, Marchioni D. 3D exoscopic surgery of lateral skull base. *Eur Arch Otorhinolaryngol.* (2020) 277:687–94. doi: 10.1007/s00405-019-05736-7
8. Kanzaki S, Takahashi S, Toda M, Yoshida K, Ogawa K. Pros and cons of the exoscope for otologic surgery [published online ahead of print, 2020 Sep 29]. *Surg Innov.* (2020) 28:360–5. doi: 10.1177/1553350620964151
9. Mamelak AN, Danielpour M, Black KL, Hagike M, Berci G. A high-definition exoscope system for neurosurgery and other microsurgical disciplines: preliminary report. *Surg Innov.* (2008) 15:38–46. doi: 10.1177/1553350608315954
10. Krishnan KG, Schöller K, Uhl E. Application of a compact high-definition exoscope for illumination and magnification in high-precision surgical procedures. *World Neurosurg.* (2017) 97:652–60. doi: 10.1016/j.wneu.2016.09.037
11. Kwan K, Schneider JR, Du V, Falting L, Boockvar JA, Oren J, et al. Lessons learned using a high-definition 3-dimensional exoscope for spinal surgery. *Oper Neurosurg.* (2019) 16:619–25. doi: 10.1093/ons/opy196
12. Lenzi R, Bleier BS, Felisati G, Muscatello L. Purely endoscopic trans-nasal management of orbital intraconal cavernous haemangiomas: a systematic review of the literature. *Eur Arch Otorhinolaryngol.* (2016) 273:2319–22. doi: 10.1007/s00405-015-3733-3
13. Dallan I, Castelnuovo P, Turri-Zanoni M, Fiacchini G, Locatelli D, Battaglia P, et al. Transorbital endoscopic assisted management of intraorbital lesions: lessons learned from our first 9 cases. *Rhinology.* (2016) 54:247–53. doi: 10.4193/Rhin15.237
14. Dzhindzhikhadze RS, Dreval' ON, Lazarev VA, Polyakov AV. Transpal'pebral'nyi keyhole-dostup v khirurgii kavernom orbity: sluchai iz praktiki i obzor literatury [The transpalpebral keyhole approach in surgery of orbital cavernomas: a case report and literature review]. *Zh Vopr Neirokhir Im N N Burdenko.* (2018) 82:73–80. doi: 10.17116/neiro201882373
15. Abdel Aziz KM, Bhatia S, Tantawy MH, Sekula R, Keller JT, Froelich S, et al. Minimally invasive transpalpebral "eyelid" approach to the anterior cranial base. *Neurosurgery.* (2011) 69(Suppl. 2):ons195–207. doi: 10.1227/NEU.0b013e31821c3ea3
16. Pirola F, Spriano G, Malvezzi L. Preliminary experience with exoscope in lacrimal surgery. *Eur Arch Otorhinolaryngol.* (2021) 278:285–8. doi: 10.1007/s00405-020-06379-9

Conflict of Interest: The authors declare that the research was conducted in the absence of any commercial or financial relationships that could be construed as a potential conflict of interest.

Publisher's Note: All claims expressed in this article are solely those of the authors and do not necessarily represent those of their affiliated organizations, or those of the publisher, the editors and the reviewers. Any product that may be evaluated in this article, or claim that may be made by its manufacturer, is not guaranteed or endorsed by the publisher.

frontiers in Surgery

CASE REPORT
published: 23 August 2021
doi: 10.3389/fsurg.2021.607417

Ventriculosternal Shunt for the Treatment of Idiopathic Normal Pressure Hydrocephalus: A Case Report

Xinxia Guo, Abdul Malik Popal, Zhoule Zhu, Chengwei Cai, Jingquan Lin, Hongjie Jiang, Zhe Zheng, Jianmin Zhang, Anwen Shao and Junming Zhu**

Department of Neurosurgery, The Second Affiliated Hospital, School of Medicine, Zhejiang University, Hangzhou, China

Background: Conventional corticospinal fluid (CSF) diversion surgery for idiopathic normal pressure hydrocephalus (iNPH) includes ventriculoperitoneal shunt and ventriculoatrial shunt. Ventriculosternal (VS) shunt may be considered if both the abdominal cavity and atrium are not feasible.

Methods: A 76-year-old woman was admitted to our hospital with gait disturbance and urinary incontinence for 2 years, and the condition aggravated in the last 1 month. Based on clinical assessment and imaging findings, the patient was diagnosed with iNPH, with surgical indications. She was on peritoneal dialysis for chronic renal failure, and a cardiac Doppler echocardiogram showed enlargement of the left atrium and decreased diastolic function of the left ventricle. Due to these conditions, we chose the sternum as the vessel for CSF absorption and performed VS shunt.

Results: No swelling, exudation, and effusion were found in the suprasternal fossa. Gait disturbance and urinary incontinence improved significantly immediately and 1 week after surgery, respectively. No shunt-related complication was reported at 16 months follow-up.

Conclusion: This case demonstrated VS shunting as a feasible and alternative for the management of hydrocephalus.

Keywords: cerebrospinal fluid shunting, ventriculosternal shunting, normal pressure hydrocephalus, intraosseous absorption, case

OPEN ACCESS

Edited by:
Massimiliano Zingales, University of Palermo, Italy

Reviewed by:
Emanuela Bologna, University of Palermo, Italy
Mario Ganau, Oxford University Hospitals NHS Trust, United Kingdom

****Correspondence:***
Anwen Shao
21118116@zju.edu.cn
Junming Zhu
dr.zhujunming@zju.edu.cn

Specialty section:
This article was submitted to Neurosurgery, a section of the journal Frontiers in Surgery

Received: *17 September 2020*
Accepted: *27 July 2021*
Published: *23 August 2021*

Citation:
Guo X, Popal AM, Zhu Z, Cai C, Lin J, Jiang H, Zheng Z, Zhang J, Shao A and Zhu J (2021) Ventriculosternal Shunt for the Treatment of Idiopathic Normal Pressure Hydrocephalus: A Case Report. Front. Surg. 8:607417. doi: 10.3389/fsurg.2021.607417

INTRODUCTION

Idiopathic normal pressure hydrocephalus (iNPH) is a common neurodegenerative disease among the elderly characterized by gait disturbance, cognitive decline, and urinary incontinence (1). In the treatment of iNPH, ventriculoperitoneal (VP) shunt, and ventriculoatrial (VA) shunt are the most commonly performed procedures to divert corticospinal fluid (CSF), both of which result in significant improvements of functional outcomes (2, 3). However, in certain patients who have peritonitis, adhesion, and cardiac insufficiency, there seems to be no standard alternative surgical method to be considered. Recently, Ming Woo et al. reported a case about ventriculosternal (VS) shunt for the management of hydrocephalus, which provided a potential option for these patients (4). In the past, the sternum has been used for volume resuscitation in an emergency situation. Macnab et al. showed that the sternal gravity infusion flow could reach 80 ml/min,

and the injector injection flow could reach 150 ml/min by testing the sternum as an alternative site for fluid resuscitation (5). Tubbs et al. demonstrated that the sternum is a plausible receptacle for CSF diversion by an experimental work (6). In this work, we report a case of iNPH for whom VS shunt was performed, and we further illustrate the feasibility of VS shunt.

CASE PRESENTATION

A 76-year-old woman was admitted to our hospital complaining of progressive gait disturbance, continuous urinary incontinence, and gradual decline in cognitive function for 2 years. She was diagnosed with Type 2 diabetes for 5 years and hypertension for 26 years, and she was on peritoneal dialysis for chronic renal failure (Primary IgA nephropathy) for 13 months. On admission, a B-ultrasound of the urinary system showed that both the kidneys were atrophied. The serum creatinine and urea values were 505 umol/L and 11.53 md/dL, respectively. Magnetic resonance imaging (MRI) showed disproportionately enlarged subarachnoid space hydrocephalus (7, 8) (**Figures 1A,B**) and dilated cerebral ventricles and cisterns, with no apparent obstacle (**Figure 1B**). Evans Index was 0.32 (**Figure 1B**). The iNPH grading scale (iNPHGS) (9) showed 2 points in cognitive impairment, 3 points in gait assessment, and 3 points in the urinary disturbance domain (**Table 1**). The mini-mental state examination (MMSE) (10)score was 23 of 30. The CSF of the tap test of the patient (11), which rated with the 10-m up test and 5-meter up & go test before, and 8 and 72 h after 30 ml of CSF removal (CSF pressure was 160 mmHg), showed improvement (**Table 2**). Laboratory studies of CFS were normal. A diagnosis of iNPH was made. Surgical treatment was indicated in this patient. However, she was on peritoneal dialysis for chronic renal failure, and a cardiac Doppler echocardiogram showed enlargement of the left atrium and decreased diastolic function of the left ventricle. Due to these conditions, and after careful evaluation, we chose the sternum as the vessel for CSF absorption. Informed consent was obtained from the patient and her family.

SURGICAL PROCEDURE

The patient was given general anesthesia and took the supine position with a slightly raised right shoulder and back. After skin preparation and draping, an arc skin incision was made at the sternal notch (**Figure 2A**), and then subcutaneous tissues were separated until the anterior edge of the bilateral sternocleidomastoid muscle and the superior border of the sternum were exposed. Next, a tunnel, approximately 3 cm long and parallel to the sternum, was drilled through the sternal manubrium by a high-speed drill (**Figure 2B**). An indwelling needle containing 10 mL of saline was used to confirm the length of the tunnel and test the intraosseous absorbability (10 mL injected in 3 min; **Figure 2C**). A subcutaneous tunnel was made from the scalp incision to the sternal notch incision with a metal strip. An adjustable pressure antisiphon shunting catheter (ProGAV 2.0, Aesculap), parallel to the sagittal line, was then inserted through the right frontal bone burr hole at the Kocher's point. The adjustable gravity valve was connected to the ventricular catheter, pressure preadjusted to 120 mm H_2O. The distal catheter was placed into the sternal manubrium, and a reserved loop was fixed at the sternum tendon of the sternocleidomastoid muscle (**Figure 2D**). After confirming that the shunt tube was unobstructed, the tunnel entrance was sealed with bone wax to prevent CSF leak. Tissue and skin of each

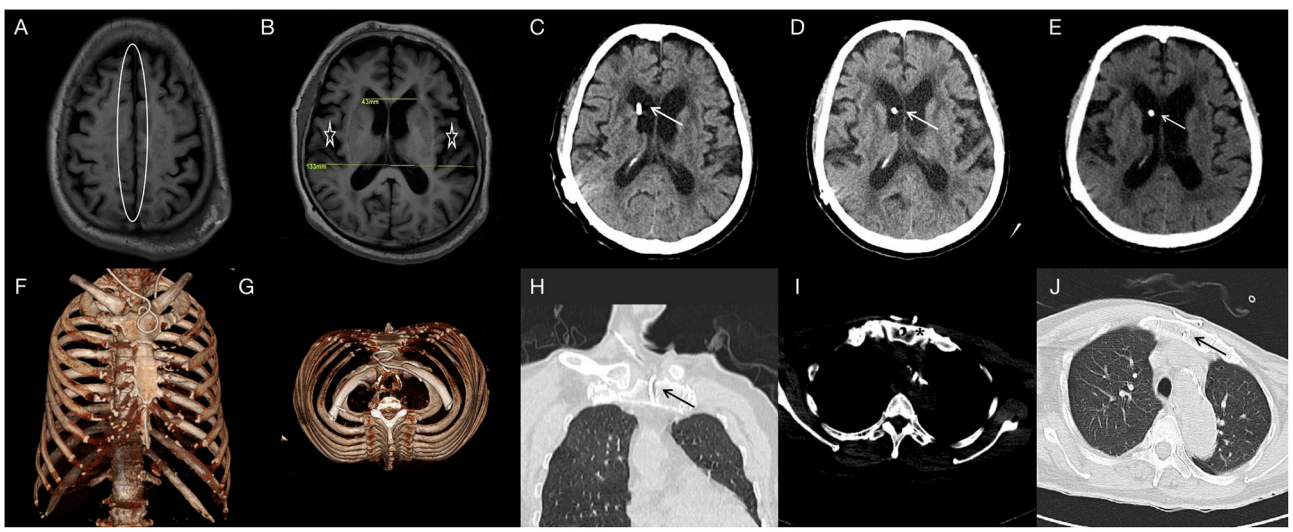

FIGURE 1 | T1FLAIR **(A,B)** brain MRI showing the narrowed sulcal spaces at the vertex (oval) and the enlarged ventricles of the brain and lateral cracks(asterisk) (DESH); Evans Index was 0.32. Two-month CT-**(C)**, 6-month CT-**(D)** and 16-month CT-**(E)** brain scan showing the catheter in position and the hydrocephalus is relieved**.** One-week three-dimensional reconstructed CT- **(F,G)** scan of the thorax showing the distal catheter *in situ*. Two-month CT- **(H,I)** and 16-month CT-**(J)** thorax scan showing the sternum is intact and the distal catheter *in situ*.

TABLE 1 | iNPH grading scale.

Grade	Definition	Before surgery	After surgery (one week)
Cognitive impairment			
0	Normal		√
1	Complaints of amnesia or inattention but no objective memory and attentional impairment	√	
2	Existence of amnesia or inattention but no disorientation of time and place		
3	Existence of disorientation of time and place but the conversation is possible		
4	Disorientation for the situation or meaningful conversation impossible		
Gait disturbance			
0	Normal		
1	complaints of dizziness of drift and dysplasia but no objective gait disturbance		√
2	unstable but independent gait		
3	walking with any support	√	
4	walking not possible		
Urinary disturbance			
0	Normal		
1	pollakiuria or urinary urgency		√
2	occasional urinary incontinence (1–3 or more times per week but less than once per day)		
3	continuous urinary incontinence (1 or more times per day)	√	
4	bladder function is almost or entirely deficient		

Positive outcomes:
(1) For gait, a positive outcome was defined as >1-point improvement in the gait section of iNPHGS.
(2) For cognition, a positive outcome was defined as >1-point improvement in the cognition section of iNPHGS.
(3) For urinary incontinence, a positive outcome was defined as >1-point improvement in the urinary incontinence section of iNPHGS.

TABLE 2 | The CSF tap test results.

Test	Before the CSF Tap Test	After 8 h	Improvement	After 72 h	Improvement
5 m Up & Go test	32 s, 32 steps	34 s, 26 steps	−6.3*, 18.8%	21 s, 21 steps	34.4, 34.4%
10 m up test	19 s, 30 steps	14 s, 23 steps	26.3, 23.3%	13 s, 21 steps	31.6, 30.0%

Positive outcomes:
(1) 10 m up test: One parameter was improved more than 20%, or two parameters were improved more than 10%.
(2) 5 m Up & Go test: A more than 10% rate improvement after the CSF Tap Test.
*(3) *The reason for this calculation result may be that the step distance of the patient is widened and the number of steps decreases during the gait test, or it may be caused by artificial measurement errors.*

incision were sutured in layers with absorbable 2-0 polyglactin-910 sutures.

POSTOPERATIVE COURSE

The patient recovered well without fever, headache, and had no shunt-related complications after surgery. No swelling, exudation, and effusion were found in the suprasternal fossa. Laboratory blood studies showed no signs of associated infection. Gait disturbance and urinary incontinence improved significantly 2 days and 1 week after surgery, respectively. The three-dimensional reconstructed thoracic CT scan suggested that the distal catheter was located in an intraosseous tunnel, and there was no complication, such as manubrium sternal fracture, pneumothorax, or mediastinal gas (**Figures 1F,G**). The MMSE score improved to 28 of 30, and the scores of all three domains of the iNPHGS were rated at 1 point (**Table 1**). At the 2-month follow-up, the scores of all three domains of the iNPHGS remained the same. The CT brain scan showed the ventricle size did not dramatically change (12), and the ventricular catheter was in place (**Figure 1C**). The CT thorax scan showed sternum was intact, and there were no shunt-related complications(**Figures 1H,I**). The patient remained in good condition and was free of shunt-related complications at the 6-month and 16-month follow-up (**Figures 1D,E,J**). The episode of care is organized as a timeline in **Figure 3**. At the 16-month postoperative follow-up, the patient did not feel any inconvenience caused by this surgical method.

DISCUSSION

The CFS diversion surgery has four basic components, namely: a proximal catheter, a reservoir, a valve, and a distal catheter (13, 14). In general, the proximal catheter drains CSF from one of the

two lateral cerebral ventricles. The reservoir provides an access to obtain CSF samples and for intracranial pressure monitoring. The valve ensures unidirectional CSF flow into the distal catheter. Traditionally, the distal catheter is tunneled subcutaneously and terminates in a cavity, which can absorb the shunted CSF (13, 15). There are variations in the placement of distal catheters such as peritoneal, atrial, sternum, etc., to adapt to different conditions of patients (15).

In this study, we reported a typical case of iNPH, who was not suitable for routine VP or VA shunt because of cardiac insufficiency and renal failure; so we introduced an alternative called VS shunt. The patient had significant improvement and no obvious complications during the 16-month follow-up.

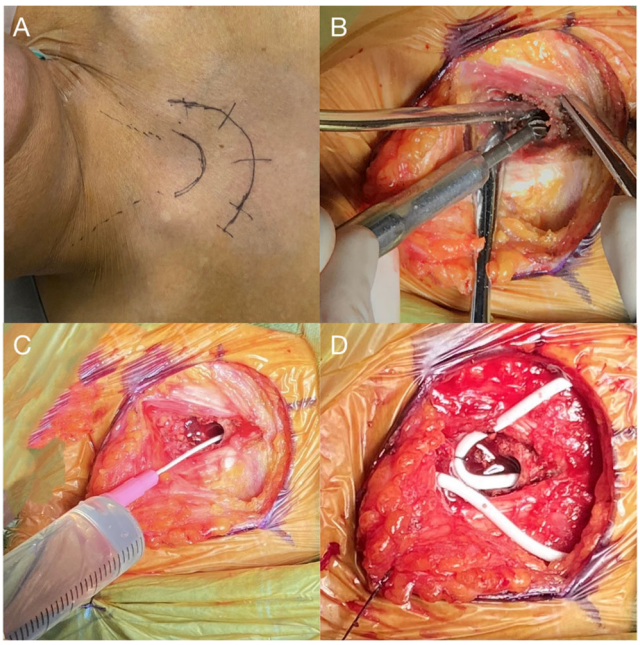

FIGURE 2 | (A) An arc skin incision for a right-sided shunt is marked. **(B)** Drilling of a 3 cm long tunnel parallel to the long axis of the sternum at its midline. **(C)** Indwelling needle placement to confirm the length of the tunnel and intraosseous absorption of 10 ml saline. **(D)** Placement of sternal catheter with a loop fixed at the sternum tendon of the sternocleidomastoid muscle.

Based on the literature, the sternum is ideal for distal catheter placement for the following reasons: (1) Its location is adequately superficial for shunt implantation (4, 16); (2) Its proximity to the skull reduces the risk of pulling and displacement caused by the overlength of the shunt catheter (4, 16); (3) It retains more red bone marrow than the tibia and humerus in adults, allowing better absorption of CSF (4, 16); (4) internal mammary vein and azygos vein, allowing adequate drainage of CSF (4, 17); (5) the post operation fasting time of VS shunt is only 6 h, to avoid patients suffer from thirst, sore throat, and hunger, and also to accelerate the recovery of normal gastrointestinal function; (6) compared with VA shunt, VS shunt avoids serious complications such as atrial thrombosis, arrhythmia or endocarditis, especially in the elderly with cardiac dysfunction.

According to existing researches, the sternum also has been supported as a feasible and alternative drainage vessel in physiology, animal experiments, and clinical cases. Physiologically, the bone marrow cavity contains abundant cavernous venous sinuses, which can communicate with the systemic circulation through the central tube, nourishing vein, and guiding vein (16). Fluids or drugs can quickly enter the circulatory system *via* the bone marrow cavity. A previous work has demonstrated that the sternum can absorb flow rates of up to 150 mL/min (5), and sternal intraosseous infusion applied as a rapid, safe, and effective vascular access when venous punctures failed in emergency treatment in adults (18). According to the above researches, CSF could be rapidly absorbed in the bone marrow cavity.

Ventriculosternal shunt was first proposed by Tubbs et al. based on an exploratory study (6), in which he first injected up to 30 L of water continuously into the manubrium sternum of five fresh human cadavers within 1 h, and no significant fluid overflows, edema, or fluid accumulation were observed in the chest or abdomen. The team then injected saline into the sternum of living rhesus monkeys for 24 h, and the MRI showed no extravascular fluid accumulation. To verify the feasibility of VS

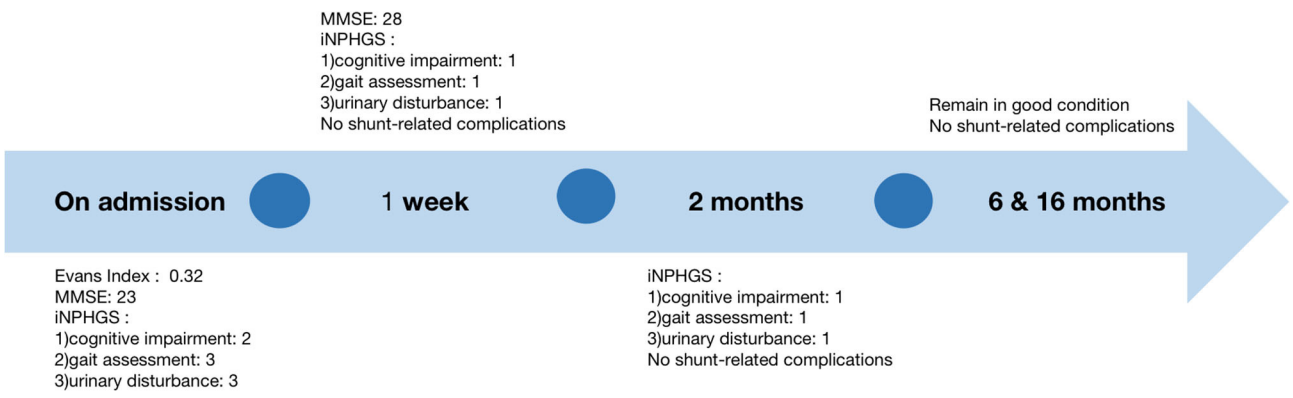

FIGURE 3 | A timeline of the follow-up of the patient.

shunt in large animals, they performed the procedure on two adult pigs. Two weeks after surgery, the conditions of both the pigs were stable without any sign of infection. There was also no evidence of osteomyelitis or CSF exudation in the autopsy. Based on these findings, Tubbs et al. argued that the manubrium sternum was an ideal "CSF container".

The first successful application of VS shunt in the treatment of hydrocephalus was reported by Ming Woo et al. In this case, the physiology and cognition of the patient were recovered to a certain extent and suffered no complications 3 years after the procedure (4). As for details of VS shunt procedure, Ming Woo et al. suggested that the length of the tunnel on the sternal manubrium should be controlled within 4 cm to avoid damage to the brachiocephalic artery by accidental puncture of the posterior sternal cortex or entry into the superior mediastinum (4). The surgeon should be aware that long-term CSF immersion may lead to osteomalacia and pathological fractures. In the later stage, attention should be paid to postoperative scar formation, especially for young patients with a family history of skin scars or dark-skinned patients. Another concern is that long-term CSF immersion may lead to osteomalacia and pathological fractures. They also mentioned the possible contraindications of VS shunt, including tracheotomy, sternal fracture or history of sternotomy, osteogenic insufficiency or severe osteoporosis, local infection, cardiac shunt from right to left, and history of shunt glomerulonephritis (4).

According to our study, we also concluded the following technical notes on VS shunt surgical procedure: (1) thoracotomy design: with the upper sternal fossa as the center, a 2/3 circular incision was formed to expose the upper sternal fossa; (2) sternal tunnel: parallel to the long axis of the sternal manubrium when drilling, with a depth of <4 cm; (3) test the absorption rate of CSF: ensure that 10 mL of saline can be absorbed within 3 min. We found that it could be challenging to test intraosseous absorbability with saline due to bleeding intraoperatively, and for further study, except the potential risks and complications mentioned above by Ming Woo et al., we propose that VS shunt, as with conventional shunt methods, can also develop complications like shunt-related idiopathic intracranial hypertension (IIH), infection, over drainage, and so on (19–21).

Otherwise, ventriculovesical (VV) shunt and ventriculo-cholecystic (VC) shunt have been reported as alternative surgeries for CSF diversion (22–25). However, Shahul Hameed et al. suggested that VV shunt should not be recommended as an alternative to peritoneum or atrium, because of the existing disadvantages, which are: it is a difficult surgical technique, fluid electrolytes depletion, and recurrent urinary tract infection and calculus formation (23). According to available reports, VC shunt is generally performed on pediatric patients. Duncan Henderson et al. reported that the VC shunt survived for 1 year in two children, who had preoperative external ventricular drain (EVD) outputs of 8 and 10 ml/h, respectively. And one child failed at day four, who had preoperative EVD of 30–35 ml/h (22). Hence, the EVD was suggested to evaluate per hour of CSF production pre-VC shunt (22), which is an invasive operation increasing the physical burden and surgical risks to patients. The reflux of bile causing an aseptic meningitis and irritation of the brain stem also have been reported after post-VC shunt by Bernstein et al. (24). Relatively, VS shunt was more feasible for this patient.

According to our knowledge, only two cases of hydrocephalus treated with VS shunt have been reported, including our case study. The limitation is that the period of follow-up time in our case is not long enough to support VS shunt as a long-term feasible alternative, although the outcome was considerable at 16-month follow-up. The potential risks and possible complications of this novel procedure have not been fully investigated as well. Despite, this the VS shunt may be a potential option for CSF diversion in the future.

CONCLUSION

The authors demonstrate the feasibility and efficacy of VS shunt for the management of iNPH in this case report. VS shunt may be a valuable option when other conventional CSF diversion procedures are ruled out.

DATA AVAILABILITY STATEMENT

The raw data supporting the conclusions of this article will be made available by the authors, without undue reservation.

ETHICS STATEMENT

The studies involving human participants were reviewed and approved by Ethics Committee of the Second Affiliated Hospital of Zhejiang University, School of Medicine. The patients/participants provided their written informed consent to participate in this study. Written informed consent was obtained from the individual(s) for the publication of any potentially identifiable images or data included in this article.

AUTHOR CONTRIBUTIONS

All authors contributed toward surgery records, drafting, and revising the article.

REFERENCES

1. Marmarou M, Bergsneider N, Relkin P, Klinge P, Black PM. Development of guidelines for idiopathic normal-pressure hydrocephalus: introduction. *Neurosurgery.* (2005) 57:S1–3. doi: 10.1227/01.NEU.0000168188.25559.0E
2. Liu A, Sankey EW, Jusue-Torres I, Patel MA, Elder BD, Goodwin CR, et al. Clinical outcomes after ventriculoatrial shunting for idiopathic normal pressure hydrocephalus. *Clin Neurol Neurosurg.* (2016) 143:34–8. doi: 10.1016/j.clineuro.2016.02.013
3. Razay G, Vreugdenhil A, Liddell J. A prospective study of ventriculo-peritoneal shunting for idiopathic normal pressure hydrocephalus. *J Clin Neurosci.* (2009) 16:1180–3. doi: 10.1016/j.jocn.2008.12.007
4. Ming Woo PY, Hung Pang PK, Chan KY, Ching Kwok JK, Ventriculosternal shunting for the management of hydrocephalus:

case report of a novel technique. *Neurosurgery*. (2015) 11:371–5. doi: 10.1227/NEU.0000000000000861
5. Macnab A, Christenson J, Findlay J, Horwood B, Johnson D, Jones L, et al. A new system for sternal intraosseous infusion in adults. *Prehosp Emerg Care*. (2000) 4:173–7.
6. Tubbs RS, Bauer D, Chambers MR, Loukas M, Shoja MM, Cohen-Gadol AA. A novel method for cerebrospinal fluid diversion: a cadaveric and animal study. *Neurosurgery*. (2011) 60:491–4. doi: 10.1227/NEU.0b013e3181ffa21c
7. Jagust WJ, Friedland RP, Budinger TF. Positron emission tomography with [18F]fluorodeoxyglucose differentiates normal pressure hydrocephalus from Alzheimer-type dementia. *J Neurol Neurosurg Psychiatry*. (1985) 48:1091–6. doi: 10.1136/jnnp.48.11.1091
8. Craven CL, Toma AK, Mostafa T, Patel N, Watkins LD. The predictive value of DESH for shunt responsiveness in idiopathic normal pressure hydrocephalus. *J Clin Neurosci*. (2016) 34:294–8. doi: 10.1016/j.jocn.2016.09.004
9. Kubo Y, Kazui H, Yoshida T, Kito Y, Kimura N, Tokunaga H, et al. Validation of grading scale for evaluating symptoms of idiopathic normal-pressure hydrocephalus. *Dement Geriatr Cogn Disord*. (2008) 25:37–45. doi: 10.1159/000111149
10. Folstein MF, Folstein SE, McHugh PR. "Mini-mental state". A practical method for grading the cognitive state of patients for the clinician. *J Psychiatr Res*. (1975) 12:189–98. doi: 10.1016/0022-3956(75)90026-6
11. Virhammar J, Cesarini KG, Laurell K. The CSF tap test in normal pressure hydrocephalus: evaluation time, reliability and the influence of pain. *Eur J Neurol*. (2012) 19:271–6. doi: 10.1111/j.1468-1331.2011.03486.x
12. Meier U, Mutze S. Correlation between decreased ventricular size and positive clinical outcome following shunt placement in patients with normal-pressure hydrocephalus. *J Neurosurg*. (2004) 100:1036–40. doi: 10.3171/jns.2004.100.6.1036
13. Chari A, Czosnyka M, Richards HK, Pickard JD, Czosnyka ZH. Hydrocephalus shunt technology: 20 years of experience from the Cambridge Shunt Evaluation Laboratory. *J Neurosurg*. (2014) 120:697–707. doi: 10.3171/2013.11.JNS121895
14. Soler GJ, Bao M, Jaiswal D, Zaveri HP, DiLuna ML, Grant RA, et al. A Review of cerebral shunts, current technologies, and future endeavors. *Yale J Biol Med*. (2018) 91:313–21.
15. Isaacs AM, Williams MA, Hamilton MG. Current update on treatment strategies for idiopathic normal pressure hydrocephalus. *Curr Treat Options Neurol*. (2019) 21:65. doi: 10.1007/s11940-019-0604-z
16. LaRocco BG, Wang HE. Intraosseous infusion. *Prehosp Emerg Care*. (2003) 7:280–5. doi: 10.1080/10903120390936950
17. J.A. Anson. Vascular access in resuscitation: is there a role for the intraosseous route? *Anesthesiology*. (2014) 120:1015–31. doi: 10.1097/ALN.0000000000000140
18. M.J. Koschel. Sternal intraosseous infusions: emergency vascular access in adults. *Am J Nurs*. (2005) 105:66–8. doi: 10.1097/00000446-200501000-00027
19. Choux M, Genitori L, Lang D, Lena G. Shunt implantation: reducing the incidence of shunt infection. *J Neurosurg*. (1992) 77:875–80. doi: 10.3171/jns.1992.77.6.0875
20. Liu A, Elder BD, Sankey EW, Goodwin CR, Jusue-Torres I, Rigamonti D. Are shunt series and shunt patency studies useful in patients with shunted idiopathic intracranial hypertension in the emergency department? *Clin Neurol Neurosurg*. (2015) 138:89–93. doi: 10.1016/j.clineuro.2015.08.008
21. Williams MA, Malm J. Diagnosis and treatment of idiopathic normal pressure hydrocephalus. *Continuum (Minneap Minn)*. (2016) 22:579–99. doi: 10.1212/CON.0000000000000305
22. Henderson D, Budu A, Horridge M, Jesurasa A, Sinha S, Ushewokunze S, et al. The ventriculo-cholecystic shunt: does CSF volume matter? *Childs Nerv Syst*. (2019) 35:1557–60. doi: 10.1007/s00381-019-04317-7
23. Shahul Hameed AS, Yousaf I, Choudhari KA. Urinary bladder calculi complicating ventriculo-vesical shunt. *Br J Neurosurg*. (2005) 19:449–50. doi: 10.1080/02688690500390458
24. Bernstein RA, Hsueh W. Ventriculocholecystic shunt. A mortality report. *Surg Neurol*. (1985) 23:31–7. doi: 10.1016/0090-3019(85)90156-9
25. Demetriades AK, Haq IZ, Jarosz J, McCormick D, Bassi S. The ventriculocholecystic shunt: two case reports and a review of the literature. *Br J Neurosurg*. (2013) 27:505–8. doi: 10.3109/02688697.2013.771135

Conflict of Interest: The authors declare that the research was conducted in the absence of any commercial or financial relationships that could be construed as a potential conflict of interest.

Publisher's Note: All claims expressed in this article are solely those of the authors and do not necessarily represent those of their affiliated organizations, or those of the publisher, the editors and the reviewers. Any product that may be evaluated in this article, or claim that may be made by its manufacturer, is not guaranteed or endorsed by the publisher.

frontiers in Surgery

CASE REPORT
published: 21 September 2021
doi: 10.3389/fsurg.2021.746034

Technical Case Report of a Cranioplasty With *ex vivo* Frozen Ostoblastic Bone Graft From Large Skull Metastasis

Pang-Shuo Perng[1], *Po-Hsuan Lee*[1], *Hao-Hsiang Hsu*[1], *Chi-Chen Huang*[1], *Chih-Yuan Huang*[1] *and Jung-Shun Lee*[1,2,3]*

[1] *Section of Neurosurgery, Department of Surgery, National Cheng Kung University Hospital, College of Medicine, National Cheng Kung University, Tainan, Taiwan,* [2] *Department of Cell Biology and Anatomy, College of Medicine, National Cheng Kung University, Tainan, Taiwan,* [3] *Institute of Basic Medical Sciences, College of Medicine, National Cheng Kung University, Tainan, Taiwan*

OPEN ACCESS

Edited by:
Philipp Taussky,
The University of Utah, United States

Reviewed by:
Lai Fung Li,
Queen Mary Hospital, Hong Kong, SAR China
Lynne Lourdes Navarrete Lucena, Bicol University, Philippines

***Correspondence:**
Jung-Shun Lee
nslee1218@gmail.com

Specialty section:
This article was submitted to Neurosurgery, a section of the journal Frontiers in Surgery

Received: *23 July 2021*
Accepted: *26 August 2021*
Published: *21 September 2021*

Citation:
Perng P-S, Lee P-H, Hsu H-H, Huang C-C, Huang C-Y and Lee J-S (2021) Technical Case Report of a Cranioplasty With ex vivo Frozen Ostoblastic Bone Graft From Large Skull Metastasis. Front. Surg. 8:746034. doi: 10.3389/fsurg.2021.746034

Objective: Liquid nitrogen cryotherapy has shown efficacy in the treatment of bone tumors of the extremities with good oncologic and functional outcomes. However, its application in metastatic skull tumors has been rarely reported and whether the adjuvant radiotherapy affects the future bone healing is not yet explored. We report an immediate cranioplasty with the resected osteoblastic bone, which underwent *ex vivo* cryotherapy, and discuss the surgical techniques and postoperative images.

Methods: A 58-year-old man with esophageal adenocarcinoma, undergoing chemoradiotherapy, presented with a rapidly enlarging scalp mass for 5 months. Imaging revealed an enhancing mass, centered in the frontal skull bone with extracranial and intracranial invasion, suggestive of osteoblastic metastasis. After preoperative transarterial embolization, the tumor was excised en bloc. Immediate cranioplasty was performed with the osteoblastic bone graft after *ex vivo* cryotherapy. It was soaked in liquid nitrogen for 20 min, thawed at room temperature for 15 min, and soaked in povidone-iodine solution for 10 min. Then, the bone graft was fixed to its original place. Pathologic examination revealed metastasis originating from the esophagus. He underwent adjuvant radiotherapy for local tumor control.

Results: He had an uneventful clinical course without any neurologic deficit. Brain imaging during the six-month follow-up showed no tumor recurrence and partial bony union.

Conclusions: Cranioplasty using an autologous bone graft with *ex vivo* cryotherapy was helpful in the reconstruction of osteoblastic metastatic skull tumor treatment. It was a simple and cost-effective procedure that achieved satisfactory cosmetic results without negatively impacting bone healing, even after adjuvant radiotherapy.

Keywords: cranioplasty, cryotherapy, metastasis, bone healing, osteoblastic differentiation

INTRODUCTION

Skullbone metastasis with extracranial and intracranial extension signifies late-stage cancer. It has been challenging to treat this entity due to the inherent hypervascularity of metastatic lesions, reconstruction of the large skull defects, wound healing issues after postoperative radiotherapy, and lack of effective adjuvant chemotherapy. Therefore, most metastatic lesions were treated with palliative radiotherapy. The advancement in adjuvant targeted therapy and intensity-modulated radiation therapy has improved the survival outcomes of patients undergoing metastasectomy (1). In addition, metastasectomy is the only means of obtaining a tissue diagnosis while immediately alleviating neurological symptoms in patients with large skull metastasis and intracracnial compression.

Most skull bone metastases are osteolytic, wherein the bony structure is destroyed by tumor cells, and the skull defect can be reconstructed with titanium meshes, polyetheretherketone, or polymethylmethacrylate. A minority of skull bone metastasis cases were osteoblastic, wherein the metastatic bone preserved its bony contour and structural integrity. Previous researches have not discussed the utility of an osteoblastic metastatic bone as an autograft after adequate treatment *ex vivo*. We report an immediate cranioplasty with a frozen osteoblastic bone graft

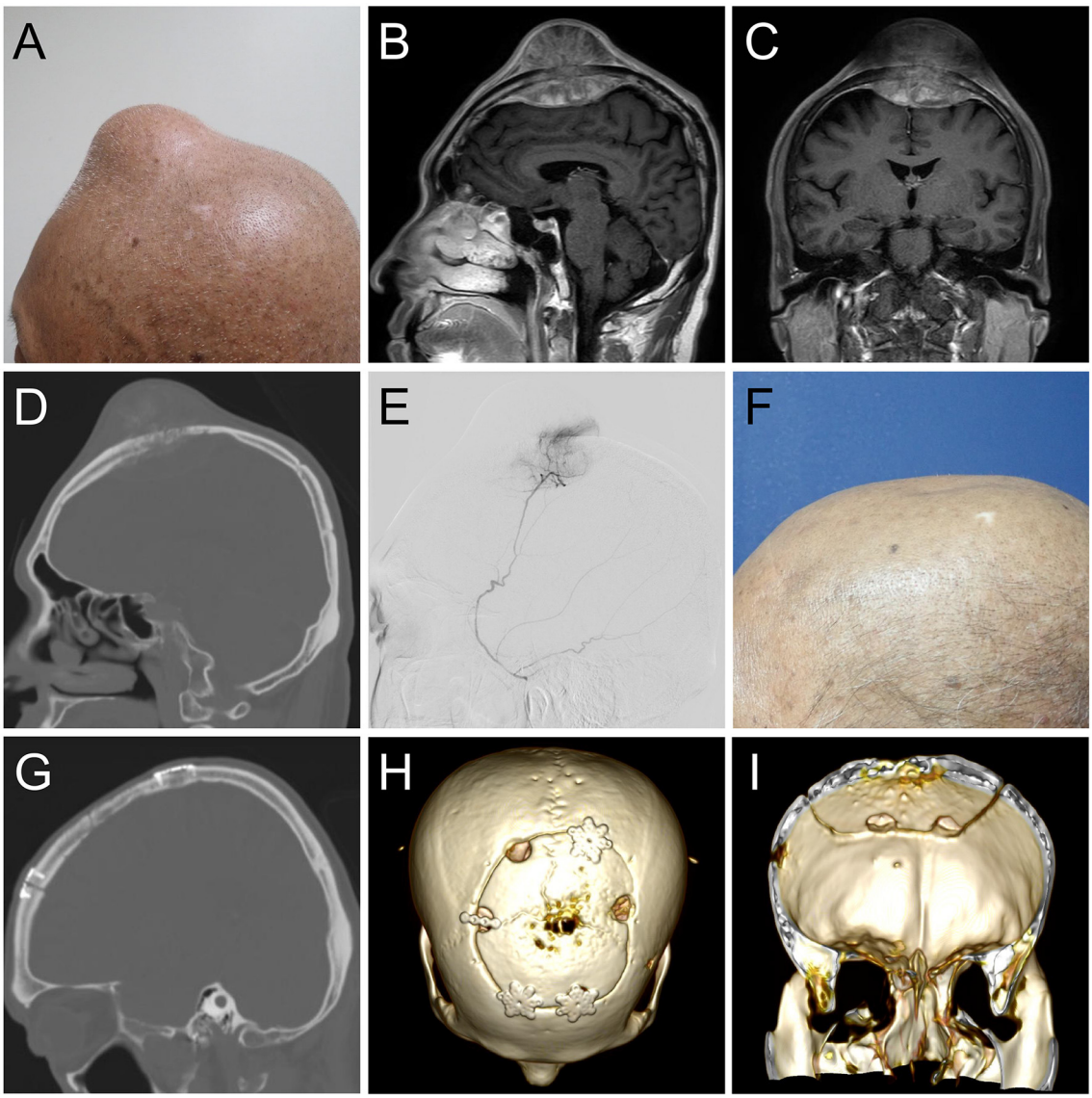

FIGURE 1 | (A) Clinical image of the 8-cm scalp tumor. **(B)** Sagittal and **(C)** coronal gadolinium-enhanced T1- weighted magnetic resonance imaging depicting a biconvex mass with extracranial and intracranial invasion, compressing bilateral brain tissue. **(D)** A sagittal computed tomography (CT) image showing an osteoblastic lesion. **(E)** Angiographic tumor staining of the left middle meningeal artery. At the 6-month follow-up **(E)**, sagittal and coronal CT **(F,G)** and 3D reconstruction image **(H,I)** illustrated normal skull contour with a solid fusion of the graft to the skull.

after removing a large skull metastasis with intracranial and extracranial extension. The surgical techniques, rationale behind tumor resection, *ex vivo* tumor eradication, and follow-up images after radiotherapy were discussed in this report.

CASE PRESENTATION

A 58-year-old man had esophageal adenocarcinoma (cT4bN3M1) with bilateral adrenal gland metastasis noted 8 months ago. He underwent eight cycles of concurrent chemoradiotherapy with cisplatin, 5-fluorouracil, and paclitaxel. He presented with a rapidly enlarging scalp mass for 5 months (**Figure 1A**). Physical examinations revealed a firm, fixed, non-tender, 8-cm mass over the midline frontal area behind the hairline. Computed tomography revealed an enlarging skull mass with osteoblastic characteristics in the frontal area along the midline. Gadolinium-enhanced magnetic resonance imaging showed a heterogeneously enhanced biconvex mass (**Figures 1B–D**). The mass had an extracranial extension and intracranial compression over the left and right frontal lobes and superior sagittal sinus. The patient was diagnosed with a metastatic skull tumor with brain compression. Thus, surgery was indicated.

SURGICAL INTERVENTION

Angiography revealed that the main tumor feeding artery came from the left and right middle meningeal arteries (**Figure 1E**). These vessels were embolized with micro-coils 5 days before surgery. Intraoperatively, an encapsulated tumor

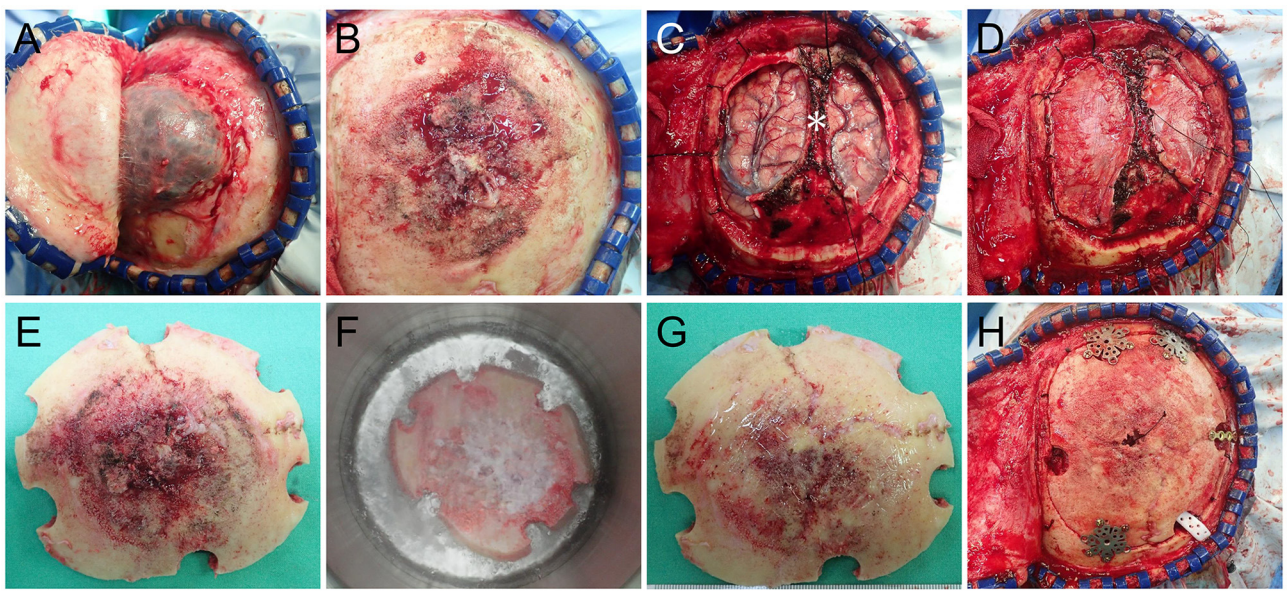

FIGURE 2 | Intraoperative images **(A)** Following reflecting the galea showing a well-demarcated extracranial tumor**. (B)** After removal of the extracranial tumor showing the osteoblastic tumor-bearing bone. **(C)** The intracranial tumor was removed with the preservation of the superior sagittal sinus (*). **(D)** Duraplasty with tensor fascia lata. **(E)** *Ex vivo* cryotherapy was done with the autologous bone graft by soaking it in liquid nitrogen for 20 min **(F)**, thawing it in room air for 10 min and soaking it in povidone-iodine solution for 15 min. The nitrogen-treated graft **(G)** was fixed back *in situ* with plates and screws **(H)**.

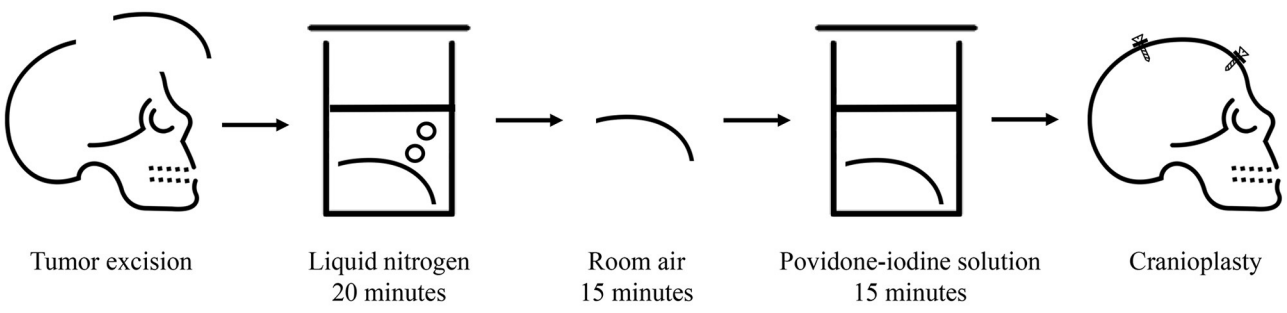

FIGURE 3 | Summary of the *ex vivo* cryotherapy.

was dissected from the subgaleal layer after a U-shaped incision (**Figure 2A**). The frozen section of the galeal biopsy showed no tumor invasion. The extracranial component was excised entirely via electrocoagulation. En bloc resection of the osteoblastic bone was performed using the craniotome under navigation guidance (**Figure 2B**). The intracranial tumor was removed per segment, and the involved dura was excised while preserving the superior sagittal sinus (**Figure 2C**). After completely removing the tumor, duraplasty was performed using a tensor fascia lata graft (**Figure 2D**). Meanwhile, the resected osteoblastic bone graft was scheduled for *ex vivo* cryotherapy (**Figures 2E–G**). First, the bone graft was soaked in liquid nitrogen for 20 min for tumor eradication. Then, it was thawed at room temperature for 15 min and soaked in diluted povidone-iodine solution for 10 min to prevent a rapid rise in temperature and for disinfection. After cryotherapy, the bone graft was fixed to the skull defect with plates and screws (**Figure 2H**). The scalp was then sutured by layers. The cryotherapy was summarized in **Figure 3** with an illustrative video (**Supplementary File**). The total amount of blood loss was 300 mL. Histopathological analysis revealed metastatic adenocarcinoma of the skull bone and excised dura, originating from the esophagus. The patient received adjuvant radiotherapy (3740 centigray/15 fractions) 1 month after surgery. During the 6-month follow-up, imagines showed no *in-situ* tumor recurrence and partial bone healing (**Figures 1F–I**). However, the patient passed away 1 year after the surgery due to primary esophageal cancer disease progression accompanied with massive gastrointestinal bleeding.

DISCUSSION

The incidence of calvarial metastasis has increased, and prompt intervention is mandatory due to its proximity to brain tissues. Various treatments have been reported for individual cases, and there has been no consensus regarding the optimal treatment. Surgery aims to maximize tumor debulking safely and achieve optimal skull reconstruction. Resection for metastatic tumors, which is characterized by hypervascularity and risks of dural sinus invasion, may lead to significant blood loss and result in surgical mobility and mortality. This ultimately results in surgical morbidity and mortality. To address this, transarterial embolization of the feeding arteries was performed according to the treatment of large convexity meningiomas (2). The left and right middle meningeal arteries were embolized 5 days before surgery. This limited the blood loss to 300 mL in our case.

Unlike osteolytic metastasis, osteoblastic metastasis has a preserved primary bone structure. Reconstruction with an autologous calvarial bone graft prevents contagion, costs less, and achieves satisfactory cosmesis. Given these advantages, the osteoblastic bone was used to perform cranioplasty immediately after adequate management *ex vivo*. The major concerns regarding reconstruction with this graft are the complete eradication of tumor cells and future bone healing after radiotherapy. To root out the tumor cells, cryotherapy with liquid nitrogen, which has been reported for the treatment of osteosarcoma of the extremities, was performed. Liquid nitrogen successfully destroys tumor cells via ice crystal formation, cell dehydration, and cell ischemia caused by thrombosis. Favorable oncologic outcomes were achieved with no tumor recurrence noted during the 65-month follow-up and a 100% 5-year recurrence-free survival rate (3). In addition, single attempt of 20-min soaking in the liquid nitrogen (−196°C) was evident to exterminate the tumor cells rather than two cycles (4). After freezing, the autologous bone graft was thawed at room temperature (20°C) and in bactericidal physiological saline (30°C) for 10 min, respectively, to prevent bony fracture formation during a rapid rise in temperature.

Postoperative radiotherapy is mandatory for skull or brain metastasis treatment, but it is not indicated as an adjuvant treatment for osteosarcoma. However, radiotherapy reduces osteogenic cells and delays bone healing (5). Furthermore, unlike bones of the extremities, the skull bones endure less physical stress and have a low proportion of hypervascularized cancellous bone, which negatively influences bone healing. Incomplete bone union can induce a higher infection rate, adjacent tissue damage, and reabsorption (6, 7). Xu et al. detected fibrous tissue and immature bone matrix in the frozen bone 12 weeks after liquid nitrogen treatment (8). These bones serve as essential pillars and provide osteoinductive properties. Despite the drawbacks of adjuvant radiotherapy in hindering bony healing and a low portion of cancellous bone, this was the first case to document bony union on computed tomography during the 6-month follow-up.

CONCLUSION

We presented an immediate cranioplasty using liquid nitrogen to treat a metastatic skull tumor with intracranial and extracranial involvement. This simple and effective method for reconstructing skull metastasis utilized the key osteoblastic characteristics and a novel cryotherapy to achieve favorable oncologic and surgical outcomes.

DATA AVAILABILITY STATEMENT

The original contributions presented in the study are included in the article/**Supplementary Material**, further inquiries can be directed to the corresponding author/s.

ETHICS STATEMENT

Ethical review and approval was not required for the study on human participants in accordance with the local legislation and institutional requirements. Written informed consent for participation was not required for this

study in accordance with the national legislation and the institutional requirements.

AUTHOR CONTRIBUTIONS

P-SP, P-HL, and H-HH: writing—original draft. C-CH and C-YH: supervision and writing—original draft. J-SL: conceptualization, writing—original draft, review, and editing. All authors contributed to the article and approved the submitted version.

SUPPLEMENTARY MATERIAL

The Supplementary Material for this article can be found online at: https://www.frontiersin.org/articles/10.3389/fsurg.2021.746034/full#supplementary-material

REFERENCES

1. Jegoux F, Malard O, Goyenvalle E, Aguado E, Daculsi G. Radiation effects on bone healing and reconstruction: interpretation of the literature. *Oral Surg Oral Med Oral Pathol Oral Radiol Endodontol.* (2010) 109:173–84. doi: 10.1016/j.tripleo.2009.10.001
2. Mirabet V, García D, Roca A, Quiroz AR, Antón J, Rodríguez-Cadarso M, et al. Cranioplasty with autologous bone flaps cryopreserved with dimethylsulphoxide: does tissue processing matter. *World Neurosurg.* (2021) 149:e582–91. doi: 10.1016/j.wneu.2021.01.131
3. Miwa S, Takeuchi A, Shirai T, Yamamoto N, Hayashi K, Nishida H, et al. Outcomes and complications of reconstruction using tumor-bearing frozen autografts in patients with metastatic bone tumors. *Anticancer Res.* (2014) 34:5569–77.
4. Sankey EW, Tsvankin V, Grabowski MM, Nayar G, Batich KA, Risman A, et al. Operative and peri-operative considerations in the management of brain metastasis. *Cancer Med.* (2019) 8:6809–31. doi: 10.1002/cam4.2577
5. Shah A, Choudhri O, Jung H, Li G. Preoperative endovascular embolization of meningiomas: update on therapeutic options. *Neurosurg Focus.* (2015) 38:E7. doi: 10.3171/2014.12.FOCUS14728
6. Thomas JD, Kehoe JL. Bone non-union. In: *StatPearls.* Treasure Island, FL: StatPearls Publishing LLC (2021).
7. Xu G, Yamamoto N, Nojima T, Hayashi K, Takeuchi A, Miwa S, et al. The process of bone regeneration from devitalization to revitalization after pedicle freezing with immunohistochemical and histological examination in rabbits. *Cryobiology.* (2020) 92:130–7. doi: 10.1016/j.cryobiol.2019.12.002
8. Yamamoto N, Tsuchiya H, Tomita K. Effects of liquid nitrogen treatment on the proliferation of osteosarcoma and the biomechanical properties of normal bone. *J Orthop Sci.* (2003) 8:374–80. doi: 10.1007/s10776-002-0626-3

Conflict of Interest: The authors declare that the research was conducted in the absence of any commercial or financial relationships that could be construed as a potential conflict of interest.

Publisher's Note: All claims expressed in this article are solely those of the authors and do not necessarily represent those of their affiliated organizations, or those of the publisher, the editors and the reviewers. Any product that may be evaluated in this article, or claim that may be made by its manufacturer, is not guaranteed or endorsed by the publisher.

frontiers in Surgery

CASE REPORT
published: 22 September 2021
doi: 10.3389/fsurg.2021.734757

Case Report: Whole-Exome Sequencing of Hypothalamic Hamartoma From an Infant With Pallister-Hall Syndrome Revealed Novel *de novo* Mutation in the *GLI3*

Yue Yang[1†], Fang Shen[2†], Xie-Pan Jing[3†], Nu Zhang[1], Shang-Yu Xu[1], Dan-Dong Li[1], Ling-Li Zhou[4], Guang-Hui Bai[5], Huang-Yi Fang[1,6], Zhong-Ding Zhang[1], Chen Pang[1,6], Jian Lin[1] and Han-Song Sheng[1]*

[1] Department of Neurosurgery, Second Affiliated Hospital of Wenzhou Medical University, Wenzhou, China, [2] Department of Surgery, Northern Hospital Epping, Epping, VIC, Australia, [3] Department of Neurosurgery, People's Hospital of Mongolian Autonomous Prefecture of Bayingolin, Korla Xinjiang, China, [4] Department of Pathology, Second Affiliated Hospital of Wenzhou Medical University, Wenzhou, China, [5] Department of Radiology, Second Affiliated Hospital of Wenzhou Medical University, Wenzhou, China, [6] School of the 2nd Clinical Medical Sciences, Wenzhou Medical University, Wenzhou, China

Background: GLI-Kruppel family member 3 (GLI3), a zinc finger transcription factor of the sonic hedgehog pathway, is essential for organ development. Mutations in *GLI3* cause several congenital conditions, including Pallister-Hall syndrome (PHS), which is characterized by polydactyly and hypothalamic hamartoma. Most patients are diagnosed soon after birth, and surgical removal of hypothalamic hamartoma in the very young is rarely performed because of associated risks.

Case presentation: A 7-month-old boy with PHS features, including a suprasellar lesion, bifid epiglottis, tracheal diverticulum, laryngomalacia, left-handed polydactyly and syndactyly, and omental hernia was referred to our service. His suprasellar lesion was partially removed, and whole-exome sequencing was applied to the resected tumor, his peripheral blood, and blood from his parents. Histopathology confirmed the diagnosis of hypothalamic hamartoma, and molecular profiling revealed a likely pathogenic *de novo* variant, c.2331C>G (p. H777Q), in *GLI3*. Magnetic resonance imaging follow-up 1 year later showed some residual tumor, and the patient experienced normal development post operation.

Conclusions: We presented a case of PHS that carries a novel *GLI3* variant. Hypothalamic hamartoma showed a distinct genetic landscape from germline DNA. These data offer insights into the underlying etiology of hypothalamic hamartoma development in patients with PHS.

Keywords: molecular profiling, whole-exome sequencing, Pallister-Hall syndrome, *GLI3*, hypothalamic hamartoma, surgical resection

OPEN ACCESS

Edited by:
Philipp Taussky,
The University of Utah, United States

Reviewed by:
George Wong,
The Chinese University of Hong Kong, Hong Kong, SAR China
Mario Ganau,
Oxford University Hospitals NHS Trust, United Kingdom

***Correspondence:**
Han-Song Sheng
shenghansong@126.com

[†] These authors have contributed equally to this work

Specialty section:
This article was submitted to Neurosurgery, a section of the journal Frontiers in Surgery

Received: *01 July 2021*
Accepted: *26 August 2021*
Published: *22 September 2021*

Citation:
Yang Y, Shen F, Jing X-P, Zhang N, Xu S-Y, Li D-D, Zhou L-L, Bai G-H, Fang H-Y, Zhang Z-D, Pang C, Lin J and Sheng H-S (2021) Case Report: Whole-Exome Sequencing of Hypothalamic Hamartoma From an Infant With Pallister-Hall Syndrome Revealed Novel de novo Mutation in the GLI3. Front. Surg. 8:734757. doi: 10.3389/fsurg.2021.734757

INTRODUCTION

Pallister-Hall syndrome (PHS) was first described in 1978 following the observation of a series of congenital features in a group of patients who died during the neonatal period (1). PHS was later identified as an autosomal dominant condition with characteristic phenotypes including hypothalamic hamartoma (HH), polydactyly, bifid epiglottis, and imperforate anus (2). Through advances in molecular testing techniques, *Gli Kruppel Family Member 3* (*GLI3*) was identified as the causative gene of PHS in 1997 (3). The availability of MRI even in remote regions contributes to a better delineation of intracranial lesions in patients with PHS. Indeed, patients with PHS are known to have a wide variety of phenotypes include anal, genitourinary, and respiratory abnormalities (4, 5).

GLI3 plays an essential role in regulating the development of multiple organ systems. Therefore, it is not surprising that different pathogenic *GLI3* variants lead to various developmental anomalies (6). Accordingly, personalized management is preferred for patients with different *GLI3* defects based on molecular studies. Major surgery has been performed to improve patient chance of survival by correcting defects such as imperforate anus. Moreover, given that patients with mild phenotypical abnormalities are more likely to survive into adulthood, cosmetic surgeries are often needed to improve their quality of life (7). HHs are associated with endocrine defects, seizures, and developmental delay in patients with PHS, and their surgical resection, if required, remains technically challenging, especially in the very young age group (8). In this study, we have successfully partially removed a HH in a 7-month-old boy diagnosed with PHS. Whole-exome sequencing (WES) of the tumor and blood samples of the patient revealed that he carried a likely pathogenic *de novo* variant in *GLI3*. Short-term clinical follow-up showed normal development in the patient. The reporting of this study conforms to CARE guidelines (9).

CASE PRESENTATION

A 7-month-old boy was referred to the Second Affiliated Hospital (also known as Yuying Children's Hospital) of Wenzhou Medical University after identification of an intracranial lesion by magnetic resonance imaging (MRI) scans that had been performed 12 days postnatally at a local hospital. He was born at full-term after an uneventful pregnancy by normal spontaneous vaginal delivery. At birth, he weighed 3.8 kg and was 50 cm in length. Physical examination on admission to our hospital revealed faltering growth (6.0 kg and 58 cm) [WHO criteria (10) at this age is 6.7–10.3, 8.3 kg (± 2 standard deviation, 50th percentile) and 64.8–73.5, 69.2 cm (± 2 standard deviation, 50th percentile)]. There were also dysmorphic features including left-hand polydactyly, syndactyly (**Figure 1a**) and a reducible omental hernia (1.5 × 1.5 cm). Flexible bronchoscopy showed bifid epiglottis, tracheal diverticulum, and laryngomalacia (**Figures 1b,c**). Neurological examination showed a normal muscle tone, strength, and reflexes. Endocrinology evaluations of pituitary, thyroid and cortisol hormones were within normal range. However, his parents reported that patient experienced frequent attacks of inappropriate laughter which suggested features of gelastic seizures. Unfortunately, electroencephalography was not available for such a small child to provide more objective evidence of seizure activities.

Computed tomography (CT) and MRI scans showed a suprasellar hypothalamic lesion suggestive of a hamartoma (**Figures 1d–f**). Surgery was performed because of parents' concerns over the faltering growth. The intracranial lesion was partially resected via transcallosal anterior interforniceal approach through the space between the internal carotid artery and optic nerve, and part of the tumor was left to avoid injuring the hypothalamus. The intraoperative diagnosis was hamartoma, and tumor samples were sent for histopathological and molecular testings. Postoperative course was uneventful, and repeated CT and MRI confirmed some residual tumor (**Figures 1g,h**). Patient was discharged 2 weeks later, and follow-up MRI 1 year later showed subtotal removal of the tumor (**Figure 1i**). Since the operation, he experienced normal growth without signs of gelastic seizures. At the clinical follow-up when he was 20-months-old, patient showed recovery of growth velocity (12 kg weight and 70 cm height). MRI at this time showed the residual tumor to be of a stable size and to be located in the tuber cinereum.

METHODS

Immunohistochemistry

Staining was performed in the hospital pathology department using an automatic staining machine and commercially available hematoxylin and eosin (H&E) staining and immunohistochemistry agents. Briefly, tumor specimens were processed into 3- to 4-μm formalin-fixed paraffin-embedded section slides. For H&E staining, slides were first deparaffinized using xylene, rehydrated using ethanol, rinsed with distilled water, stained with H&E, and dehydrated. Slides were cover-slipped using Permount (Thermo Fisher Scientific, MA, USA).

For immunohistochemistry, antigens were first retrieved with either heat-induced epitope retrieval (62°C for 1 h) or citrate antigen retrieval buffer (95–100°C for 20 min). Then endogenous peroxidases were blocked with 1.5% hydrogen peroxide for 5 min. Slides were first incubated with primary antibodies against the following antigens including epidermal growth factor receptor (EGFR), glial fibrillary acidic protein (GFAP), epithelial membrane antigen (EMA), cytokeratins (CK), Sry-related HMg-Box gene 10 (SOX-10), S-100, P-glycoprotein (P-gp), cluster of differentiation 99 (CD 99), vimentin, neurofilament (NF) or synaptophysin (SYN) for 1–2 h per protocols. Then slides were incubated with horseradish peroxidase-linked secondary antibody (Thermo Fisher Scientific, MA, USA) for 30 min to 1 h at room temperature. All antibodies were ready to use without need of dilution. Diaminobenzidine tetrahydrochloride (Thermo Fisher Scientific, MA, USA) was sequentially added for 5 min then washed with phosphate-buffered saline for chromogenic detection. Slides were counterstained with hematoxylin before being mounted with Permount. All reagents were provided by Fuzhou Maixin Biotech Co., Ltd. (Fuzhou, China) and

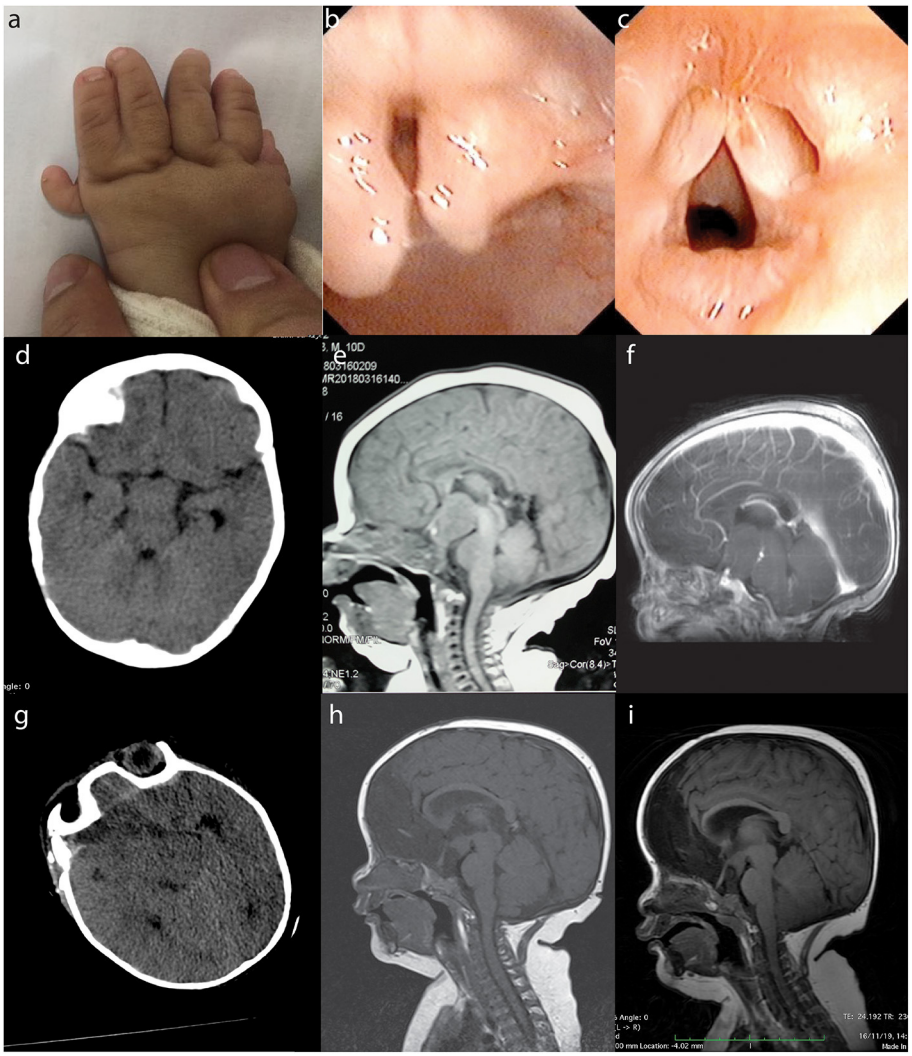

FIGURE 1 | PHS in a 7-month-old boy. The patient presented with typical morphological features of PHS such as polydactyly and syndactyly (**a**: left hand), bifid epiglottis **(b)**, and laryngomalacia **(c)**. Preoperative CT (**d**: at 7 months of age), non-contrast MRI (**e**: 12 days postnatal), and contrast-enhanced MRI (**f**: 7 months of age) showed a suprasellar lesion. Postoperative CT **(g)** and MRI **(h)** revealed subtotal removal of the lesion, and follow-up MRI 1 year later showed no tumor regrowth **(i)**. PHS, Pallister–Hall syndrome; CT, computed tomography; MRI, magnetic resonance imaging.

Beijing Zhongshan Golden Bridge Biotechnology Co. Ltd (Beijing, China).

DNA Extraction and WES

DNA was isolated from tumor tissues, the patient's peripheral lymphocytes, and his parents' peripheral lymphocytes as described before (11). The quality of isolated DNA was assessed by using 1% agarose gel electrophoresis and Qubit® DNA Assay Kit in Qubit® 2.0 Fluorometer (Life Technologies, CA, USA).

The WES protocol was similar to the one we used previously (11). Briefly, DNA libraries were prepared using the Agilent SureSelect Human All Exon kit (Agilent Technologies, Santa Clara, CA, USA) following the manufacturer's recommendations, and index codes were applied to each sample. A total of 0.6 μg genomic DNA per sample was used as input material for DNA sample preparation. Library products were purified using the AMPure XP system (Beckman Coulter, Beverly, MA, USA) and quantified using a high-sensitivity DNA assay on the Agilent Bioanalyzer 2100 system (Agilent Technologies, USA). Clustering of the index-coded samples was performed on a cBot Cluster Generation System using the HiSeq PE Cluster Kit (Illumina, CA, USA) according to the manufacturer's instructions. After cluster generation, the DNA libraries were sequenced using the Illumina HiSeq platform, and 150 bp paired-end reads were generated.

Variant Calling and Bioinformatics Analysis

FASTQ files of obtained exomes first underwent quality control to generate high-quality clean data. Valid sequencing data were then mapped to the reference human genome (UCSC

hg19) by Burrows-Wheeler Aligner software to obtain initial mapping results in BAM format (12). SAMtools, Picard (http://broadinstitute.github.io/picard/), and Genome Analysis Toolkit (13) were used to sort BAM files and carry out duplicate marking, local realignment, and base quality recalibration to generate a final BAM file to compute the sequence coverage and depth. SAMtools mpileup (14) and bcftools performed variant calling and identification of single nucleotide polymorphisms (SNPs) and insertions and deletions (InDels). Somatic single nucleotide variants (SNVs) were detected by muTect (15), and somatic InDels by Strelka (16). Control-FREEC (17) was used to identify somatic copy number variation (CNV). The novelty of the mutation identified was verified by searching several publicly available databases, including ExAC, 1000 Genomes Project, and ESP6500. MutationTaster online software was used to evaluate the disease-causing potential of sequenced genetic alterations (18). Comprehensive visualization of gene mutations reported in the literature was performed by ProteinPaint, a web application for visualizing genetic lesions (19).

Sanger Sequencing for Validation

The primers used for *GLI3* amplification were as follows: forward, 5'-TGAAACCCCAATCATGGACTC-3' and reverse, 5'-AGATGCATGGTCTGATGTAGAACTC-3'. PCR was conducted with 28 cycles of denaturation (94°C for 30 s), annealing (58°C for 30 s), and extension (72°C for 60 s). Reactions were performed in a Line-Gene 9600 Plus thermal cycler (BIOER, Hangzhou Bioer Technology Co., Ltd., Hangzhou, China). Reaction volumes were 20 μL that contained 1 μL DNA template, 1 μL each of forward and reverse primers, and 10 μL Premix Taq (Takara Bio Inc., Shiga, Japan) including deoxynucleotides and Tris-borate ethylenediaminetetraacetic acid as a buffer. Amplified DNA fragments were recovered from a low melting temperature agarose gel, purified with a Magnetic Beads Genomic DNA Extraction Kit (Enriching Biotechnology Ltd., Shanghai, China), and subjected to direct sequencing analysis using an automated ABI-3730 Sequencer (Applied Biosystems; Thermo Fisher Scientific, Inc., MA, USA).

RESULTS

Histopathological Examination

H&E staining revealed clusters of small neurons intermixed with glia and relatively sparse large neurons. IHC analysis showed positive staining for GFAP, P-gp, S-100, vimentin, and SYN, and partial staining for EGFR. Staining for NF, SOX-10, CD99, CK, and EMA was negative. This staining pattern was compatible with a diagnosis of hamartoma with both neural and glial components (**Figure 2**) (20–22).

Genetic Analysis

Cluster analysis showed similarity between peripheral blood lymphocytes samples from the patient and his father, while the tumor sample was more distinctive (data not shown). SNV analysis revealed that many SNPs in coding sequence (CDS) regions were common among the samples sequenced, with 45.39% of SNPs being shared by four samples, and 27.09% shared by three samples. A detailed comparison of SNP distributions in the genome and CDS regions showed differences between tumor samples and patient peripheral blood lymphocyte samples (**Figure 3A**). A similar trend was also observed in the InDel distribution in the genome and CDS (**Figure 3B**). These results indicate that the tumor gained further *de novo* mutations compared with germline cells. Somatic mutation analysis of the tumor sample revealed a total of 32 SNVs and six InDels. Among them, two SNVs (including missense SNV in POM121: c.A1456T:p.T486S) and one InDel (non-frameshift deletion of OLFM2: c.595_636del:p.199_212del) were identified in the CDS region. There was also a notable increase in CNV ($n = 352$) in the tumor sample compared with peripheral blood lymphocyte samples. These results suggest that the tumor sample had a different mutational burden compared with germline cells.

Analysis of *GLI3* Variants

Following *GLI3* variants annotation, we observed variants c.C2993T (p.P998L) and c.A547G (p.T183A) in the germline cells of the patient and both parents, suggesting that they might be benign. The missense variant c.C2331G (p.H777Q) was predicted to be deleterious using MutationTaster and was only found in patient germline and tumor cells, suggesting a deleterious potential with *de novo* origin. This was further validated by Sanger sequencing (**Figure 4**). This variant was also absent from several public databases, including the ExAC, 1000 Genomes Project, and ESP6500. More than 40 pathogenic *GLI3* variants in CDS regions have been identified since 1993 in patients diagnosed with PHS (23). Literature review revealed this novel variant, c.C2331G (p.H777Q), was previously reported in a PHS patient with rare metopic suture fusion (24). These findings, together with our own, are shown in **Figure 5**.

DISCUSSION

PHS was originally described as a lethal condition in 1978 (25) with distinctive features including HH, postaxial or central polydactyly, anal atresia, and bifid epiglottis observed in the neonatal period (26, 27). It is now clear that PHS is not always lethal, and some patients survive into adulthoods (28). Clinical diagnosis of PHS would not be difficult when a constellation of phenotypical features as mentioned above is observed. Ideally, targeted genetic testing of the *GLI3* should be followed to confirm the clinical suspicion if resources are available (29). Nevertheless, early detection and personalized management such as endocrinal intervention for growth hormone deficits (30) improve patient outcomes. In sporadic HH, WES showed somatic mutations within genes comprising the sonic hedgehog (SHH) pathway (including *GLI3*) in up to 37% of cases (31). To our knowledge, this is the first report on WES of HH from cases of PHS which identified a novel *GLI3* variant both in tumor and germline DNA. Moreover, WES revealed additional *de novo* mutations in tumor DNA, indicating a different genetic landscape between tumor and germline DNA in our current case.

Despite mainly being of autosomal dominant inheritance, about 25% of PHS cases (32), include our patient, acquired through *de novo* mutations in *GLI3*. Defects in *GLI3* lead to

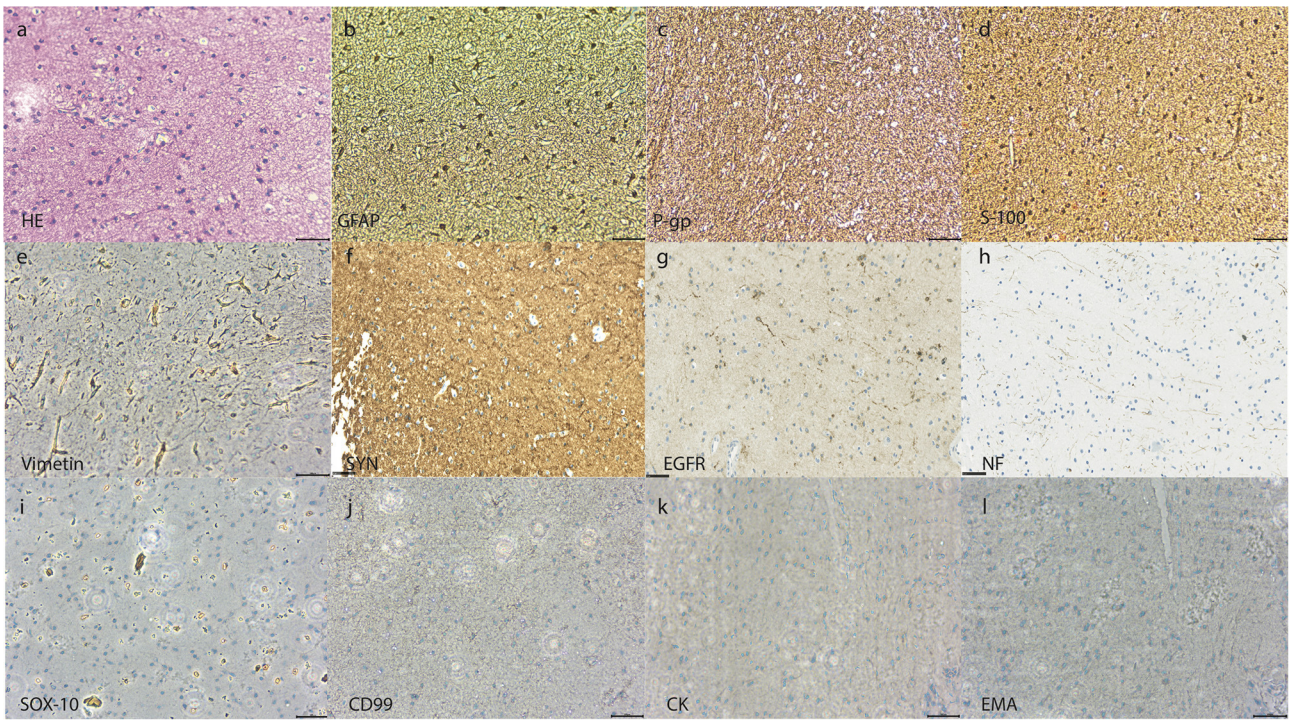

FIGURE 2 | Pathological examination of the suprasellar hypothalamic lesion. H&E staining showing clusters of small neurons intermixed with glia and relatively sparse large neurons **(a)**. IHC (magnification ×400) showing positive staining for GFAP **(b)**, P-gp **(c)**, S-100 **(d)**, vimentin **(e)**, and synaptophysin **(f)**, and partial positive staining for EGFR **(g)**. Negative staining was seen for neurofilament **(h)**, SOX-10 **(i)**, CD99 **(j)**, CK **(k)**, and EMA **(l)** (Scale bar = 100 um). H&E, hematoxylin and eosin; IHC, immunohistochemistry; GFAP, glial fibrillary acidic protein; P-gp, P-glycoprotein; SYN, synaptophysin; EGFR, epidermal growth factor receptor; NF, neurofilament; SOX-10, Sry-related HMg-Box gene 10; CD 99, cluster of differentiation 99; CK, cytokeratins; EMA, epithelial membrane antigen.

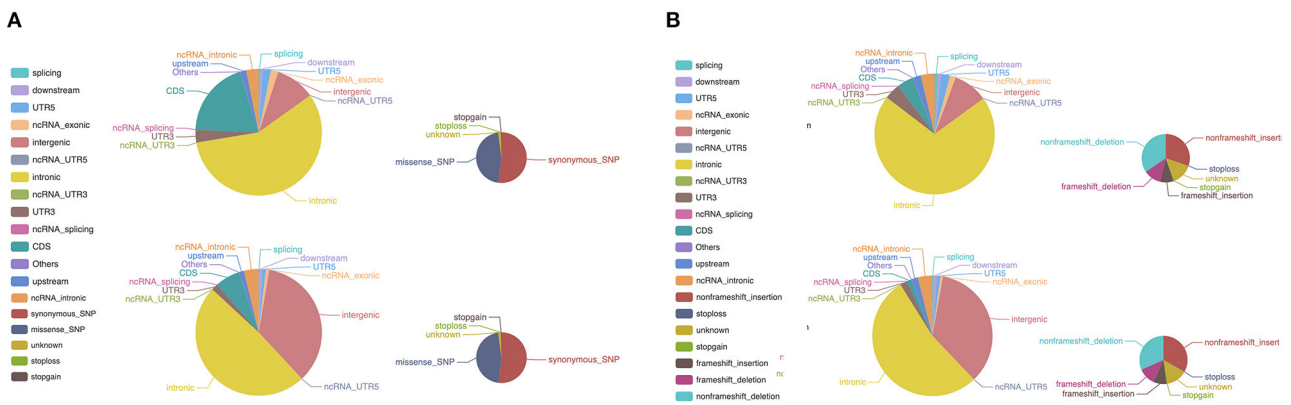

FIGURE 3 | WES of the patient tumor sample and peripheral blood lymphocyte sample. **(A)** Differences in the distribution of SNPs between the tumor sample and peripheral blood lymphocyte sample. The larger pie charts represent the genome, and the smaller ones the CDS. **(B)** A similar pattern was observed in the distribution of InDels between the tumor sample and peripheral blood lymphocyte sample. The larger pie charts represent the genome, and the smaller ones the CDS. WES, whole-exome sequencing; SNP, single nucleotide polymorphism; CDS, coding sequence; InDels, insertions and deletions.

dysregulation of the SHH signaling, which plays an essential role in multiple organ development. It was not until 2005 that the molecular mechanism underlying PHS was elucidated (33). This showed that most pathogenic mutations occur in the middle third of the *GLI3* gene (exons 13–15). To date, more than 40 pathogenic *GLI3* variants in patients with PHS have been reported (23). The majority of mutations are frameshift and nonsense mutations. In the present study, we identified the c.C2331G (p.H777Q) missense variant in our patient, which adds to the knowledge of pathogenic *GLI3* variants responsible

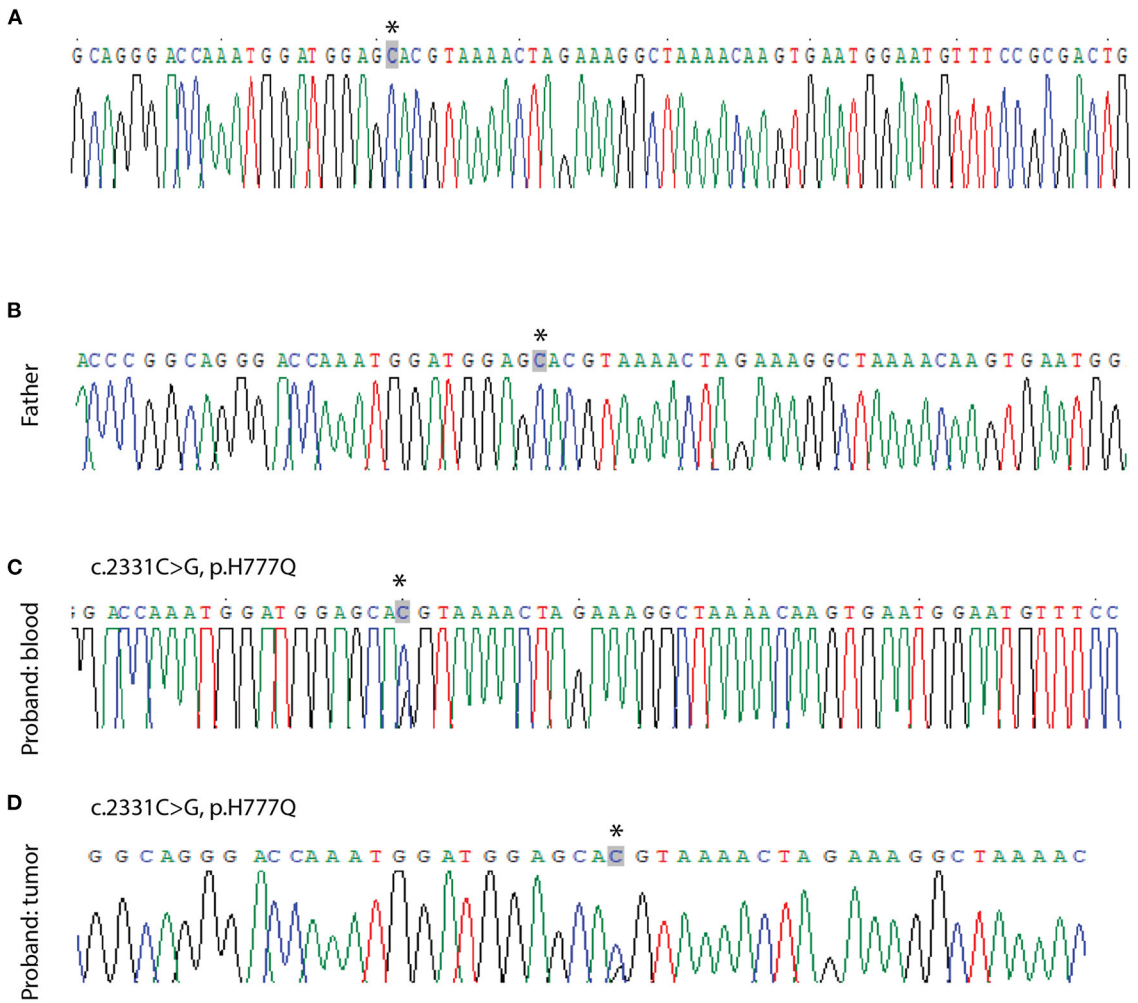

FIGURE 4 | Sanger sequencing validation of point mutations in *GLI3*. No mutation is seen in the peripheral blood lymphocyte sample from the patient's mother **(A)** and father **(B)**. A c.2331C>G mutation is seen in the patient's blood sample **(C)** and tumor sample **(D)**. Arrows indicate the ivariant.

for PHS phenotypes (34). This variant in exon 14 of *GLI3* was only previously reported in a PHS patient with a rare feature of metopic suture fusion (24). Interestingly, despite sharing the same variant, no metopic suture fusion was observed in our case on his CT scan at 7-months-old (data not shown).

Surgical management of HH at a very young age is challenging (35). Our report on the subtotal HH removal was performed in the youngest patient to date. The decision to operate was based on the following reasons: first and foremost, despite no obvious endocrinal/neurological deficits on examination, the patent's parents requested the operation because of the patient's slow growth rate and signs of gelastic seizures (30, 36). HH related epilepsy has been shown to start during the 1st year of life, typically as classic gelastic seizures (37) or less frequently as dacrystic seizures (38). Without surgical intervention, most gelastic seizures progress to tonic, myoclonic, or secondarily generalized seizures types (39). To minimize surgical-related trauma, only subtotal tumor removal was performed, which was confirmed by postoperative MRI. Follow-up MRI 1 year later showed no tumor regrowth, and the patient regained growth rate at the follow-ups. Nevertheless, Chibbaro et al. have described endoscopic resection of HH that lead to complete removal of the lesions and control of epileptic activity (40). This surgical advancement is important as it is paving the way toward minimal invasiveness management of those lesions, even in the very young.

Our study has several limitations. First, the surgical resection of HH might be arguable given its relatively benign biological behavior. Besides, surgical removal carries the risk of iatrogenic injury like any other intracranial procedure. Nevertheless, short-term follow-up showed our patient regained growth velocity without any complication. However, long-term follow-up is required to evaluate the

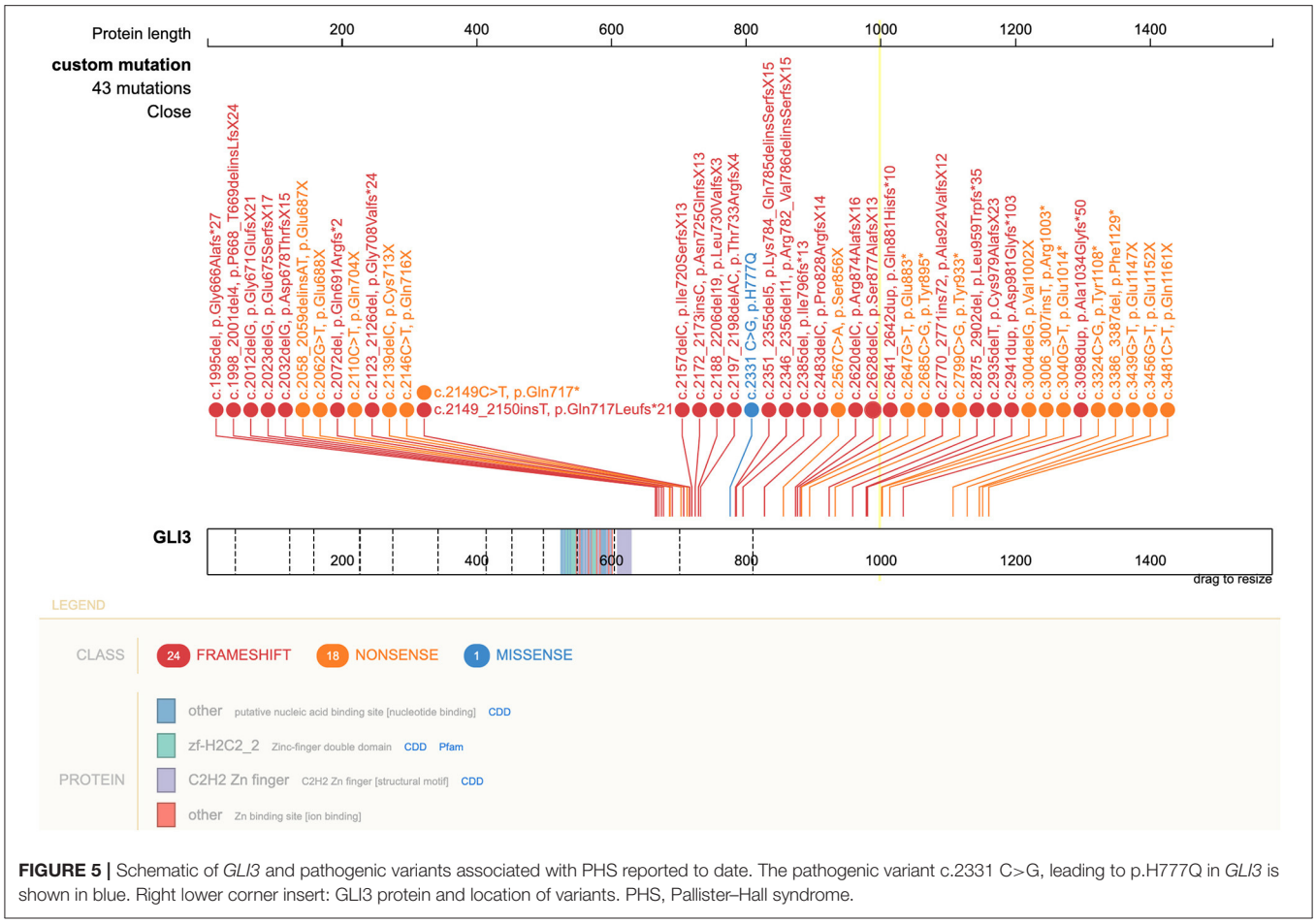

FIGURE 5 | Schematic of *GLI3* and pathogenic variants associated with PHS reported to date. The pathogenic variant c.2331 C>G, leading to p.H777Q in *GLI3* is shown in blue. Right lower corner insert: GLI3 protein and location of variants. PHS, Pallister–Hall syndrome.

benefits of early surgical intervention. Third, only two patients with PSH have ever been reported to carry the c.2331C>G (His777Glu) variant, and it is unclear how it alters the biochemical domains of GLI3 and subsequent signaling pathways. Further laboratory-based study is needed to elucidate this.

DATA AVAILABILITY STATEMENT

The datasets presented in this study can be found in online repositories. The names of the repository/repositories and accession number(s) can be found at: NCBI [accession: PRJNA743577].

ETHICS STATEMENT

Written informed consent was obtained from the relevant individual(s), and/or minor(s)' legal guardian/next of kin, for the publication of any potentially identifiable images or data included in this article.

AUTHOR CONTRIBUTIONS

FS, YY, and X-PJ conceived and wrote the manuscript and performed sequencing studies. NZ and S-YX performed tissue biopsies. Z-DZ, S-YX, and D-DL performed data collection and statistical analysis. L-LZ performed pathological evaluations. G-HB performed radiological evaluations. H-YF, Z-DZ, and CP performed validation studies. JL and H-SS reviewed the manuscript. All authors contributed to the article and approved the submitted version.

FUNDING

This study was supported by Zhejiang Province Science and Technology Program (Grant No. 2016C33213), Wenzhou Municipal Science and Technology Program (Grant No. Y20180665), Zhejiang Province Science and Technology Program (Grant No. 2021KY794), Wenzhou Municipal Science and Technology Bureau (Grant No. 2020Y0278), and Ningbo Natural Science Foundation (Grant No. 2018A610256).

REFERENCES

1. Hall JG. Pallister-Hall syndrome has gone the way of modern medical genetics. *Am J Med Genet C Semin Med Genet.* (2014) 166C:414–8. doi: 10.1002/ajmg.c.31419
2. Biesecker LG. *Pallister-Hall Syndrome*. (2000). Available online at: https://www.ncbi.nlm.nih.gov/books/NBK1465/ (accessed May 18, 2018).
3. Kang S, Graham JM, Olney AH, Biesecker LG. GLI3 frameshift mutations cause autosomal dominant Pallister-Hall syndrome. *Nat Genet.* (1997) 15:266–8. doi: 10.1038/ng0397-266
4. Hall JG. The early history of Pallister-Hall syndrome-Buried treasure of a sort. *Gene.* (2016) 589:100–3. doi: 10.1016/j.gene.2016.01.003
5. Squires LA, Constantini S, Miller DC, Wisoff JH. Hypothalamic hamartoma and the Pallister-Hall syndrome. *Pediatr Neurosurg.* (1995) 22:303–8. doi: 10.1159/000120920
6. Freese K, Driess S, Bornholdt D, Shoenle EJ, Seidel H, Tinschert S, et al. Gene symbol: GLI3. Disease: Pallister-Hall syndrome. *Hum Genet.* (2003) 112:103.
7. Courtney E, Swee DS, Ishak D, Ngeow J. A delayed diagnosis of Pallister-Hall syndrome in an adult male following the incidental detection of a hypothalamic hamartoma. *Hum Genome Var.* (2018) 5:31. doi: 10.1038/s41439-018-0031-9
8. Ng YT, Kerrigan JF, Prenger EC, White WL, Rekate HL. Successful resection of a hypothalamic hamartoma and a Rathke cleft cyst. *Case report. J Neurosurg.* (2005) 102:78–80. doi: 10.3171/ped.2005.102.1.0078
9. Gagnier JJ, Kienle G, Altman DG, Moher D, Sox H, Riley D, et al. The CARE Guidelines: Consensus-based clinical case reporting guideline development. *Glob Adv Health Med.* (2013) 2:38–43. doi: 10.7453/gahmj.2013.008
10. Group WHOMGRS. WHO Child Growth Standards based on length/height, weight and age. *Acta Paediatr Suppl.* (2006) 450:76–85. doi: 10.1111/j.1651-2227.2006.tb02378.x
11. Sheng HS, Shen F, Zhang N, Yu LS, Lu XQ, Zhang Z, et al. Whole exome sequencing of multiple meningiomas with varying histopathological presentation in one patient revealed distinctive somatic mutation burden and independent clonal origins. *Cancer Manag Res.* (2019) 11:4085–95. doi: 10.2147/CMAR.S202394
12. Li H, Durbin R. Fast and accurate short read alignment with Burrows-Wheeler transform. *Bioinformatics.* (2009) 25:1754–60. doi: 10.1093/bioinformatics/btp324
13. DePristo MA, Banks E, Poplin R, Garimella KV, Maguire JR, Hartl C, et al. A framework for variation discovery and genotyping using next-generation DNA sequencing data. *Nat Genet.* (2011) 43:491–8. doi: 10.1038/ng.806
14. Li H, Handsaker B, Wysoker A, Fennell T, Ruan J, Homer N, et al. The Sequence Alignment/Map format and SAMtools. *Bioinformatics.* (2009) 25:2078–9. doi: 10.1093/bioinformatics/btp352
15. Cibulskis K, Lawrence MS, Carter SL, Sivachenko A, Jaffe D, Sougnez C, et al. Sensitive detection of somatic point mutations in impure and heterogeneous cancer samples. *Nat Biotechnol.* (2013) 31:213–9. doi: 10.1038/nbt.2514
16. Saunders CT, Wong WS, Swamy S, Becq J, Murray LJ, Cheetham RK. Strelka: accurate somatic small-variant calling from sequenced tumor-normal sample pairs. *Bioinformatics.* (2012) 28:1811–7. doi: 10.1093/bioinformatics/bts271
17. Boeva V, Popova T, Bleakley K, Chiche P, Cappo J, Schleiermacher G, et al. Control-FREEC: a tool for assessing copy number and allelic content using next-generation sequencing data. *Bioinformatics.* (2012) 28:423–5. doi: 10.1093/bioinformatics/btr670
18. Schwarz JM, Rodelsperger C, Schuelke M, Seelow D. MutationTaster evaluates disease-causing potential of sequence alterations. *Nat Methods.* (2010) 7:575–6. doi: 10.1038/nmeth0810-575
19. Zhou X, Edmonson MN, Wilkinson MR, Patel A, Wu G, Liu Y, et al. Exploring genomic alteration in pediatric cancer using ProteinPaint. *Nat Genet.* (2016) 48:4–6. doi: 10.1038/ng.3466
20. Kerrigan JF, Parsons A, Tsang C, Simeone K, Coons S, Wu J. Hypothalamic hamartoma: Neuropathology and epileptogenesis. *Epilepsia.* (2017) 58 Suppl 2:22–31. doi: 10.1111/epi.13752
21. Coons SW, Rekate HL, Prenger EC, Wang N, Drees C, Ng YT, et al. The histopathology of hypothalamic hamartomas: study of 57 cases. *J Neuropathol Exp Neurol.* (2007) 66:131–41. doi: 10.1097/nen.0b013e3180302090
22. Yamada S, Wood CP, Shah JA, Vida J, Parisi JE, Jentoft ME. Hypothalamic hamartoma with neurofibrillary tangles. *Neuropathology.* (2016) 36:480–4. doi: 10.1111/neup.12296
23. Demurger F, Ichkou A, Mougou-Zerelli S, Le Merrer M, Goudefroye G, Delezoide AL, et al. New insights into genotype-phenotype correlation for GLI3 mutations. *Eur J Hum Genet.* (2015) 23:92–102. doi: 10.1038/ejhg.2014.62
24. Braddock SR, Lipinski RJ, Williams MS, Carey JC. 35(th) Annual David W Smith Workshop on Malformations and Morphogenesis: abstracts of the 2014 annual meeting. *Am J Med Genet A.* (2015) 167A:1685–740. doi: 10.1002/ajmg.a.37107
25. Jaiman S, Nalluri H, Aziz N, Kolar G. Pallister-Hall syndrome presenting as an intrauterine fetal demise at 39 weeks' gestation. *Indian J Pathol Microbiol.* (2012) 55:100–3. doi: 10.4103/0377-4929.94873
26. Dunham C, McFadden D, Dahlgren L, Butler B, Hamilton S, McKinnon M. Congenital hypothalamic "hamartoblastoma" versus "hamartoma": suggestions for neuropathologic terminology emanating from a mid-gestational autopsy case of pallister-hall syndrome. *Pediatr Dev Pathol.* (2018) 21:324–31. doi: 10.1177/1093526617701338
27. Kremer S, Minotti L, Thiriaux A, Grand S, Satre V, Le Bas JF, et al. Epilepsy and hypothalamic hamartoma: look at the hand Pallister-Hall syndrome. *Epileptic Disord.* (2003) 5:27–30.
28. Talsania M, Sharma R, Sughrue ME, Scofield RH, Lim J. Familial pallister-hall in adulthood. *Neuro Endocrinol Lett.* (2017) 38:329–31.
29. Ler GYL, Liew WK, Lim J, Lim JY, Ong LY, Tang PH, et al. Teaching NeuroImages: hypothalamic hamartoma and polydactyly: Think Pallister-Hall syndrome. *Neurology.* (2019) 93:e1016–7. doi: 10.1212/WNL.0000000000008580
30. Feuillan P, Peters KF, Cutler GB, Biesecker LG. Evidence for decreased growth hormone in patients with hypothalamic hamartoma due to Pallister-Hall syndrome. *J Pediatr Endocrinol Metab.* (2001) 14:141–9. doi: 10.1515/JPEM.2001.14.2.141
31. Hildebrand MS, Griffin NG, Damiano JA, Cops EJ, Burgess R, Ozturk E, et al. Mutations of the sonic hedgehog pathway underlie hypothalamic hamartoma with gelastic epilepsy. *Am J Hum Genet.* (2016) 99:423–9. doi: 10.1016/j.ajhg.2016.05.031
32. Al-Qattan MM, Shamseldin HE, Salih MA, Alkuraya FS. GLI3-related polydactyly: a review. *Clin Genet.* (2017) 92:457–66. doi: 10.1111/cge.12952
33. Johnston JJ, Olivos-Glander I, Killoran C, Elson E, Turner JT, Peters KF, et al. Molecular and clinical analyses of Greig cephalopolysyndactyly and Pallister-Hall syndromes: robust phenotype prediction from the type and position of GLI3 mutations. *Am J Hum Genet.* (2005) 76:609–22.
34. Johnston JJ, Sapp JC, Turner JT, Amor D, Aftimos S, Aleck KA, et al. Molecular analysis expands the spectrum of phenotypes associated with GLI3 mutations. *Hum Mutat.* (2010) 31:1142–54. doi: 10.1002/humu.21328
35. Dericioglu N, Saygi S, Akalan N. Transcallosal endoscopic resection of hypothalamic hamartoma in a case with Pallister-Hall syndrome. *Epileptic Disord.* (2011) 13:209–13. doi: 10.1684/epd.2011.0440
36. Boudreau EA, Liow K, Frattali CM, Wiggs E, Turner JT, Feuillan P, et al. Hypothalamic hamartomas and seizures: distinct natural history of isolated and Pallister-Hall syndrome cases. *Epilepsia.* (2005) 46:42–7. doi: 10.1111/j.0013-9580.2005.68303.x
37. Mittal S, Mittal M, Montes JL, Farmer JP, Andermann F. Hypothalamic hamartomas. Part 1. Clinical, neuroimaging, and neurophysiological characteristics. *Neurosurg Focus.* (2013) 34:E6. doi: 10.3171/2013.3.FOCUS1355
38. Burghardt T, Basha MM, Fuerst D, Mittal S. Crying with sorrow evoked by electrocortical stimulation. *Epileptic Disord.* (2013) 15:72–5. doi: 10.1684/epd.2013.0559
39. Valentin A, Lazaro M, Mullatti N, Cervantes S, Malik I, Selway RP, et al. Cingulate epileptogenesis in hypothalamic hamartoma. *Epilepsia.* (2011) 52:e35–9. doi: 10.1111/j.1528-1167.2011.03060.x

40. Chibbaro S, Cebula H, Scholly J, Todeschi J, Ollivier I, Timofeev A, et al. Pure endoscopic management of epileptogenic hypothalamic hamartomas. *Neurosurg Rev.* (2017) 40:647–53. doi: 10.1007/s10143-017-0822-3

Conflict of Interest: The authors declare that the research was conducted in the absence of any commercial or financial relationships that could be construed as a potential conflict of interest.

Publisher's Note: All claims expressed in this article are solely those of the authors and do not necessarily represent those of their affiliated organizations, or those of the publisher, the editors and the reviewers. Any product that may be evaluated in this article, or claim that may be made by its manufacturer, is not guaranteed or endorsed by the publisher.

frontiers in Surgery

CASE REPORT
published: 14 December 2021
doi: 10.3389/fsurg.2021.775560

Case Report: Creeping Growth in Lymphoplasmacyte-Rich Meningioma—A Radiologic Variant

Jiuhong Li[1,2†], Xin Zan[1†], Min Feng[3], Xueyun Deng[4], Si Zhang[1] and Wenke Liu[1*]*

[1] Department of Neurosurgery, West China Hospital, Sichuan University, Chengdu, China, [2] West China School of Medicine, Sichuan University, Chengdu, China, [3] Department of Pathology, West China Hospital, Sichuan University, Chengdu, China, [4] Department of Neurosurgery, The Second Clinical Medical College of North Sichuan Medical College, Nanchong Central Hospital, Nanchong, China

Lymphoplasmacyte-rich meningioma (LRM) is a rare histologic subtype of meningioma. Creeping-growth pattern is uncommon in meningioma, and the mechanism is unclear. Here, we report a 44-year-old man presented with extremities weakness for 2 months and incontinence for 2 weeks. Head and neck MRI revealed diffuse creeping-growth nodular meningeal masses with skull base, tentorium, sella area, and C1-6 vertebral plane involvement. An operation was carried out, cervical and lower clivus part of the lesion was resected, but gross total resection could not be achieved due to the widespread lesions. Pathologic examination revealed the diagnosis of LRM. The patient is free from progression clinically 3 months postoperatively. We also conducted a systematic literature review about LRM with creeping-growth pattern. A total of only nine cases (including the present case) of creeping-growth LRMs were included and analyzed in terms of clinical manifestations, radiological features, treatment, and outcome. LRMs show a higher rate (7.5%) of creeping-growth pattern than other types of meningiomas. The average creeping length of all creeping-growth LRMs was 11.4 ± 10.9 cm (range, 3–30 cm). Most cases (66.7%) had obvious peritumoral edema. Total removal rate is low (33.3%), and two of them (22.2%) received biopsy, followed by steroids treatment (or further immunosuppressive drugs therapy) and radiotherapy. The recurrence rate is higher than conventional LRMs (22.2 vs. 11.3%), and one patient (11.1%) died 11 months after treatment. Creeping-growth pattern in LRM may be considered as a general radiologic variant. The recurrence rate is higher compared with LRM with round/swelling pattern. We speculated that the pathogenesis of creeping growth in LRM may be associated with damage of lymphatic systems of the central nervous system.

Keywords: creeping-growth, lymphoplasmacyte-rich meningioma, mechanism, lymphatic system, case report

OPEN ACCESS

Edited by:
Mario Ganau,
Oxford University Hospitals NHS Trust, United Kingdom

Reviewed by:
Salvatore Chibbaro,
Neurosurgery Department, Strasbourg University Hospital, France
Rahul Shah,
Oxford University Hospitals NHS Trust, United Kingdom

****Correspondence:***
Si Zhang
zhangsi198712@126.com
Wenke Liu
8592237@qq.com

† These authors have contributed equally to this work and share first authorship

Specialty section:
This article was submitted to Neurosurgery, a section of the journal Frontiers in Surgery

Received: *14 September 2021*
Accepted: *15 November 2021*
Published: *14 December 2021*

Citation:
Li J, Zan X, Feng M, Deng X, Zhang S and Liu W (2021) Case Report: Creeping Growth in Lymphoplasmacyte-Rich Meningioma—A Radiologic Variant. Front. Surg. 8:775560. doi: 10.3389/fsurg.2021.775560

INTRODUCTION

Intracranial meningioma represents the most common primary brain tumor (1). Radiologically, they frequently behave as swelling dura-based masses (2). Meningiomas with creeping-growth pattern are a rare occurrence and are frequently misdiagnosed preoperatively (3–5). Lymphoplasmacyte-rich meningioma (LRM) is probably the rarest histologic subtype of meningioma, accounting for around 1% of all intracranial meningiomas (6, 7). It is characterized by

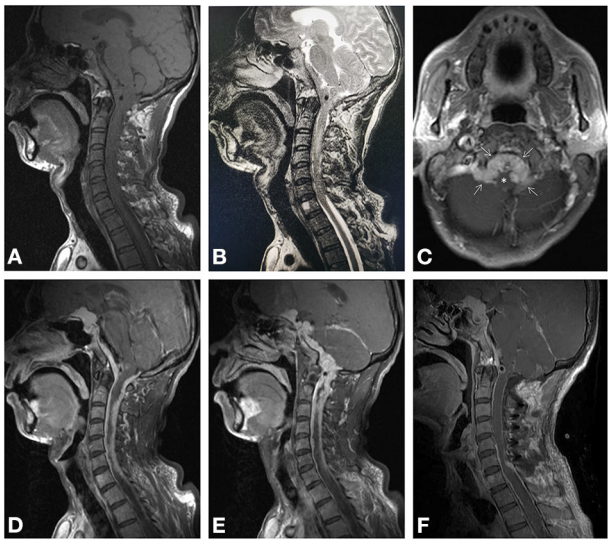

FIGURE 1 | Magnetic resonance imaging. Preoperative imaging revealed isointense lesions on T1-weighted **(A)** and T2-weighted imaging **(B)**, compressing the spinal cord. Axial enhanced T1-weighted imaging **(C)** revealed enhanced lesion located at midline premedullary cistern and lateral medullary cisterns (*arrows*), compressing the brainstem (*asterisk*). Sagittal enhanced T1-weighted imaging **(D, E)** showed multiple nodular lesions continuously creeping through the tentorium and meninges of sellar region, skull base, and C1–C6. Postoperative-enhanced MRI **(F)** proved the spinal and lower region of clivus of the tumor was totally removed.

infiltration of lymphoplasmacyte that overshadows the meningioma components (8). We reported a patient with LRM who presented with diffuse creeping-growth nodular meningeal masses with skull base, tentorium, sella area, and C1-6 vertebral plane involvement radiologically. Eight additional cases of creeping-growth LRM were identified in the literature and were also presented. The mechanism of creeping growth in LRM is unclear. Therefore, we also made a hypothesis to elucidate the mechanism of this rare growth pattern in LRM based on lymphatic systems of the central nervous system (CNS).

CASE PRESENTATION

A 44-year-old man presented with extremities weakness for 2 months and incontinence for 2 weeks. He had a history of hospitalization in another hospital 1 month ago. The electromyography testing results of limbs were normal and brain plain MRI showed no obvious abnormalities. A diagnosis of symptomatic parkinsonism (encephalitis-induced most likely) was made, and Madopar was prescribed for 2 weeks, but the symptoms did not alleviate and incontinence occurred. Thus, an indwelling urinary catheter was placed. The dosage of Madopar was gradually increased, but the symptoms did not alleviate. Two weeks later, he was transferred to our hospital. His temperature was 37.6°C on admission. Physical examination disclosed decreased muscle strength of extremities (muscle strength grade III for the left and IV for the right) and Babinski sign positive for lower limbs. White blood count was normal; HIV testing was negative. Head and neck MRI showed creeping-growth isointense lesions on T1- and T2-weighted images, compressing the spinal cord (**Figures 1A,B**). After administration of gadolinium, diffuse creeping-growth nodular meningeal masses with skull base, tentorium, sella area, and C1-6 vertebral plane involvement were detected, compressing medulla and adjacent spinal cord (**Figures 1C–E**). Routine urine examination of the patient showed that the white blood cell count was 44/HP, and pus cells were detected. The patient received levofloxacin instillation for 7 days and the temperature went normal. A preliminary diagnosis of meningeal inflammatory lesion was made based on radiological manifestations. Subsequently, he underwent an operation. The patient was placed with a left lateral decubitus position, and we used a posterior midline approach. We formed the bone flap (within 4 cm above foramen magnum) and removed posterior arch of C1, performed laminotomy of C2–C6. During operation, creeping-growth subdural masses surrounding the medulla and the spinal cord were detected, with a clear boundary. We mainly used ultrasonic aspiration to achieve tumor debulking and micro-scissors to achieve separation. The cervical and lower clivus part of the lesion was resected; however, gross total resection could not be achieved due to the widespread lesions. Finally, long-segment laminoplasty of C2–C6 and cranioplasty of occipital bone were performed. Postoperative MRI confirmed the total resection of the cervical and lower clivus part of the lesion (**Figure 1F**). The muscle strength of extremities of the patient recovered to normal level, and the Babinski sign was negative for lower limbs 4 days after surgery. Then he discharged and was transferred to our two-way referral hospital. The patient is free from progression clinically 3 months postoperatively (**Figure 2**). A histological test revealed that the tumor stroma was surrounded by prominent lymphocytes and plasmocytes. The tumor cells were positive for EMA, P63, PR, and negative for GFAP, Oligo2, and CK; lymphocytes were positive for LCA, CD3, and CD20; plasmocytes were positive for CD138, partly positive for IgG and IgG4, which is consistent with an LRM (**Figure 3**). A multidisciplinary team (Neurosurgery, Neurology, Oncology, and Pathology team) discussion for the patient was performed, and we recommended adjuvant radiotherapy while the patient refused. Thus, we recommended regular imaging follow-up, and if the tumor had sign of progression, stereotactic radiotherapy should be performed and the patient agreed.

LITERATURE REVIEW

This study was conducted and reported according to the Preferred Reporting Items for Systematic Reviews and Meta-Analysis statement.

Search Strategy and Article Selection

The PubMed and Embase databases were searched for case reports and series relevant to LRM published up to December

Abbreviations: CNS, central nervous system; LRM, lymphoplasmacyte-rich meningioma.

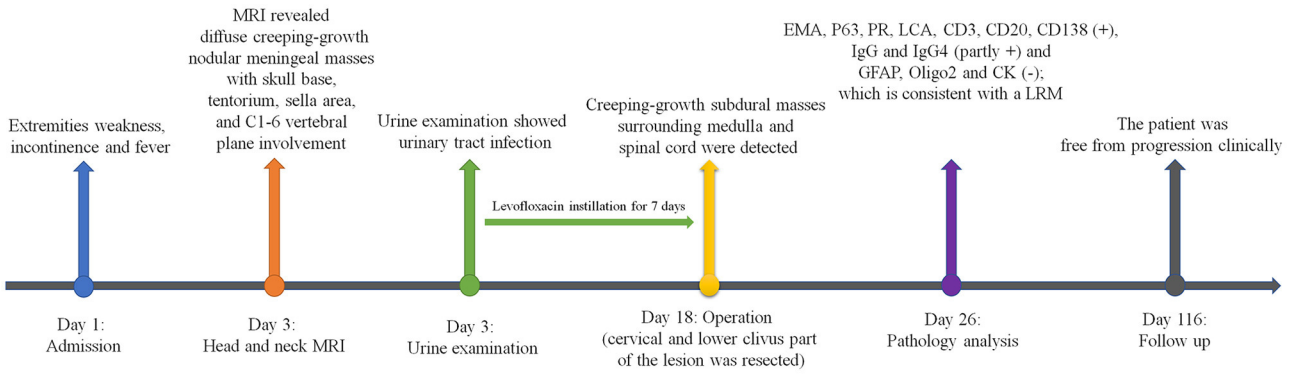

FIGURE 2 | Timeline of the case presentation.

31, 2020. "Lymphoplasmacyte," "rich," "lymphoplasmacyte-rich," and "meningioma" were used as either keywords or medical subject headings. In addition, the references cited in selected articles were hand-searched and reviewed to identify additional potentially eligible studies. Titles and abstracts of all articles were screened. Only articles describing cases of creeping-growth LRM were selected. Articles without any radiological imaging were excluded; articles published in languages other than English were also excluded from the study. References from relevant reviews were hand-searched. Subsequently, relevant articles were retrieved and evaluated independently by two authors (JL and XZ). A cross-reference check of the citations of each included relevant article was done to ensure that no relevant studies were missed by the computerized database search. Disagreements regarding the inclusion of studies were resolved by the judgment of a third author (SZ).

Data Extraction

Two authors (JL and XZ) independently extracted the following characteristics from the included studies: setting, study type, demographic data of presented patients, duration, tumor location, radiologic findings, treatment, outcome, and follow-up. The length of creeping growth in cases with complex skull base involvement is determined by the maximal creeping length on the axial, coronal, and sagittal planes.

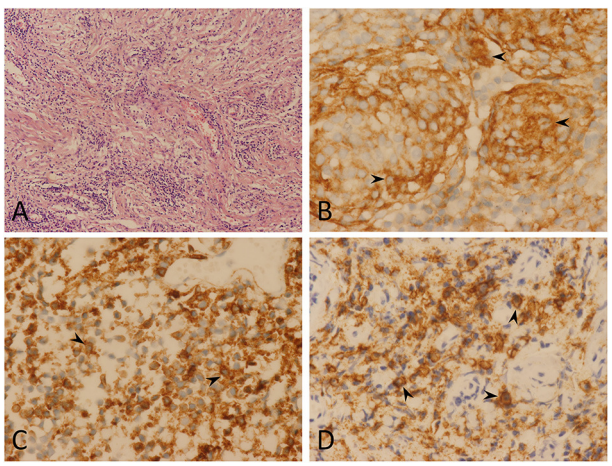

FIGURE 3 | Pathological findings. Hematoxylin and eosin (magnification, ×100) **(A)** showing lymphoplasmacytes infiltrated the tumor stroma, overshadowing the meningioma component. Immunohistochemistry testing showed epithelial membrane antigen positive (*arrowheads*) (magnification, ×400) **(B)**, CD20 positive (*arrowheads*) (magnification, ×400) **(C)**, and CD138 positive (*arrowheads*) (magnification, ×400) **(D)**. In conclusion, pathological findings indicate a lymphoplasmacyte-rich meningioma.

RESULT

Our search identified 46 potential citations for full-text evaluation. Eight cases of creeping-growth LRM from five different publications between 1997 and 2018 could be extracted from the literature and matched the inclusion criteria of our study.

Till now, around 120 cases of LRM have been reported in the English literature, and nine cases (7.5%) of creeping-growth LRM (including the present case) have been reported (4, 5, 9–12). The key characteristics of all reported creeping-growth LRM are summarized in **Supplementary Table 1**. There were five male and four female patients. The mean age was 40.8 ± 12.8 years (range, 22–55 years). Unlike other histologic subtypes of meningiomas, no female predominance was observed (0.8:1), which was similar to the literature report (4, 11). Most cases (55.6%) were non-skull base masses (**Supplementary Table 1**). The average creeping length of all creeping-growth LRMs was 11.4 ± 10.9 cm (range, 3–30 cm). Most cases (62.5%) had obvious peritumoral edema, higher than that (40%) of round LRMs reported by Tao et al. (11). Total removal rate is low (33.3%) due to the wide-spread lesion. Two of them (22.2%) received biopsy, followed by steroids treatment (or further immunosuppressive drugs therapy) and radiotherapy. The recurrence rate is higher than conventional LRMs (22.2 vs. 11.3%) and one patient (11.1%) died 11 months after treatment (11).

DISCUSSION

Lymphoplasmacyte-rich meningioma was firstly described by Banerjee and Blackwood in 1971, which was characterized by infiltration of lymphoplasmacyte that overshadows the meningioma components (8). It is probably the rarest histologic subtype of meningioma, accounting for around 1% of all intracranial meningiomas and was classified as WHO grade I tumor (6, 7). The pathogenesis, radiologic features, and outcome of this subtype of meningioma remain unclear because of their rarity. Here, we report an extremely rare case of LRM with a creeping-growth pattern mimicking idiopathic hypertrophic pachymeningitis and examine previously reported cases of creeping-growth LRM in an attempt to provide an up-to-date summary of the condition and illustrate the possible mechanism of this rare kind of growth pattern.

DIFFERENTIAL DIAGNOSIS

For subdural masses with creeping growth, the most common preoperative diagnosis can be a subdural hematoma, lymphoma, dural metastasis, and sarcoma. However, our study suggests that meningiomas should also be included in the differential diagnosis. Subdural LRMs usually have "dural tail sign" and are more likely to show extensive uneven thickening of nearby meninges and peritumoral edema (4). Patients with subdural hematoma usually have a brain-trauma history, with surrounding edema on T2-weighted image and no enhancement on enhanced MRI. Subdural lymphomas tend to be primary ones such as mucosal-associated lymphoid tissue lymphomas, usually with nodular/lobulate borders and leptomeningeal extension (13–17). Dural metastasis lesions usually demonstrate hyperintensity on T2-weighted imaging and have a history of systemic primary neoplasm, especially from melanoma, breast, and prostate cancers (16, 18, 19). Sarcomas tend to affect pediatric or younger patients and are usually accompanied by systemic leukemia (20). Other differential diagnoses include empyema or granuloma, neurosarcoidosis, tuberculosis, inflammatory pseudotumor, idiopathic hypertrophic pachymeningitis and Rosai–Dorfman disease (5, 12–14, 16, 18, 19, 21, 22). Thus, when dealing with subdural masses, neurosurgeons should at least be reminded of the possibility of LRM, and further examinations such as enhanced MRI should be considered which would be helpful for the differential diagnosis.

THERAPEUTIC STRATEGY

As for treatment of creeping-growth LRM, surgical resection is the optimal treatment modality to achieve pathological diagnosis, alleviate symptoms, and sometimes cure the disease (4, 5). However, the total removal rate is very challenging in some cases because of the wide-creeping lesion, which is hard to expose and resect (4, 5, 9, 10). As summarized in **Supplementary Table 1**, two patients had recurrence, and they both received incomplete resection. Thus, we hold that for patients receiving incomplete resection, radiotherapy should be recommended to achieve better tumor control. Hirunwiwatkul et al. (5) performed a biopsy to achieve pathological diagnosis of an LRM extending from planum sphenoidale down along the clivus to the foramen magnum and then prescribed prednisone and later azathioprine, followed by fractionated radiotherapy. And the patient was free from recurrence for over 6 months. Therefore, we hold that for creeping-growth LRM, a comprehensive treatment program (surgery, steroids, and immunosuppressive treatment combined with radiotherapy) could be recommended, especially for those receiving incomplete resection.

THE LYMPHATIC SYSTEM OF CNS

In 2015, Louveau et al. (23) discovered functional lymphatic vessels lining the venous sinuses in mice, which could drain both fluid and immune cells from cerebrospinal fluid–interstitial fluid flow. Absinta et al. (24) then demonstrated the existence of true lymphatic vessels in humans by non-invasive MRI, which run parallel to the venous sinus and alongside branches of the middle meningeal artery. Meningeal lymphatic vessels, together with the perineural sheaths surrounding cranial and spinal nerves and arachnoid granulations are thought to be three distinct kinds of outflow sites of cerebrospinal fluid in recent years (25). Meningeal lymphatic systems are mainly located within the dura mater and carry fluid, macromolecules, and immune cells, such as plasmocytes and lymphocytes, to the draining deep cervical lymph nodes (26).

POSSIBLE MECHANISM OF CREEPING-GROWTH PATTERN IN LRM

Radiologically, meningioma frequently manifests as swelling dura-based mass (1, 2). The creeping-growth pattern of meningiomas is rare; however, LRMs show a higher rate (7.5%) of creeping-growth pattern than other types of meningioma (1, 27). The mechanism of creeping growth in LRM is unclear. Yamaki et al. (12) hold that microscopically tumor component of LRM is almost replaced by abundant inflammatory cells; thus, LRM may behave differently from conventional meningioma radiologically. Liu et al. (28) suggest that lymphoplasmacytes could form cuff-like structure around the vascular tissue and damage the blood–brain barrier, thus causing enhancement on post-contrast MRI. We initially elucidate this rare phenomenon based on the lymphatic systems of the CNS.

We speculated that the mechanism of creeping growth in LRM might be as follows: (1) meningioma grows and erodes the meningeal lymphatic systems; (2) meningioma may even keep growing and transmitting to adjacent dura mater through the highway of the lymphatic system. (3) meningiomas express chemotactic agents such as inflammatory and chemotactic cytokines to assemble lymphocytes and plasmocytes; (4) vast lymphocytes and plasmocytes subsequently keep leaking from the lymphatic structure, overshadowing the meningioma

components; and (5) lymphocytes and plasmocytes change the microenvironment of the tumor and prevent the gathering and adhering of meningioma components or destroy/hamper the formation of peritumoral fibrin, restraining the swelling growth of the tumor, and thus LRM tends to grow diffusely along the meninges. In our case, the meningioma grows as continuous multiple nodular pattern probably under the influence of prominent infiltrated lymphoplasmacytes instead of forming a regular shape (swelling/round) of a meningioma (**Figures 1A–E**). In addition, the margin of case 4 (**Supplementary Table 1**) reported by Luo et al. is quite near the superior sagittal sinus and transverse sinus (4). Furthermore, case 2 (**Supplementary Table 1**) showed the vicinity of the tumor and occipital sagittal sinus (4). These cases indicated that the pathogenesis of LRM might be associated with the lymphatic system, especially the wider lymphatic vessels alongside intracranial venous sinuses. For the case treated in our hospital reported by Yang et al. (9), the whole intracranial dura mater was involved, which indicated the meningioma components may be transmitted through the meningeal lymphatic system to reach such widespread meninges. As for those LRMs behaving as swelling pattern, the destruction of the meningeal lymphatic systems may occur while the tumor is relatively large, whereas the infiltrated immune cells could not reshape the tumor.

The hypothesis that the pathogenesis of LRM associates with CNS lymphatic system damage could interpret the following four aspects of LRM behaviors. (1) Massive lymphocytes and plasmocytes infiltrating the tumor is uncommon, which means they are most likely to originate from lymphatic systems rather than blood vessels or cerebrospinal fluid. (2) Many creeping-growth LRMs could reach a creeping length of over 10 cm. The extraordinary diffuse involvement of dura mater may be attributed to the lymphatic system pathway transfusion. (3) It could explain why LRM may behave as regular (swelling/round) shape or a relatively higher rate (around 10%) of creeping-growth pattern than other histologic subtypes of meningiomas due to the different stages of lymphatic system damage. (4) The lymph proteins leaking from lymphatic systems or the dysfunction of cerebrospinal fluid absorbing caused by lymphatic destruction could further induce brain edema, which is compatible with the high rate (62.5%) of severe peritumoral edema in creeping-growth LRM (29).

The strength of our study is that we reviewed all the cases of creeping-growth LRMs and concluded that LRMs show a higher rate of creeping growth compared with other histological meningiomas; thus, the creeping-growth pattern in LRMs may be considered as a common radiologic variant. In addition, we proposed a hypothesis that the pathogenesis of LRMs may be associated with damage of lymphatic systems, which could nicely explain why LRM may behave as regular (swelling/round) shape or a relatively higher rate (around 10%) of creeping-growth pattern than other histologic subtypes of meningiomas due to the different stage of lymphatic system damage. The limitations of our study are retrospective in nature. Furthermore, because of financial limitations and local medical insurance policy restrictions, we could not obtain sufficient data regarding genetic conditions. Moreover, some cases of the literature were lost to follow-up. Finally, no evidence from the experiments confirming the mechanism of creeping growth of LRM existed. Therefore, further investigations, such as tracing the origin of lymphoplasmacytes, analyzing the function of infiltrated lymphocytes and plasmocytes, the possible chemotactic agents expressed by LRM, and exploring genetic differences, are necessary to elucidate the preferred mechanisms of creeping growth in LRM.

CONCLUSION

Lymphoplasmacyte-rich meningiomas show a higher rate (7.5%) of creeping-growth pattern than other types of meningiomas and may be considered as a general radiologic variant. Currently, though total removal is challenging, surgical resection is the optimal treatment to cure the disease and relieve the symptoms. The recurrence rate is higher compared with LRM with round/swelling pattern. We proposed a hypothesis that the pathogenesis of creeping growth in LRM may be associated with damage of the lymphatic systems of the CNS.

DATA AVAILABILITY STATEMENT

The original contributions presented in the study are included in the article/**Supplementary Material**, further inquiries can be directed to the corresponding authors.

ETHICS STATEMENT

The studies involving human participants were reviewed and approved by Ethics Committee of West China Hospital of Sichuan University. Written informed consent was obtained from the patient and his legal representatives for the publication. Written informed consent was obtained from the individual(s) for the publication of any potentially identifiable images or data included in this article.

AUTHOR CONTRIBUTIONS

XZ, SZ, and WL contributed to the conception and design of the study. JL, MF, and XD developed the methodology. JL, XZ, MF, XD, SZ, and WL helped in the acquisition and analysis of data. JL, XZ, and MF involved in writing, reviewing, and revision of the manuscript. MF and WL provided the technical and material support. SZ and WL supervised the study. All authors have read and approved the manuscript.

All authors contributed to the article and approved the submitted version.

FUNDING

This work was supported by the Youth Program of the National Natural Science Foundation of China (Nos. 81701174 and 81801178); the Program of Science & Technology Department of Sichuan Province (No. 2020YFS0222).

ACKNOWLEDGMENTS

The authors appreciate the patient's collaboration in this work.

SUPPLEMENTARY MATERIAL

The Supplementary Material for this article can be found online at: https://www.frontiersin.org/articles/10.3389/fsurg.2021.775560/full#supplementary-material

REFERENCES

1. Whittle IR, Smith C, Navoo P, Collie D. Meningiomas. *Lancet.* (2004) 363:1535–43. doi: 10.1016/S0140-6736(04)16153-9
2. Buetow MP, Buetow PC, Smirniotopoulos JG. Typical, atypical, and misleading features in meningioma. *Radiographics.* (1991) 11:1087–106.
3. Wu C, Liu J, Yang C. Meningioma mimics chronic subdural hematoma: a case report and discussion of differential diagnosis. *Neurol India.* (2012) 60:549–50. doi: 10.1148/radiographics.11.6.1749851
4. Yongjun L, Xin L, Qiu S, Jun-Lin Z. Imaging findings and clinical features of intracal lymphoplasmacyte-rich meningioma. *J Craniofac Surg.* (2015) 26:e132–7. doi: 10.1097/SCS.0000000000001193
5. Hirunwiwatkul P, Trobe JD, Blaivas M. Lymphoplasmacyte-rich meningioma mimicking idiopathic hypertrophic pachymeningitis. *J Neuroophthalmol.* (2007) 27:91–4. doi: 10.1097/WNO.0b013e31806773a5
6. Bhat AR, Wani MA, Kirmani AR, Ramzan AU. Histological-subtypes and anatomical location correlated in meningeal brain tumors (meningiomas). *J Neurosci Rural Pract.* (2014) 5:244–9. doi: 10.4103/0976-3147.133568
7. Louis DN, Perry A, Reifenberger G, von Deimling A, Figarella-Branger D, Cavenee WK, et al. The 2016 world health organization classification of tumors of the central nervous system: a summary. *Acta Neuropathol.* (2016) 131:803–20. doi: 10.1007/s00401-016-1545-1
8. Banerjee AK, Blackwood W. A subfrontal tumour with the features of plasmocytoma and meningioma. *Acta Neuropathol.* (1971) 18:84–8. doi: 10.1007/BF00684477
9. Yang X, Le J, Hu X, Zhang Y, Liu J. Lymphoplasmacyte-rich meningioma involving the whole intracranial dura mater. *Neurology.* (2018) 90:934–5. doi: 10.1212/WNL.0000000000005532
10. Cha YJ, Lee SK, Chang JH, Kim SH. Report of a rare case of atypical lymphoplasmacyte-rich meningioma in the tentorium mimicking idiopathic hypertrophic pachymeningitis. *Brain Tumor Pathol.* (2016) 33:216–21. doi: 10.1007/s10014-016-0254-8
11. Tao X, Wang K, Dong J, Hou Z, Wu Z, Zhang J, et al. Clinical, radiologic, and pathologic features of 56 cases of intracranial lymphoplasmacyte-rich meningioma. *World Neurosurg.* (2017) 106:152–64. doi: 10.1016/j.wneu.2017.06.143
12. Yamaki T, Ikeda T, Sakamoto Y, Ohtaki M, Hashi K. Lymphoplasmacyte-rich meningioma with clinical resemblance to inflammatory pseudotumor. Report of two cases. *J Neurosurg.* (1997) 86:898–904. doi: 10.3171/jns.1997.86.5.0898
13. Smith AB, Horkanyne-Szakaly I, Schroeder JW, Rushing EJ. From the radiologic pathology archives: mass lesions of the dura: beyond meningioma-radiologic-pathologic correlation. *Radiographics.* (2014) 34:295–312. doi: 10.1148/rg.342130075
14. Iwamoto FM, Abrey LE. Primary dural lymphomas: a review. *Neurosurg Focus.* (2006) 21:E5. doi: 10.3171/foc.2006.21.5.6
15. Goetz P, Lafuente J, Revesz T, Galloway M, Dogan A, Kitchen N. Primary low-grade B-cell lymphoma of mucosa-associated lymphoid tissue of the dura mimicking the presentation of an acute subdural hematoma. Case report and review of the literature. *J Neurosurg.* (2002) 96:611–4. doi: 10.3171/jns.2002.96.3.0611
16. Lim M, Kheok SW, Lim KC, Venkatanarasimha N, Small JE, Chen RC. Subdural haematoma mimics. *Clinical Radiol.* (2019) 74:663–75. doi: 10.1016/j.crad.2019.04.013
17. Starr CJ, Cha S. Meningioma mimics: five key imaging features to differentiate them from meningiomas. *Clinical Radiol.* (2017) 72:722–8. doi: 10.1016/j.crad.2017.05.002
18. Chourmouzi D, Potsi S, Moumtzouoglou A, Papadopoulou E, Drevelegas K, Zaraboukas T, et al. Dural lesions mimicking meningiomas: a pictorial essay. *World J Radiol.* (2012) 4:75–82. doi: 10.4329/wjr.v4.i3.75
19. Ganau M, Gallinaro P, Cebula H, Scibilia A, Todeschi J, Gubian A, et al. Intracranial metastases from prostate carcinoma: classification, management, and prognostication. *World Neurosurg.* (2020) 134:e559–e65. doi: 10.1016/j.wneu.2019.10.125
20. Catana D, Koziarz A, Cenic A, Nath S, Singh S, Almenawer SA, et al. Subdural hematoma mimickers: a systematic review. *World Neurosurg.* (2016) 93:73–80. doi: 10.1016/j.wneu.2016.05.084
21. Gupta RK, Kumar S. Central nervous system tuberculosis. *Neuroimaging Clin N Am.* (2011) 21:795–814, vii–viii. doi: 10.1016/j.nic.2011.07.004
22. Sandoval-Sus JD, Sandoval-Leon AC, Chapman JR, Velazquez-Vega J, Borja MJ, Rosenberg S, et al. Rosai-Dorfman disease of the central nervous system: report of 6 cases and review of the literature. *Medicine.* (2014) 93:165–75. doi: 10.1097/MD.0000000000000030
23. Louveau A, Smirnov I, Keyes TJ, Eccles JD, Rouhani SJ, Peske JD, et al. Structural and functional features of central nervous system lymphatic vessels. *Nature.* (2015) 523:337–41. doi: 10.1038/nature14432
24. Absinta M, Ha SK, Nair G, Sati P, Luciano NJ, Palisoc M, et al. Human and nonhuman primate meninges harbor lymphatic vessels that can be visualized noninvasively by MRI. *Elife.* (2017) 6:e29738. doi: 10.7554/eLife.29738.018
25. Rasmussen MK, Mestre H, Nedergaard M. The glymphatic pathway in neurological disorders. *Lancet Neurol.* (2018) 17:1016–24. doi: 10.1016/S1474-4422(18)30318-1
26. Raper D, Louveau A, Kipnis J. How do meningeal lymphatic vessels drain the CNS? *Trends Neurosci.* (2016) 39:581–6. doi: 10.1016/j.tins.2016.07.001
27. Buerki RA, Horbinski CM, Kruser T, Horowitz PM, James CD, Lukas RV. An overview of meningiomas. *Future Oncol.* (2018) 14:2161–77. doi: 10.2217/fon-2018-0006
28. Liu JL, Zhou JL, Ma YH, Dong C. An analysis of the magnetic resonance imaging and pathology of intracal lymphoplasmacyte-rich meningioma. *Eur J Radiol.* (2012) 81:968–73. doi: 10.1016/j.ejrad.2011.02.014
29. West CA, Fischer GA, Young AJ, He C, Su M, Mentzer SJ. Biochemical changes in the efferent lymph plasma after oxazolone stimulation. *Dev Comp Immunol.* (2002) 26:111–9. doi: 10.1016/s0145-305x(01)00043-x

Conflict of Interest: The authors declare that the research was conducted in the absence of any commercial or financial relationships that could be construed as a potential conflict of interest.

Publisher's Note: All claims expressed in this article are solely those of the authors and do not necessarily represent those of their affiliated organizations, or those of the publisher, the editors and the reviewers. Any product that may be evaluated in this article, or claim that may be made by its manufacturer, is not guaranteed or endorsed by the publisher.

frontiers in Surgery

CASE REPORT
published: 24 January 2022
doi: 10.3389/fsurg.2021.773371

Internal Maxillary Artery-Radial Artery-Middle Cerebral Artery Bypass and STA-MCA Bypass for the Treatment of Complex Middle Cerebral Artery Bifurcation Aneurysm: A Case Report

Chaojue Huang†, Shixing Qin†, Guan Cao, Wei Huang* and Yongjia Yu*

Department of Neurosurgery, First Affiliated Hospital of Guangxi Medical University, Nanning, China

OPEN ACCESS

Edited by:
Philipp Taussky,
The University of Utah, United States

Reviewed by:
Lai Fung LI,
Queen Mary Hospital, Hong Kong SAR, China
Jorge Marcelo Mura,
Instituto de Neurocirugía, Chile

***Correspondence:**
Chaojue Huang
310046542@qq.com
Wei Huang
13977166636@126.com

†*These authors have contributed equally to this work and share first authorship*

Specialty section:
This article was submitted to Neurosurgery, a section of the journal Frontiers in Surgery

Received: *09 September 2021*
Accepted: *13 December 2021*
Published: *24 January 2022*

Citation:
Huang C, Qin S, Cao G, Huang W and Yu Y (2022) Internal Maxillary Artery-Radial Artery-Middle Cerebral Artery Bypass and STA-MCA Bypass for the Treatment of Complex Middle Cerebral Artery Bifurcation Aneurysm: A Case Report. Front. Surg. 8:773371. doi: 10.3389/fsurg.2021.773371

Background: Children's complex middle cerebral artery (MCA) aneurysm is a relatively rare occurrence. When the huge aneurysm is located in the MCA bifurcation with an inconspicuous neck and involving numerous arteries, intravascular interventional surgery or aneurysm clipping are often difficult treatment options. At this point, high flow bypass revascularization is necessary as a treatment to preserve cerebral blood flow. In recent years, the internal maxillary artery (IMA) has gradually become the mainstream donor artery of thw high flow bypass. We performed internal maxillary artery -radial artery-middle cerebral artery (IMA-RA-MCA) and superficial temporal artery-middle cerebral artery (STA-MCA) bypass as the treatment of a complex MCA bifurcation aneurysm in consideration of the patient's condition and the advantage of the IMA. According to the author, this case is the youngest reported case of IMA-RA-MCA bypass at present.

Case Description: A male child, 7 years and 8 months, was admitted to the hospital due to "recurrent headache for more than 9 months," DSA indicated that there was a large wide-necked aneurysm at the bifurcation of the right MCA M1 segment, with a size of about 1.16*1.58*1.32 cm. The inflow path of the aneurysm was in front of M1 bifurcation, and one outflow path originated from the aneurysm body, and another small outflow path attached to the aneurysm body. After completing the preoperative evaluation, an extended pterional approach with zygomatic osteotomy was performed to fully expose the aneurysm and IMA, harvesting the left radial artery at the same time, then a STA-MCA bypass, IMA-RA-MCA bypass, and aneurysm trapping were performed. postoperative re-examination showed that bypass vessels and the distal middle artery vessels were patent and the aneurysm disappeared, the child has no neurological dysfunction.

Conclusions: IMA-RA-MCA bypass is an effective high-flow cerebral blood reconstruct scheme in the treatment of complex middle cerebral artery bifurcation aneurysms. This case can provide a reference for the surgical treatment of complex middle cerebral artery bifurcation aneurysms in children.

Keywords: pediatric complex aneurysm, middle cerebral artery bifurcation aneurysm, internal maxillary artery, superficial temporal artery, extracranial-to-intracranial bypass, high flow bypass

INTRODUCTION

Nowadays, intracranial aneurysms are mostly treated by intravascular therapy. Especially in recent years, flow diversion devices (FDDs) have been widely proved to be safe for the treatment of complex cerebrovascular diseases, which is greatly expanding the indications for intracranial aneurysm treatment. However, traditional microsurgery is still difficult to replace in the treatment of MCA M1 bifurcation aneurysms, especially when aneurysms have complex morphology and involve multiple branching arteries.

Complex aneurysms of the middle cerebral artery are rare in children. In this case, the patient was too young and the wide-neck aneurysm was located at the bifurcation of MCA and numerous vessels were involved. Considering long-term prognosis, graft length and other factors, MA-RA-MCA + STA-MCA bypass was performed. According to the author, this case is the youngest reported case of IMA-RA-MCA bypass at present.

CASE DESCRIPTION

General Information and Preoperative Preparation

A male child, aged 7 years and 8 months, was admitted to the hospital on April 22, 2021 due to "recurrent headache for more than 9 months" without other complaints of discomfort. About 4 days before admission, the child had a paroxysmal headache, and head CT suggested a high-density shadow in the right sylvian fissure (Possibly meningioma? AVM?) He was transferred to our hospital for further diagnosis and treatment. Cranial nerve and nervous system examination showed no abnormalities. DSA indicated that there was a wide-necked aneurysm at the bifurcation of the M1 segment of the right middle cerebral artery, about 1.16*1.58*1.32 cm in size. The inflow path of the aneurysm was in the front of M1 bifurcation, and one outflow artery branch was seen to originate from the aneurysm, and another small artery attached to the aneurysm was suspected to be another outflow artery, as shown in **Figures 1A,B**. Hunt-Hess grade I.

After discussion by various experts in our ward, the cerebrovascular reconstruction plan was decided, the IMA-RA-MCA bypass and aneurysm trapping were preliminarily proposed after the aneurysm's outflow arteries were adequately explored, STA bypass would be performed when necessary. A preoperative CTA, color ultrasound of the radial artery, and Allen test were completed to evaluate whether the IMA and radial artery were suitable for bypass grafting. The relevant preoperative examination and operation diagram is shown in **Figure 2**.

Abbreviations: CT, computed tomography; CTA, CT-angiography; CTP, CT-perfusion; DSA, digital subtraction angiography; MRI, Magnetic resonance imaging; RA, Radial artery; RAG, Radial artery graft; MCA, Middle cerebral artery; IMA/IMAX, Internal maxillary artery; STA: Superficial temporal artery; mRS, modified Rankin Scale; EC-IC: extracranial-to-intracranial; IC-IC: intracranial-to-intracranial; ECA, external carotid artery.

Surgical Procedure

Excluding other surgical contraindication, the extended pterional approach with zygomatic osteotomy was performed, the skull base bone of the inferior temporal fossa was fully bitten to better explore and obtain IMA. The right IMA was explored and exposed with the aid of intraoperative neuronavigation and doppler, the diameter of the IMA was about 2.0 mm, then it was separated and exposed with a length of about 1.5 cm.

The M1 segment of the right MCA, the aneurysm, anterior cerebral artery, and internal carotid artery were exposed (**Figure 1A**). The exploration showed that two branches of the MCA emanated from the aneurysm, one of which was larger and emitted two branching arteries, confirming the preoperative conjecture (comparing **Figures 3A,B** with **Figure 1B**). During the intracranial operation, the other group of surgeons explored the radial artery of the left forearm. The diameter of the radial artery was about 2.0 mm and the blood flow was patent, 10 cm was cut for use after measuring the distance, rinsing the radial artery lumen with heparin-saline to prevent vasospasm.

The right STA-MCA end-to-side bypass was performed for the smaller outflow path (**Figure 3C** The white arrow). The recipient artery was blocked for 25 min during the STA-MCA bypass. The end-to-side bypass of the radial artery and the larger outflow path was performed continuously (**Figure 3C** The yellow arrow). The recipient artery was blocked for 22 min during the RA-M2 bypass. The lateral skull base bone of the inferior temporal fossa was fully bitten when we exposed IMA as mentioned above, RAG exits the right sylvian fissure and follows the surface of the temporal lobe toward the inferior temporal fossa, and the inferior temporal fossa enters to meet IMA through the dura and the skull window of the bottom of the temporal lobe (**Figures 3E,F**). Then the IMA-RA end-to-side bypass was performed (**Figure 3D** The yellow arrow), the recipient artery was blocked for 35 min during IMA-RA bypass. The distal part of the IMA was clipped after bypass artery blood flow was evaluated by intraoperative doppler.

Finally, the proximal M1 segment of the aneurysm was separated and exposed again, the outflow path and inflow path of the aneurysm were trapped, respectively. Intraoperative fluorescence angiography showed that the bypass vessels were patent and the aneurysm blood supply disappeared (**Figures 3E,F**). The aneurysm's blood was continuously blocked for 1 h, and there was no change of motor evoked potential, somatosensory evoked potential or other monitoring indicators in intraoperative electrophysiological monitoring.

During the operation, blood pressure was strictly controlled at the normal level, and 10-0 prolene vascular sutures were used for anastomosis. After bypass, the dura, lateral pterygoid muscle, and temporalis muscle were rested and sutured. The skull flap was properly clipped to avoid excessive compression of bypass arteries and was rested and fixed with the zygoma. Intraoperative images are shown in **Figure 3**.

Postoperative Management and Follow-Up

The patient was routinely given intensive care, blood pressure control, and anticoagulant medication as planned after bypass surgery. The postoperative anticoagulant regimen was to take aspirin 50 mg/qd the first day after surgery and take it 6 months

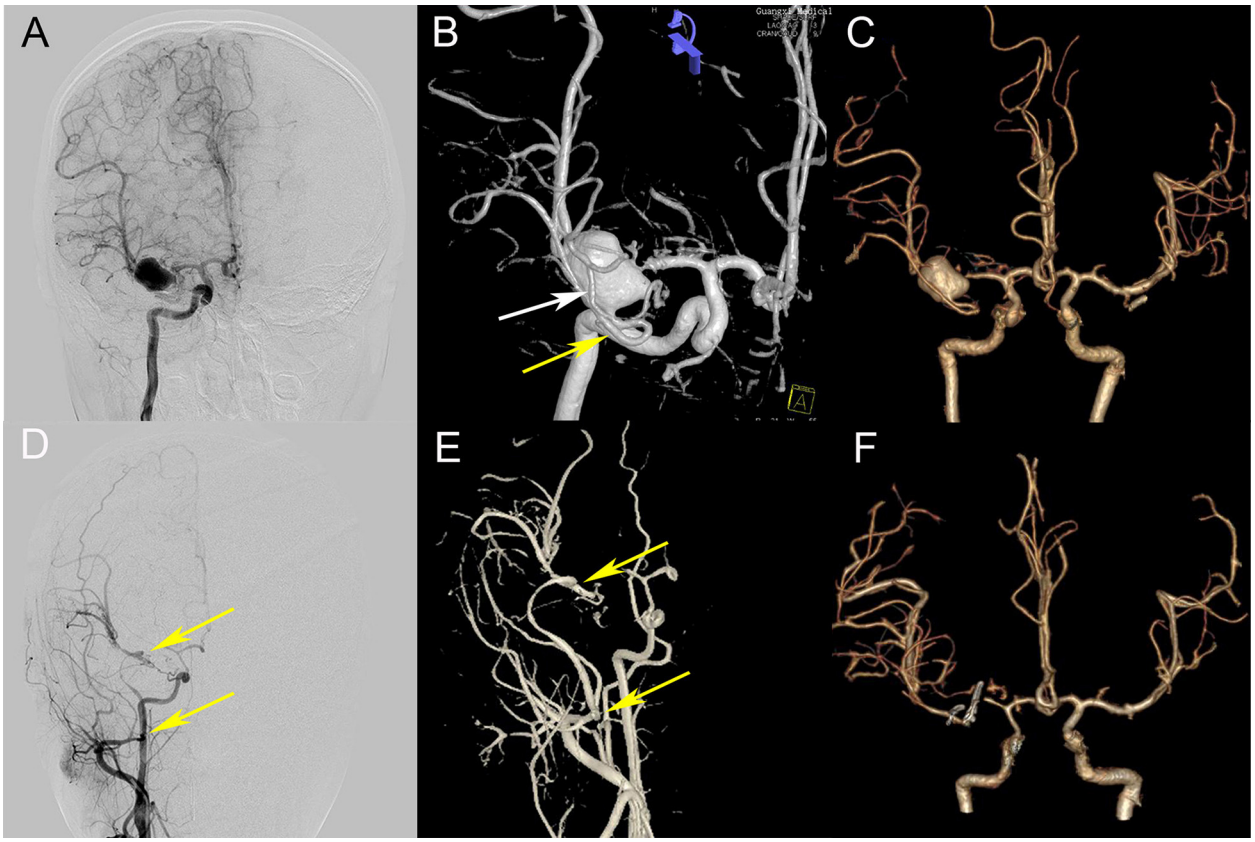

FIGURE 1 | Preoperative and postoperative comparison. **(A,B)** Preoperative DSA (A, frontal view; B, anterior upper view) showing an aneurysm at the bifurcation of M1, a small outflow path (the white arrow) and a larger outflow path (the yellow arrow) at the lateral side of the aneurysm; **(C)** Preoperative CTA 3D reconstruction; **(D,E,F)** Postoperative DSA and CTA showed that the IMX-RA-M2 bypass artery was patent (two yellow arrows indicate the RAG anastomosis), the aneurysm disappeared, and the distal artery of MCA was clearly developed (comparing C and F).

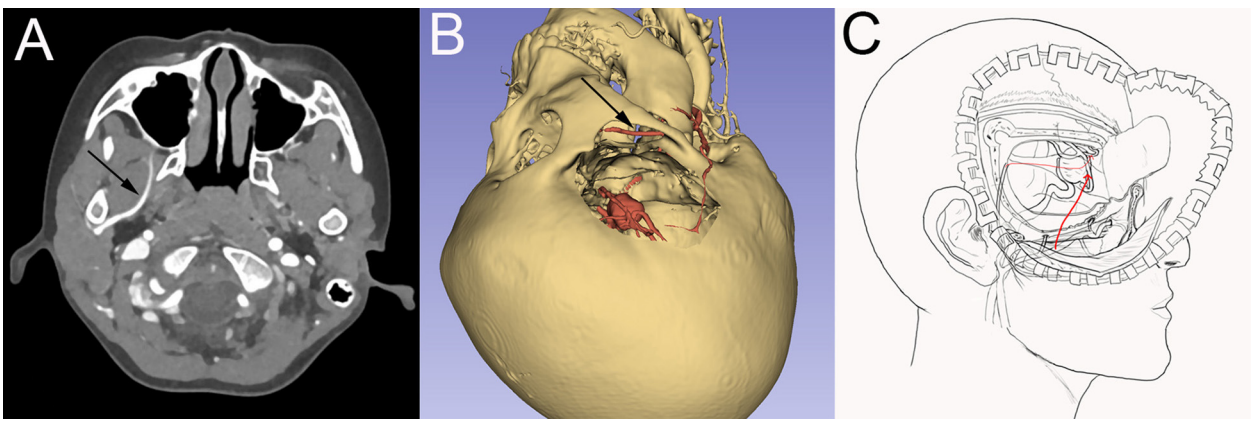

FIGURE 2 | Preoperative examination and surgical design. **(A)** Preoperative CTA showed that the right internal maxillary artery was located deep inside the lateral wing muscle. **(B)** Preoperative 3D display of bone window, aneurysm, and internal maxillary artery, the black arrow is the internal maxillary artery; **(C)** Schematic diagram of bypass surgery.

postoperatively regularly. Sodium valproate and nimodipine were routinely given to prevent epilepsy and cerebral vasospasm, too. CT before discharge showed no obvious bleeding or infarction. CTA and CTP showed improved blood perfusion in the right MCA supplying area, the distal trunk and branches of the MCA were also well-developed, as shown in **Figures 3E,F**.

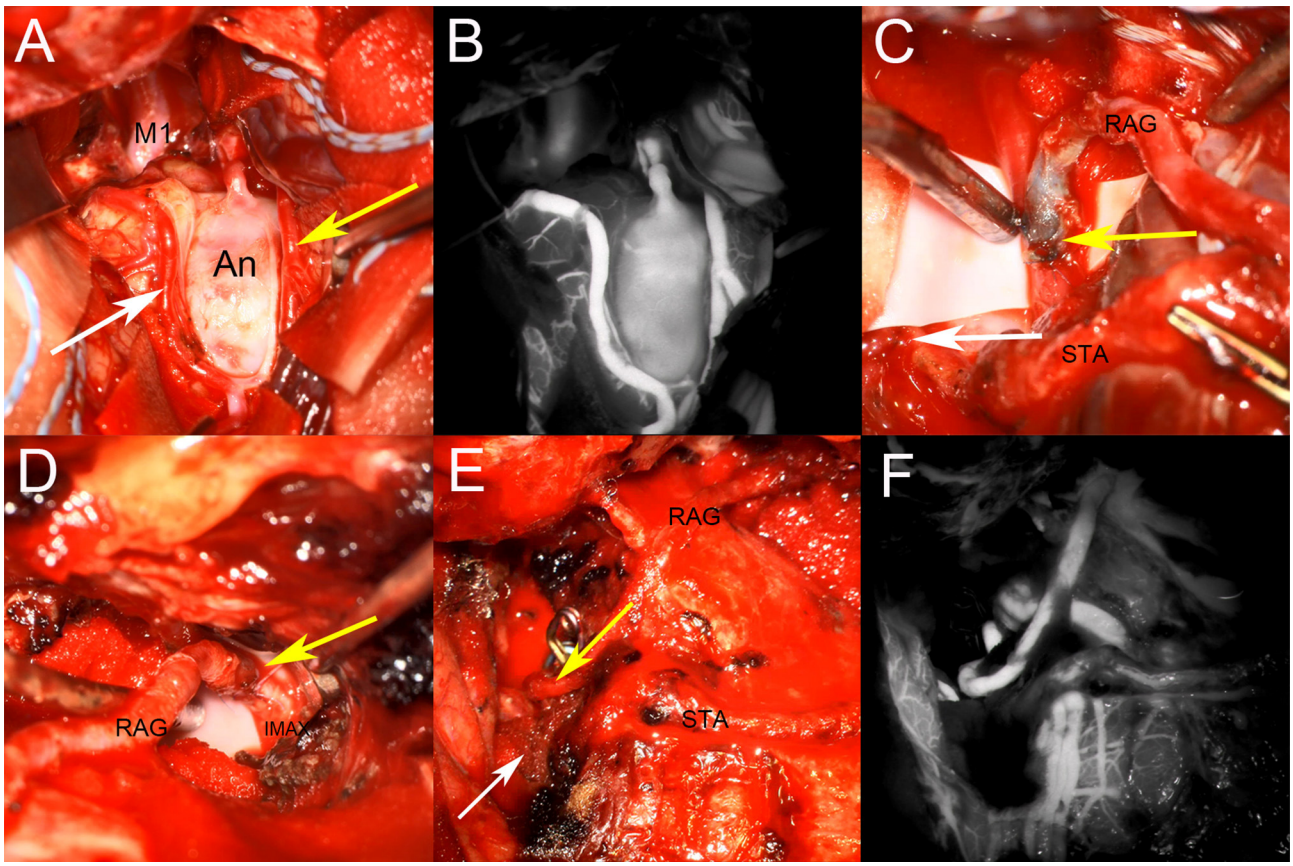

FIGURE 3 | Intraoperative images. **(A)** Aneurysm inflow artery and outflow artery were explored. Two outflow paths were affirmed, location of STA-M2 and RA-M2 anastomosis were indicated by white and yellow arrows; **(B)** Indocyanine green video angiography after aneurysm exploration; **(C)** Arteries conditions after end-to-side anastomosis of intracranial parts, the white arrow indicate STA-M2 anastomosis, and the yellow arrow indicate RA-M2 anastomosis; **(D)** The yellow arrow indicate RA-IMA end-to-side anastomosis; **(E,F)** The aneurysm was isolated after the completion of the bypass, and indocyanine green video angiography showed that the aneurysm disappeared and the reconstructed arteries were patent.

MRI indicated a small cerebral infarction in the external capsule area, but the child had no obvious neurological dysfunction.

The child complained of no neurological dysfunction and the daily life was the same as before in follow-up 6 months after the operation. He only had slight discomfort of his left fingers, and often subconsciously gripped the left finger to relieve the symptoms, but there was no paleness of extremities, numbness, or other symptoms, mRS = 1. DSA was re-examined 6 months after the operation, the IMA-RA-M2 bypass were patent and RAG diameter slightly increased than before, and the rest were roughly the same as the DSA 3 months before.

DISCUSSION

As to complex aneurysms located in the MCA bifurcation, considering the aneurysm wide-neck, involving potential lenticulostriate arteries and multiple branching arteries, conventional aneurysm clipping and endovascular treatment is often difficult to completely resect or isolate the aneurysm, and safeguard cerebral blood flow at the same time. So cerebral vascular reconstruction surgery is very necessary for such a circumstance.

In terms of the selection of reconstruction methods, Due to the complex vascular route of the aneurysm at the MCA bifurcation, it is generally accepted that middle or high flow bypass should be performed in the need of reconstructing the blood supply from MCA. Lawton consider that middle or high flow bypass is the preferred treatment for MCA bifurcation aneurysms (1). Combined bypass is a combination of two or more bypass procedures based on the six single bypass procedures summarized by Lawton et al. requiring more than two intraoperative anastomoses, such as double branch replantation using extracranial blood supply branch, double branch replantation using intracranial blood supply branch, IC-IC bypass + EC-IC bypass, etc. For unruptured MCA bifurcation aneurysms, single EC-IC high-flow bypass, or double STA- MCA bypass (2–4) can also be used as reconstruction schemes.

Combined with the characteristics of preoperative examination in this case, the risk of aneurysm clipping or interventional embolization is high on account of the bifurcation of MCA in children is complicated and the diameter is small.

Moreover, considering the long-term prognosis and the risk of aneurysm rupture, aneurysm trapping is the first choice. In addition, as the most commonly used extracranial blood supply artery, the blood flow provided by STA is related to the diameter and the recipient artery of the intracranial artery (2). Successful treatments of STA-MAC bypass that can provide blood flow >100 mL/min have been reported previously (2, 3, 5, 6), but the anterior and parietal branches of STA are relatively thin in this case, and the diameter is about 0.5 mm, so it is difficult to replace blood supply effectively if a double STA-MCA bypass is performed alone (5). Therefore, STA can only be used as a secure blood supply artery, and cannot replace the role of a high-flow blood supply artery. It should be noted that in this case, STA was not clearly displayed in postoperative angiography (**Figures 1D,E**), which was considered for two reasons: (1) the formation of small thrombosis in STA; (2) the blood supply of IMA-RA-M2 had completely replaced distal blood of MAC and the pressure difference at the anastomosis of STA-MCA was too small to display STA. We think the second point is the main reason.

Prior STA-M2 bypass provides partial blood flow to the brain during high-flow bypass artery occlusion, ensuring security when performing the complex and difficult high flow bypass afterwards. Once the high flow bypass failed, the STA can still guarantee part of effective blood artery blood supply to the brain. Therefore, the final plan was STA-M2 bypass first, followed by IMA-RA-M2 bypass, then to finally trap the aneurysm.

Compared with the intracranial insertion bypass, extracranial double-branch replantation of extracranial blood supply, or external carotid artery (ECA)-graft-MCA single-branch high-flow bypass previously, the core characteristic of this case's scheme is using the IMA as a high-flow donor artery for a seven-year-old child, which reflects the advantages of the IMA-RA-MCA bypass. In recent years, with the development of research and technical practice, the advantages of IMA as a high-flow bypass donor artery in the treatment of complex MCA arteries aneurysms have been well-established (7), and there have been many successful cases and case series reports (8–12), confirming that the IMA can be a safe and efficient high-flow donor artery. Compared with ECA, IMA has many advantages such as a single cranial incision, shorter distance from the intracranial recipient artery which reduces the length of the graft, thus reducing the risk of postoperative bypass vessel torsion, and the deeper location can effectively avoid compression, etc (9). Furthermore, the disadvantages are that the position of IMA is deep and difficult to expose, and the technical requirements of the operator are higher. In our case, due to the young age, the length of the RA graft that can be provided is limited. If performing ECA-RA-MCA bypass, it usually needs to intercept 16–18 cm RA graft (13–15). However, the seven-year-old child's short forearm makes it difficult to intercept such a length, and there is a risk of bypass vessel torsion at the same time.

The application of IMA can fully reflect its advantages and effectively solve the problems such as limited graft length (16). Generally, the second and third segments of IMA, namely the pterygoid and the Pterygopalatine segments, are used as bypass donor arteries (17, 18). To better obtain IMA, there have been numerous reports exploring more appropriate approaches and craniotomy techniques to expose IMA in recent years (19–21). Considering the operating space required for bypass surgery, we agree with the experience of Professor Xiang'en Shi's team at Beijing Sanbo Brain Hospital (9, 10, 22), Zygomatic arch was removed and the skull base bone was bitten off when necessary to fully expose the inferior temporal fossa during craniotomy so that the pterygoid segment of IMA can be fully separated. In this case, no serious masticatory muscle-related complications occurred. Preoperative CTA was performed to predict IMA location, and intraoperative neuronavigation and doppler probe assisted detection of IMA helped to obtain IMAX more efficiently and safely.

In terms of graft selection, RA has good matching, convenient for preoperative evaluation and acquisition, and good postoperative patency, but vasospasm and other complications should be paid attention to. Previous studies have pointed out that the RA is not suitable to be used as the graft artery in children younger than 12 years old (9, 16), but there is also case reported that the RA was used as the graft artery in the treatment of MCA in a 4-year-old child (23). In this case, preoperative examination and intraoperative vascular matching showed that RA was suitable for bypass grafting. The diameter of RA was matched with MCA, and postoperative fluorescence angiography showed that the artery was patent. Only 10 cm of RA was needed to effectively avoid postoperative forearm ischemia, and results of postoperative follow-up were good.

In addition, intraoperative electrophysiological monitoring ensures the control of the risk of occlusion and provides a feasible and effective judgment on the blood flow recovery after bypass. Real-time fluorescein angiography after bypass also confirmed patency of blood flow, and preoperative and postoperative CTP comparisons confirmed no severe cerebral ischemia events. Postoperative MRI showed local subacute cerebral infarction in the right external capsule area, but the child had no neurological dysfunction.

Finally, as a case study with a single sample size, and a short follow-up time, this case can still provide a reference for children's complicated aneurysms cases at that age. Larger case studies with long-term follow-up should be conducted in the future to more fully evaluate the advantages of this type of bypass surgery in the treatment of complex MCA aneurysms in children.

CONCLUSIONS

IMA-RA-MCA bypass can be used as an effective high-flow bypass to reconstruct the blood flow at MCA bifurcation, combined with STA-MCA bypass, it can safely treat complex aneurysms at MCA bifurcation. As a high-flow donor artery, IMA has advantages in bypass surgery for children with complex aneurysms of MCA. This case can provide a reference for the treatment of complex aneurysms of MCA bifurcation in children of this age.

DATA AVAILABILITY STATEMENT

The original contributions presented in the study are included in the article/supplementary material, further inquiries can be directed to the corresponding author/s.

ETHICS STATEMENT

Written informed consent was obtained from the minor's legal guardian/next of kin for the publication of any potentially identifiable images or data included in this article.

AUTHOR CONTRIBUTIONS

CH and WH: conceptualization and study design. SQ and GC: data collection, literature research, and manuscript drafting. CH, WH, and YY: revision and funding. All authors contributed to the article and approved the submitted version.

FUNDING

This work was supported by the Guangxi Medical and Health Key Scientific Research Project (No. Z20190610).

REFERENCES

1. Tayebi M, Huang W, Benet A, Kola O, Lawton MT. Bypass surgery for complex middle cerebral artery aneurysms: an algorithmic approach to revascularization. *J Neurosurg.* (2017) 127:463–79. doi: 10.3171/2016.7.JNS16772
2. Hu P, Zhang HQ, Li XY, Tong XZ. Double-barrel superficial temporal artery to proximal middle cerebral artery bypass to treat complex intracranial aneurysms: a reliable high blood flow bypass. *World Neurosurg.* (2019) 125:e884–90. doi: 10.1016/j.wneu.2019.01.203
3. Wang G, Zhang X, Gou Y, Wen Y, Zhang G, Li M, et al. A hybrid strategy for patients with complex cerebral aneurysm: STA-MCA bypass in combination with endovascular embolization. *Front Neurol.* (2020) 11:614601. doi: 10.3389/fneur.2020.614601
4. Hu P, Zhang HQ, Li XJ. Double-barrel STA to proximal MCA bypass and proximal parent artery occlusion for a fusiform superior clinoidal ICA aneurysm. *Acta Neurochir.* (2018) 160:1939–1943. doi: 10.1007/s00701-018-3652-3
5. Nussbaum ES, Kallmes KM, Lassig JP, Goddard JK, Madison MT, Nussbaum LA. Cerebral revascularization for the management of complex intracranial aneurysms: a single-center experience. *J Neurosurg.* (2018) 131:1–11. doi: 10.3171/2018.4.JNS172752
6. Wessels L, Fekonja LS, Vajkoczy P. Bypass surgery of complex middle cerebral artery aneurysms-technical aspects and outcomes. *Acta Neurochir.* (2019) 161:1981–91. doi: 10.1007/s00701-019-04042-9
7. Nossek E, Langer DJ. Internal maxillary artery to middle cerebral artery cranial bypass: the new "work horse" for cerebral flow replacement. *World Neurosurg.* (2018) 115:44–6. doi: 10.1016/j.wneu.2018.03.214
8. Wang L, Lu S, Qian H, Shi X. Internal maxillary bypass for complex pediatric aneurysms. *World Neurosurg.* (2017) 103:395–403. doi: 10.1016/j.wneu.2017.04.055
9. Wang L, Cai L, Lu S, Qian H, Lawton MT, Shi X. The history and evolution of internal maxillary artery bypass. *World Neurosurg.* (2018) 113:320–32. doi: 10.1016/j.wneu.2018.02.158
10. Wang L, Lu S, Cai L, Qian H, Tanikawa R, Shi X. Internal maxillary artery bypass for the treatment of complex middle cerebral artery aneurysms. *Neurosurg Focus.* (2019) 46:E10. doi: 10.3171/2018.11.FOCUS18457
11. Doherty RJ, Moneley D, Brennan P, Javadpour M. Internal maxillary artery to middle cerebral artery bypass for a complex recurrent middle cerebral artery aneurysm: case report and technical considerations. *Br J Neurosurg.* (2020) 1–4. doi: 10.1080/02688697.2020.1849545
12. White TG, Klironomos G, Langer DJ, Katz J, Dehdashti AR. Combined internal maxillary artery to middle cerebral artery and *in situ* middle cerebral to middle cerebral artery bypass for complex middle cerebral artery aneurysm: 3-dimensional operative video. *Oper Neurosurg.* (2020) 18:E121–22. doi: 10.1093/ons/opz166
13. Mohit AA, Sekhar LN, Natarajan SK, Britz GW, Ghodke B. High-flow bypass grafts in the management of complex intracranial aneurysms. *Neurosurgery.* (2007) 60:ONS105-22; discussion ONS122-3. doi: 10.1227/01.NEU.0000249243.25429.EE
14. Alasmari WA. The morphometric anatomy and clinical importance of the radial artery. *Folia Morphol.* (2020) 80:839–44. doi: 10.5603/FM.a2020.0139
15. Kamijo K, Matsui T. Acute extracranial-intracranial bypass using a radial artery graft along with trapping of a ruptured blood blister-like aneurysm of the internal carotid artery. Clinical article. *J Neurosurg.* (2010) 113:781–5. doi: 10.3171/2009.10.JNS09970
16. Kocaeli H, Andaluz N, Choutka O, Zuccarello M. Use of radial artery grafts in extracranial-intracranial revascularization procedures. *Neurosurg Focus.* (2008) 24:E5. doi: 10.3171/FOC/2008/24/2/E5
17. Nossek E, Costantino PD, Eisenberg M, Dehdashti AR, Setton A, Chalif DJ, et al. Internal maxillary artery-middle cerebral artery bypass: infratemporal approach for subcranial-intracranial (SC-IC) bypass. *Neurosurgery.* (2014) 75:87–95. doi: 10.1227/NEU.0000000000000340
18. Zaki Ghali MG, Srinivasan VM, Britz GW. Maxillary artery to intracranial bypass. *World Neurosurg.* (2019) 128:532–40. doi: 10.1016/j.wneu.2019.03.015
19. Li X, Orscelik A, Vigo V, Kola O, El-Sayed IH, Abla AA, et al. Microsurgical techniques for exposing the internal maxillary artery in cerebral revascularization surgery: a comparative cadaver study. *World Neurosurg.* (2020) 143:e232–42. doi: 10.1016/j.wneu.2020.07.112
20. Peto Nouri M, Agazzi S, Langer D, Dehdashti AR. Pterygo-maxillary fissure as a landmark for localization of internal maxillary artery for use in extracranial-intracranial bypass. *Oper Neurosurg.* (2020) 19:E480–6. doi: 10.1093/ons/opaa177
21. Rodriguez Rubio R, Kola O, Tayebi Meybodi A, Tabani H, Feng X, Burkhardt JK, et al. Minimally invasive exposure of the maxillary artery at the anteromedial infratemporal fossa. *Oper Neurosurg.* (2019) 16:79–85. doi: 10.1093/ons/opy051
22. Wang L, Shi X, Qian H. Is internal maxillary artery bypass feasible without zygomatic osteotomy? *World Neurosurg.* (2017) 104:1004. doi: 10.1016/j.wneu.2017.01.134
23. Mrak G, Paladino J, Stambolija V, Nemir J, Sekhar LN. Treatment of giant and large fusiform middle cerebral artery aneurysms with excision and interposition radial artery graft in a 4-year-old child: case report. *Neurosurgery.* (2014) 1(Suppl. 10):E172–7; discussion E177. doi: 10.1227/NEU.0000000000000168

Conflict of Interest: The authors declare that the research was conducted in the absence of any commercial or financial relationships that could be construed as a potential conflict of interest.

Publisher's Note: All claims expressed in this article are solely those of the authors and do not necessarily represent those of their affiliated organizations, or those of the publisher, the editors and the reviewers. Any product that may be evaluated in this article, or claim that may be made by its manufacturer, is not guaranteed or endorsed by the publisher.

frontiers in Surgery

CASE REPORT
published: 16 March 2022
doi: 10.3389/fsurg.2022.842830

Coexistence of Pituitary Adenoma and Primary Pituitary Lymphoma: A Case Report and Review of the Literature

Shangjun Ren[1†], *Qingyang Lu*[2†], *Yilei Xiao*[1], *Yiming Zhang*[1], *Lianqun Zhang*[1], *Bin Li*[3] *and Mengyou Li*[1*]

[1] Department of Neurosurgery, Liaocheng People's Hospital, Liaocheng, China, [2] Department of Pathology, Liaocheng People's Hospital, Liaocheng, China, [3] Department of Neurosurgery, Beijing Neurosurgical Institute, Capital Medical University, Beijing, China

OPEN ACCESS

Edited by:
Philipp Taussky,
The University of Utah, United States

Reviewed by:
Nguyen Minh Duc,
Pham Ngoc Thach University of Medicine, Vietnam
Selfy Oswari,
Indonesia National Brain Center / Universitas Padjadjaran, Indonesia

***Correspondence:**
Mengyou Li
limengyou@163.com

[†] These authors have contributed equally to this work and share first authorship

Specialty section:
This article was submitted to Neurosurgery, a section of the journal Frontiers in Surgery

Received: 24 December 2021
Accepted: 16 February 2022
Published: 16 March 2022

Citation:
Ren S, Lu Q, Xiao Y, Zhang Y, Zhang L, Li B and Li M (2022) Coexistence of Pituitary Adenoma and Primary Pituitary Lymphoma: A Case Report and Review of the Literature. Front. Surg. 9:842830. doi: 10.3389/fsurg.2022.842830

In the pituitary sella, the coexistence of pituitary adenoma and primary pituitary lymphoma is exceedingly rare. Thus far, only six cases have been reported. Here, we present the seventh case of coexisting pituitary adenoma and primary pituitary lymphoma, which was difficult to differentiate from other sellar tumors. To our knowledge, this is the first case of the prolactin subtype of the pituitary adenoma in literature. We have also systematically reviewed the literature and summarized the characteristics of coexisting pituitary adenoma and lymphoma. We believe this report provides a new clinical reference for the diagnosis and treatment of collision tumors of pituitary adenoma and lymphoma.

Keywords: collision tumor, pituitary adenoma (PA), pituitary lymphoma, DLBCL - diffuse large B cell lymphoma, review

INTRODUCTION

Collision tumor in the sellar region is a rare condition; it refers to two coexisting tumors of different shapes attached to each other. Typically, a collision tumor in the sellar region is characterized by the coexistence of pituitary adenoma and another tumor. Reportedly, the pituitary adenoma can be associated with meningioma (1), Rathke's cleft cyst (2), craniopharyngioma (3), gangliocytoma (4), and other neoplasms. Among them, the coexistence of pituitary adenoma and primary pituitary lymphoma is extremely rare. It is difficult to distinguish it from other sellar region tumors, and the perioperative diagnosis is difficult because the clinical and radiological manifestations of most cases are similar to pituitary adenomas. Only six cases of pituitary adenoma associated with lymphoma have, thus far, been reported. Here, we report the seventh case and systematically review the literature.

CASE PRESENTATION

In May 2020, a 41-year-old Asian male was hospitalized with a history of intermittent stabbing headache, without progressive deterioration of visual acuity or visual field. **Table 1** presents the results of the endocrine examination. Brain CT showed a tumor with calcification in the sellar region (**Figure 1A**). The brain MRI showed that the sellar floor was eroded; further, the

TABLE 1 | Endocrine examination results.

Hormone	Level measured	Normal levels
GH	0.51 ng/ml	0.014-5.219 ng/ml
PRL	11 ng/ml	3.7-17.9 ng/ml
ACTH	**94.05 pg/ml**	10.1-57.6 pg/ml
TSH	**6.84 mIU/L**	0.465-4.680 mIU/L

Bold text indicates abnormal data.
GH, growth hormone; PRL, prolactin, ACTH, adrenocorticotropic hormone; TSH, thyroid-stimulating hormone.

pituitary stalk was not clear. The tumor showed hypointensity in both T1-weighted and T2-weighted MRI images. A contrast-enhanced MRI showed a significant enhancement of under-homogeneity (**Figures 1B–E**). These radiological manifestations indicated that the sellar mass was pituitary adenoma.

The patient underwent endoscopic endonasal transsphenoidal tumor resection. A tough tumor was encountered in the sphenoid sinus and sellar region. The tumor was abnormally hypervascular, and there was bone inside the tumor. The volume of intraoperative bleeding was about 200 mL. By the end of the surgery, all the tumors were removed in pieces. Postoperatively, the patient recovered well. The symptoms of headache were significantly relieved. Pathological results showed sparsely granulated lactotroph adenoma combined with primary pituitary diffuse large B-cell lymphoma (**Figure 1F**). The immunohistochemistry results are shown in **Table 2**.

A postoperative head MRI showed that there was no residual tumor in the sellar region. A PET-CT scan did not show increased uptake in the pituitary gland and other parts. The results of bone marrow puncture showed that the degree of proliferation was V/VII, G:E = 2.3:1, and nuclear heterogeneous cells were occasionally seen. Then, he received four cycles of chemotherapy. The R-MI protocol (rituximab+methotrexate+ifosfamide) was used, accompanied by supportive treatment.

The patient underwent follow-up examinations at postoperative 6 months and 1 year. The patient was generally in good condition, and the tumor did not recur. A series of brain MRIs showed no evidence of tumor regrowth (**Figures 1G–J**). The patient will continue to be followed up.

DISCUSSION

Collision tumors of pituitary adenoma and primary pituitary lymphoma in the sellar region are extremely rare. We systematically reviewed the literature to identify the characteristics of coexisting pituitary adenoma and lymphoma. To our knowledge, thus far, only seven cases have been reported, including this case. We have summarized the characteristics of these seven cases (5–10) and presented them in **Table 3**.

The pathophysiological mechanism of tumorigenesis remains unclear, as there are only a very small number of cases currently reported. The local immune changes in the pituitary gland may be brought about by tumorigenesis. It is reported that primary pituitary lymphoma can develop in immunosuppressed individuals (11). At the same time, the occurrence and development of pituitary adenomas are closely related to immune infiltration (12). Whether immune-related mechanisms are involved in the occurrence of collision tumors is still poorly understood and needs to be investigated in more patients.

The coexistence of pituitary adenoma and primary pituitary lymphoma has no special clinical manifestations. The most common clinical manifestation is headache; it was noted in 5 of 7 cases (**Table 3**). Whether the patient's vision and visual field are affected mainly depends on the size of the tumor. Eyesight decline or visual field defect in patients occurred in five cases, but not in the present report (**Table 3**). Imaging findings are similar to pituitary adenomas, which makes preoperative diagnosis very challenging (**Figure 1**). Pathology is the gold standard for diagnosis. The diagnosis of collision tumor of pituitary adenoma and primary pituitary lymphoma in all seven cases was confirmed by pathology. The subtypes of pituitary adenoma can be follicle-stimulating hormone (FSH), Thyroid-stimulating hormone (TSH), Growth hormone (GH), Adrenocorticotropic hormone (ACTH), or Prolactin (PRL). The FSH subtype of pituitary adenoma is the most common (**Table 3**). This case report was the first to suggest the PRL subtype of pituitary adenoma. The subtypes of pituitary lymphoma are also not consistent. It can be T-cell lymphoblastic lymphoma (T-LBL) or diffuse large B-cell lymphoma (DLBCL). It is different from primary pituitary lymphoma. The most common subtypes of primary pituitary lymphoma are B-cell lymphoma, followed by T cell and NK/T cell types (13).

Surgical management is the most important treatment option for collision tumors of pituitary adenoma and primary pituitary lymphoma. The patients in the six previous cases underwent surgical treatment. In Au et al.'s (6) case report, the patient was an 82-year-old man. Perhaps because of advanced age, the patient did not undergo surgical resection after tumor biopsy but underwent radiotherapy. With the development of neuroendoscopic technology, endoscopic transnasal resection of collision tumors in the sellar region has become the treatment of choice. In our case, the patient underwent endoscopic endonasal transsphenoidal tumor resection. In the end, all the tumors were removed in pieces. If the tumor is completely resected and there is no evidence of systemic lymphoma, no additional radiotherapy is required. However, DLBCL is a highly malignant lesion. To prevent tumor recurrence, chemotherapy can be used appropriately. If the tumor remains or there is evidence of systemic lymphoma, additional radiotherapy or chemotherapy is required. Chemotherapy was used in three cases (**Table 3**). The classic chemotherapy drug is methotrexate. The external beam radiation of the head was used in three cases (6–8). In the case report by Romeike et al. (7), we found that radiotherapy

Abbreviations: CT, Computed tomography; MRI, Magnetic resonance imaging; FSH, Follicle-stimulating hormone; TSH, Thyroid-stimulating hormone; GH, Growth hormone; PRL, Prolactin; T-LBL, T-cell lymphoblastic lymphoma; DLBCL, Diffuse large B-cell lymphoma; PET, Positron emission tomography.

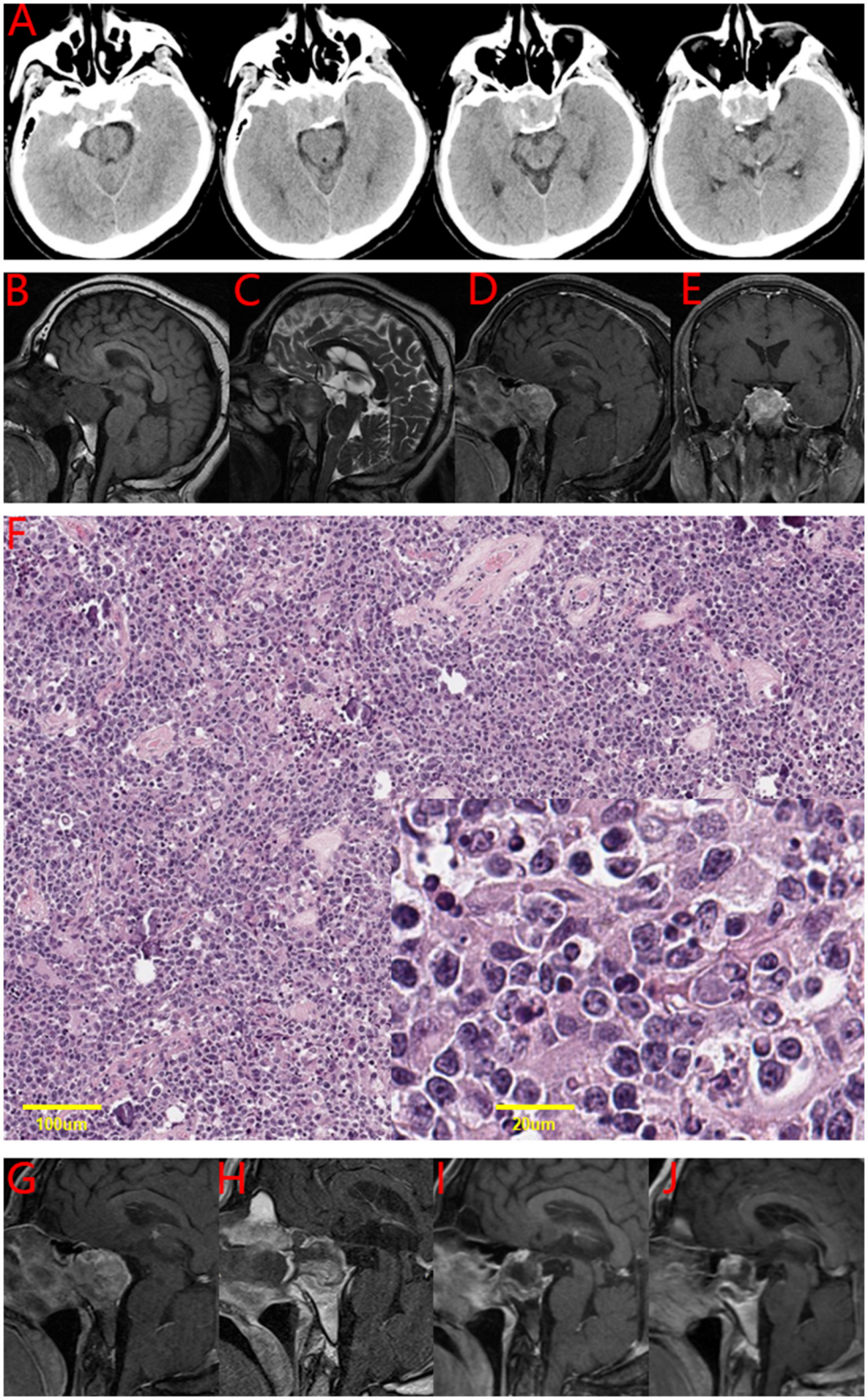

FIGURE 1 | The imaging and pathological results of the patient. **(A)** Brain CT of the patient in this case. Brain CT showed a tumor in the sellar region with calcification. **(B-E)** Brain MRI of the patient in this case. **(B)** T1-weighted image: sellar region tumor is imaged in the same intensity as the cerebral cortex. **(C)** T2-weighted image: a slightly longer signal. **(D)** and **(E)** post-gadolinium image: significant enhancement of under-homogeneity. **(F)** Hematoxylin and eosin stain of the tumor tissue in this case. Primary pituitary diffuse large B-cell lymphoma combined with sparsely granulated lactotroph adenoma. **(G-J)** A series of MRIs of the patient in this case. **(G)** Preoperative **(H),** postoperative **(I),** 6 months after the operation **(J),** and 12 months after the operation.

TABLE 2 | Immunohistochemistry results.

Biomarker	Result
CD45, CD20, CD79α, CD10, Bcl-6, c-MYC, MUM1, Pit-1, PRL, Syn, CK18	Positive (+)
Bcl-2, SF-1, T-Pit, GH, TSH, FSH, LH, ACTH	Negative [-]

TABLE 3 | Summary cases of coexistence of pituitary adenoma and pituitary lymphoma.

Case report	Age/Sex	Symptoms	Treatment	Subtype of PA	Subtype of PL	Recurrence
Kuhn. (5)	67/F	VD, VFD	ST	FSH	T-LBL	Yes (6 Mo)
Au. (6)	82/M	HA, VD, VFD	BIOP, RT	TSH	DLBCL	ND
Romeike. (7)	64/F	HA, VFD	ST, MT, RT	FSH	T-LBL	No (19 Mo)
Martinez. (8)	71/F	VFD	ST, RT	GH	DLBCL	No (12 Mo)
Ban. (9)	74/M	HA	ST, MT	FSH	DLBCL	No (32 Mo)
Gupta. (10)	55/F	HA, VD	ST	ACTH	T-LBL	ND
Present case	41/M	HA	ST, MT	PRL	DLBCL	No (12 Mo)

PA, pituitary adenoma; PL, pituitary lymphoma; F, female; M, male; VD, visual deterioration; VFD, visual field defect; HA, headache; ST, surgical treatment; BIOP, biopsy; RT, radiation therapy; MT, medical treatment; FSH, follicle-stimulating hormone; TSH, thyroid-stimulating hormone; GH, growth hormone; PRL, prolactin; T-LBL, T-cell lymphoblastic lymphoma; DLBCL, diffuse large B-cell lymphoma; Mo, month; ND, not described.

and chemotherapy were used after the subtotal removal of the lesion. A thorough postoperative examination, including brain MRI, PET-CT, bone marrow aspirate, and bone marrow trephine biopsy, are necessary to reveal any sign of systemic manifestation of the lymphoma spread.

The recurrence rate after total resection is low, but there is still recurrence. In the case report by Kuhn et al. published in 1999 (5), the tumor recurred 6 months after the operation. Perhaps, the available surgical technology then was not optimal, failing to completely remove the tumor in the first operation. Moreover, the patient did not receive chemotherapy and radiotherapy after the first operation. The patient, therefore, had to undergo a second operation. The control of collision tumors is more difficult than simple pituitary adenoma, so the follow-up cycle needs to be prolonged. We suggest that the follow-up should be extended to more than 3 years after the initial operation. If the tumor relapses, a reoperation is still the first choice, but radiotherapy and chemotherapy need to be considered after the operation.

CONCLUSIONS

The coexistence of pituitary adenoma and primary pituitary lymphoma in the sellar region is extremely rare. The disease diagnosis, tumor control, and overall survival are more challenging to achieve for collision tumors than for pituitary adenomas alone. The gross total resection of both tumors is very important for satisfactory tumor control. The follow-up assessment of patients should be appropriately prolonged.

LIMITATION

Because the patient's preoperative diagnosis was a conventional pituitary adenoma, video recording was not performed during the operation. Therefore, there are no intraoperative images. Furthermore, the report lacks neuro-ophthalmological examination, because the patient claimed to have normal visual acuity and field. Lastly, only 1-year postoperative follow-up was performed on the patient. We plan to continue to monitor the situation of this patient.

DATA AVAILABILITY STATEMENT

The raw data supporting the conclusions of this article will be made available by the authors, without undue reservation.

ETHICS STATEMENT

Written informed consent was obtained from the individual(s) for the publication of any potentially identifiable images or data included in this article.

AUTHOR CONTRIBUTIONS

ML conceived the study and edited the final manuscript. SR and QL collected the clinical data and performed a literature review. YZ confirmed the pathological analysis. BL reviewed the clinical notes and produced the draft manuscript. YX and LZ conceived the research and helped with the writing of the manuscript. All authors read and approved the final manuscript.

FUNDING

This work was supported by grants from the Taishan Scholar Project of Shandong Province of China (tsqn202103200) and the National Natural Science Foundation of China (81701159).

REFERENCES

1. Zhao Y, Zhang H, Lian W, Xing B, Feng M, Liu X, et al. Collision tumors composed of meningioma and growth hormone-secreting pituitary adenoma in the sellar region: Case reports and a literature review. *Medicine (Baltimore).* (2017) 96:e9139. doi: 10.1097/MD.0000000000009139
2. de Almeida Verdolin A, Lamback EB, Ventura N, Guasti A, da Mata Pereira PJ, Gadelha MR, et al. Collision sellar lesions: coexistence of pituitary adenoma and Rathke cleft cyst-a single-center experience. *Endocrine.* (2020) 68:174–81. doi: 10.1007/s12020-019-02149-8
3. Hasegawa H, Jentoft ME, Young WF Jr, Lakomkin N, Van Gompel JJ, Link MJ, et al. Collision of Craniopharyngioma and Pituitary Adenoma: Comprehensive Review of an Extremely Rare Sellar Condition. *World Neurosurg.* (2021) 149:e51–62. doi: 10.1016/j.wneu.2021.02.091
4. Tanriover N, Aydin O, Kucukyuruk B, Abuzayed B, Guler H, Oz B, et al. Endoscopic approach to a collision tumor of growth hormone-secreting adenoma and gangliocytoma in the pituitary gland. *J Craniofac Surg.* (2014) 25:1277–9. doi: 10.1097/SCS.0000000000000580
5. Kuhn D, Buchfelder M, Brabletz T, Paulus W. Intrasellar malignant lymphoma developing within pituitary adenoma. *Acta Neuropathol.* (1999) 97:311–6. doi: 10.1007/s004010050990
6. Au WY, Kwong YL, Shek TW, Leung G, Ooi C. Diffuse large-cell B-cell lymphoma in a pituitary adenoma: an unusual cause of pituitary apoplexy. *Am J Hematol.* (2000) 63:231-2. doi: 10.1002/(sici)1096-8652(200004)63:4<231::aid-ajh14>3.0.co;2-z
7. Romeike BF, Joellenbeck B, Stein H, Loddenkemper C, Hummel M, Firsching R, et al. Precursor T-lymphoblastic lymphoma within a recurrent pituitary adenoma. *Acta Neurochir (Wien).* (2008) 150:833–6. doi: 10.1007/s00701-008-1585-y
8. Martinez JH, Davila Martinez M, Mercado de Gorgola M, Montalvo LF, Tome JE. The coexistence of an intrasellar adenoma, lymphocytic hypophysitis, and primary pituitary lymphoma in a patient with acromegaly. *Case Rep Endocrinol.* (2011) 2011:941738. doi: 10.1155/2011/941738
9. Ban VS, Chaudhary BR, Allinson K, Santarius T, Kirollos RW. Concomitant Primary CNS Lymphoma and FSH-Pituitary Adenoma Arising Within the Sella. Entirely Coincidental? *Neurosurgery.* (2017) 80:E170–5. doi: 10.1093/neuros/nyw003
10. Gupta RK, Saran RK, Srivastava AK, Jagetia A, Garg L, Sharma MC, et al. cell lymphoblastic lymphoma/leukemia within an adrenocorticotropic hormone and thyroid stimulating hormone positive pituitary adenoma: a cytohistological correlation emphasizing importance of intra-operative squash smear. *Neuropathology.* (2017) 37:358–64. doi: 10.1111/neup.12375
11. Duan L, Liu J, Zhang Y, Cui L, Zhai X, Pan B, et al. Primary Pituitary Lymphoma in Immunocompetent Patients: A Report on Two Case Studies and the Review of Literature. *Front Endocrinol (Lausanne).* (2020) 11:562850. doi: 10.3389/fendo.2020.562850
12. Dai C, Liang S, Sun B, Kang J. The Progress of Immunotherapy in Refractory Pituitary Adenomas and Pituitary Carcinomas. *Front Endocrinol (Lausanne).* (2020) 11:608422. doi: 10.3389/fendo.2020.608422
13. Tarabay A, Cossu G, Berhouma M, Levivier M, Daniel RT, Messerer M. Primary pituitary lymphoma: an update of the literature. *J Neurooncol.* (2016) 130:383–95. doi: 10.1007/s11060-016-2249-z

Conflict of Interest: The authors declare that the research was conducted in the absence of any commercial or financial relationships that could be construed as a potential conflict of interest.

Advantages of publishing in Frontiers

OPEN ACCESS
Articles are free to read for greatest visibility and readership

FAST PUBLICATION
Around 90 days from submission to decision

HIGH QUALITY PEER-REVIEW
Rigorous, collaborative, and constructive peer-review

TRANSPARENT PEER-REVIEW
Editors and reviewers acknowledged by name on published articles

Frontiers
Avenue du Tribunal-Fédéral 34
1005 Lausanne | Switzerland

Visit us: www.frontiersin.org
Contact us: frontiersin.org/about/contact

REPRODUCIBILITY OF RESEARCH
Support open data and methods to enhance research reproducibility

DIGITAL PUBLISHING
Articles designed for optimal readership across devices

FOLLOW US
@frontiersin

IMPACT METRICS
Advanced article metrics track visibility across digital media

EXTENSIVE PROMOTION
Marketing and promotion of impactful research

LOOP RESEARCH NETWORK
Our network increases your article's readership